

HBRC Journal

Volume 2, Number 1, January 2006
ISSN: 1687-4048
DEP: 12479/2004

Contents

Concrete Properties of Ternary Cementitious Systems Containing Fly Ash and Silica Fume: M. Anwar	1
Evaluation of Concrete Properties by Using Demolished Aggregates: Z. S. Houssieen	11
Recycling of Cement Kiln Dust and Waterglass Sludge in the Manufacture of Acid Resistant Masonry Units: M. S. El-Mahlawy and T. M. El-Sokkary	23
Modeling of Openings in Masonry Infill Panels in R.C. Frames, 2d Approach: M. O. El Seify, M. M. El-Attar, A. M. Ragab, and O. A. Hodhod	36
Effect of Steel Fiber (SF) Content on Behavior of High Strength Reinforced Concrete Circular Columns: S. S. Yousef, H. M. Abd El-Latif, H. H. Bahnasawy and M. A. Metawea	50
Lateral Stability of Deep-Thin Flanged I-Shaped Beams with Vertical Stiffeners: S. S. Safar	60
Fatigue Strength of Corrugated Steel Bolted Lap Joints Under Flexure: H. E. H. Mohammed	75
The Influence of Principal Axes on Dynamic Behaviour of Irregular Structures: K. Z. Soliman	86
Effect of Clay Soil Deposits on Ground Motion Characteristics and on Structure Behavior: K. Z. Soliman And A. T. M. Farid	96

Technical Note

Manufacturing High Quality Rotating Biological Contactor's for the UK Water Industry: D. Mba, R.H. Bannister and G.E. Findlay	106
---	-----

HBRC News

115

Vol. 2 No. 1
January 2006
ISSN: 1687-4048
DEP: 12479/2004

Vol. 2 No. 1

January 2006

ISSN: 1687-4048

DEP: 12479/2004

HBRC Journal



Housing & Building National Research Center

87 El-Tahrir St. Dokki 11511 P.O.BOX 1770 Cairo, EGYPT
Phone: 00202-7617062 Fax.: 00202-3367179
www.hbrc.edu.eg, journal@hbrc.edu.eg

BOARD OF DIRECTORS

Prof. Ali Sherif Abdel Faiad (HBRC Chairman) Prof. Omaina A. Salah El-Din (Board Head)
Prof. Adel I. El-Mallawany (Deputy)
Prof. Hamdy A. El-Sayed
Prof. Fayrouz F. El-Dib
Prof. Shadia N.El-Ibiary
Prof. Heba H. Bahnasawy
Prof. Khadiga I. Abdel - Ghani
Prof. M. M. Abdel - Razik

BOARD OF EDITORS

Prof. Adel I. El-Mallawany (Head)
Prof. Amira Abd El-Rahman (Deputy)
Dr. Nadia M. Nofal
Dr. Khalid M. El-Zahaby
Dr. Dinna K. Shehayeb
Dr. Ashraf M. Kamal
Dr. Ashraf M. Fadel
Dr. Amr A. El-Hefnawy
Dr. Tarek M. El-Sokkary
Dr. Tarek M. Bahaa
Dr. Tarek M. Attia
Dr. Mohamed M. Abdel-Rahman
Mr. Mohamed E. Metwally

EDITORIAL OFFICE

Eng. Bastamy El-Touny
Eng. Ghada Daa
Eng. Anwar M. Mohamed



Published By:

**Housing & Building
National Research Center**

Tel./Fax. : (20)(2) 7617062
(20)(2) 3367179

HBRC Web Site
www.hbrc.edu.eg

E-mail:
Journal@hbrc.edu.eg

Copyright HBRC 2004
ISSN :1687-4048
DEP: 12479/2004

For Subscription Information,
please Contact HBRC.

CONCRETE PROPERTIES OF TERNARY CEMENTITIOUS SYSTEMS CONTAINING FLY ASH AND SILICA FUME

M. Anwar

Associate professor, Construction Research Institute, NWRC, Delta-Barrage 13621, Egypt.

ABSTRACT

This research presents the results from laboratory studies on the properties of concrete that contains ternary blends of Portland cement, fly ash, and silica fume. Selected nine concrete mixtures are prepared with water to cementitious material ratio of 0.4. The concrete mixtures were designed to have the same degree of workability and percentage of air content. The measured properties of fresh concrete include the slump, air content, and unit weight. The investigated properties of hardened concrete include the compressive strength, tensile strength, dynamic elastic modulus, and static young's modulus. The results indicate that concretes made with these systems generally show good fresh and hardened properties since the combination of fly ash and silica fume is somewhat synergistic. Fly ash appears to compensate for some of the workability problems associated with the use of silica fume, whereas the silica fume appears to compensate for the relatively low early strength of fly ash concrete.

Keywords: Concrete, Binary, Ternary, Portland Cement, Fly Ash, Silica Fume.

INTRODUCTION

Continuous generation of waste by-products possessing hydraulic and pozzolanic properties, creates not only acute environmental problems, but additionally outlines a need for their greater utilization in different market sectors. The construction sector is clearly the one that, at the moment, absorbs the majority of such materials, by incorporating them in hydraulic binders as supplementary cementing materials [1]. For a variety of reasons, the concrete construction industry is not sustainable. First, it consumes huge quantities of virgin materials. Second, the principal binder in concrete is Portland cement, the production of which is a major contributor to greenhouse gas emissions that are implicated in global warming and climate change. Third, many concrete structures suffer from lack of durability which has an adverse effect on the resource productivity of the industry. Because the high-volume fly ash concrete system addresses all three sustainability issues, its adoption will enable the concrete construction industry to become more sustainable [2].

In the last few decades, fly ash, blast-furnace slag and silica fume have been increasingly used as mineral additives in cement and concrete. The use of these artificial pozzolans can achieve not only economical and ecological benefits but technical benefits as well. It is generally agreed that, with proper selection of admixture, mixture proportioning and curing technique, mineral additives can greatly improve the durability of concrete [3]. Nevertheless, it is also well established that mineral additives may reduce early strength of concrete, especially with high cement replacement rates [4,5]. The loss of early strength may be compensated by: (1) curing under elevated temperature [6], (2) chemical activation [7,8], (3) high fineness cement and additives [9,10] and (4) more than one to one replacement of cement by mineral additives and lower water to cementitious materials ratio (W/C) [11,12].

In recent years, it has been reported that ternary blended cements could substantially improve the performance of concrete compared with the conventional binary blended cements or regular Portland cement. Ternary blended cement consisting of Portland cement, granulated

blast-furnace slag and fly ash (PC-SL-FA system) was developed in Japan for mass concrete construction due to its very low heat of hydration [13]. This system can be treated as slag cement incorporating fly ash. The addition of fly ash can increase workability and reduce bleeding of slag cement concrete. However, the strength development of this system is relatively slower at early age [14]. By incorporating silica fume in slag cement or fly ash cement, the ternary PC-SL-SF (Portland cement, blast-furnace slag and silica fume) and PC-FA-SF (Portland cement, fly ash and silica fume) blended cements were developed and commercially manufactured in Canada [15].

Similar to the effect of silica fume addition in Portland cement, the fluidity of PC-SL-SF system cement is impaired by silica fume. The addition of a water-reducing agent or a superplasticizer is inevitable for PC-SL-SF system cement. Fly ash in PC-FA-SF system may have water-reducing effect depending on its quality that may totally or partially compensate the increased water requirement caused by silica fume. By incorporating 25% fly ash and up to 5% silica fume, the flow of mortar had no significant change compared to ASTM Type I cement mortar [16]. It was also reported that addition of silica fume could only slightly increase the early strength of PC-FA-SF system cement. The strength did not increase so much at and after 28 days because $\text{Ca}(\text{OH})_2$ produced was preferentially consumed by the pozzolanic reaction of silica fume, thereby decreasing extensively the quantity of $\text{Ca}(\text{OH})_2$ available for the fly ash [17].

The main purpose of this paper is to study the mechanical properties of the concrete of binary and ternary cementitious systems. Binary and ternary cementitious systems of Portland cement, silica fume and fly ash with various combinations will be investigated. The effect of the changing in the replacement percents of fly ash and silica fume on the properties of concrete will be examined. The measured properties were included fresh concrete properties (slump, air content and unit weight) and hardened concrete properties such as compressive strength, tensile strength, static Young's modulus, and dynamic elastic modulus.

EXPERIMENTAL PROGRAM OUTLINE

At this stage it is not clear how the Ordinary Portland cement (OPC), silica fume (SF) and fly ash (FA) work together therefore, this research was carried out to find out how these ternary cementitious systems affect the concrete properties. Nine concrete mixtures are prepared with water/cementitious material ratio of 0.4 and sand/gravel ratio of 0.66. The measured properties of fresh concrete include slump, unit weight, and air content (the concrete mixtures designed to achieve slump of 10 ± 2 cm and air content of $4 \pm 1\%$). The evaluated properties of hardened concrete include compressive strength, tensile strength, static elastic modulus, and dynamic elastic modulus. Table 1 shows the binary and ternary systems of combination of Portland cement, silica fume and fly ash while the mix proportions of concrete mixtures are summarized in Table 2.

Table 1. Binary And Ternary Systems of Portland Cement, Silica Fume and Fly Ash

Mix No.	OPC %	Fly Ash (FA) %	Silica Fume (SF) %	Binary or Ternary System
1	100	---	---	Control
2	85	15	---	OPC-FA
3	75	25	---	OPC-FA
4	95	---	5	OPC-SF
5	90	---	10	OPC-SF
6	80	15	5	OPC-FA-SF
7	75	25	5	OPC-FA-SF
8	70	15	10	OPC-FA-SF
9	65	25	10	OPC-FA-SF

The used materials selected from commercial available construction materials in Japan. The properties of the used OPC comply with Japanese Industrial Standard (JIS). The properties of

used OPC, SF and FA are listed in Table 3. The properties of used sand and gravel are represented in Table 4. Fig.1 shows the particle size distribution of used aggregates. The used chemical admixtures are two types, the first is high performance superplasticizer, high range water reducing admixture includes air entraining effect, the second is air entraining agent.

Table 2. Mix Proportions of the Concrete Mixtures

Mix No.	kg/m ³							Ad		AE
	W	OPC	FA	SF	Sand	Gravel		C %	kg/m ³	kg/m ³
						20mm	15mm			
1	164	410.0	0.0	0.0	680	512	510	0.95	3.895	1.025
2		348.5	61.5	0.0	672	506	504	0.90	3.690	3.075
3		307.5	102.5	0.0	668	503	501	0.80	3.280	3.690
4		389.5	0.0	20.5	677	510	508	0.95	3.895	0.410
5		369.0	0.0	41.0	674	508	506	1.00	4.100	0.410
6		328.0	61.5	20.5	670	504	502	0.90	3.690	1.845
7		287.0	102.5	20.5	665	501	499	0.90	3.690	3.280
8		307.5	61.5	41.0	667	502	500	0.90	3.690	1.845
9		266.5	102.5	41.0	662	499	497	0.90	3.690	2.050

W: Water, OPC: Ordinary Portland Cement, FA: Fly Ash, SF: Silica Fume, Ad: Chemical admixture (High performance superplasticizer, high range water reducing admixture includes air entraining effect), AE: Air Entraining Agent.

Table 3. Properties of Used Portland Cement, Silica Fume and Fly Ash

Constituents	Ordinary Portland Cement (OPC)	Fly Ash (FA)	Silica Fume (SF)
Specific gravity	3.16	2.32	2.24
Surface area (cm ² /g)	3310	3910	153000
Loss on ignition, L.O.I	2.05	1.95	1.30
Silicon dioxide, SiO ₂	22.0	45.0	94.90
Magnesium oxide, MgO	1.12	N/A	0.61
Sulfur trioxide, SO ₃	2.13	N/A	0.33
Chloride Ion, Cl ⁻	0.011	N/A	0.048

Table 4. Properties of the Used Aggregates

Materials type	Sand	Gravel	
		20 mm	15 mm
Specific gravity	2.55	2.56	2.55
Water absorption (%)	1.23	2.50	2.67
Nominal maximum size (mm)	---	20	
Fineness modulus	2.68	6.72	

Gravel 20 mm : Gravel 15 mm = 1:1

The materials were batched into the mixer as follows: first; coarse aggregate followed by sand, then cementitious materials (OPC, FA, and SF are mixed well before batched into the mixer) added to the mixer. The total mixing time is three minutes divided into two stages, starting with 60 seconds dry mixing and then the required water (mixed with chemical admixture) is added

within 30 seconds, then mixer continues for the next 1.5 minutes of mixing. After casting, the concrete moulds were compacted by the use of a vibrator. The samples were finished, stripped from their moulds the day after casting. The specimens were cured under water till the testing time.

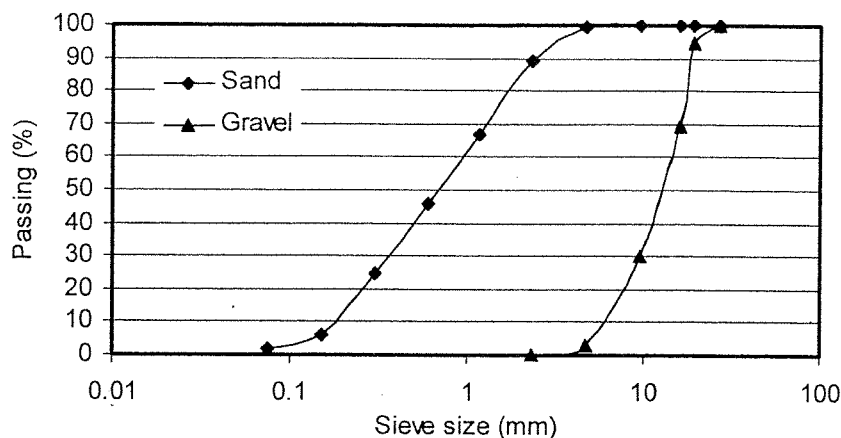


Fig. 1: Particle Size Distribution of Used Aggregate.

The hardened concrete properties were measured by means of destructive and non-destructive tests. Compressive strength and tensile strength are performed via the destructive tests, while the static young's modulus and dynamic elastic modulus were carried out via the non-destructive ones. The compressive strength and dynamic elastic modulus were measured at 3, 7, 28 and 90 days while the tensile strength (cylinder of 15 cm diameter and height 30 cm) and static young's modulus were measured at 28 days. The modulus of elasticity is determined on laboratory specimens subjected to longitudinal (horizontally or vertically) vibration at their natural frequency, and is therefore known as the dynamic elastic modulus. Japanese Industrial Standard (JIS) prescribes the use of specimens similar to those employed in the determination of the modulus of rupture, i.e. beams 10 by 10 by 40 cm or cylinder 10 cm in diameter by 20 cm in height. The specimen is put horizontally or vertically on Young's Modulus Rigidity Meter. In this work, concrete specimens (prism of 10 x 10 x 40 cm) were used to measure the dynamic elastic modulus. Determination of these properties was undertaken at the facilities of Department of Safety Systems Construction Engineering, Kagawa University, Japan, according to the specifications provided by JIS.

PROPERTIES OF FRESH CONCRETE

As mentioned before, the measured properties of fresh concrete include slump, air content (the concrete mixtures designed to achieve slump of 10 ± 2 cm and air content of 4 ± 1 %) and unit weight. Dose of the used chemical admixtures (high performance superplasticizer and air entraining agent) are changed to achieve the designed values of slump and air content. The measured values of slump, air content and unit weight are shown in Figs. 1, 2, and 3, respectively.

During proportioning and mixing the concrete mixtures, it is noticed that fly ash mixtures need high dose of the air entraining agent to achieve the designed air content while silica fume mixtures need low dose of the air entraining agent. Concerning the superplasticizer, silica fume mixtures need higher dose than those of fly ash ones. The mixtures include ternary systems of fly ash and silica fume show that both silica fume and fly compensate each other regarding the dose of air entraining agent and superplasticizer. The measured values of slump and air content fall within the designed range, i.e., all measured slump are 10 ± 2 cm and air content of 4 ± 1 % as shown in Figs. 2 and 3. The results of unit weight of concrete change according to the type of used cementitious materials as shown in Fig. 4. This attributed to change in the

specific gravity of the cementitious materials and air content. Moreover, results show that type of cementitious materials system plays significant role in produced fresh concrete.

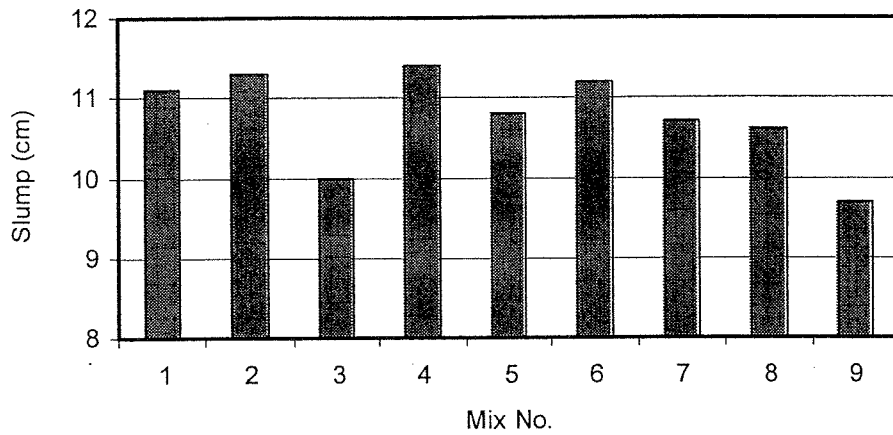


Fig.2. Slump of the Studied Concrete Mixtures.

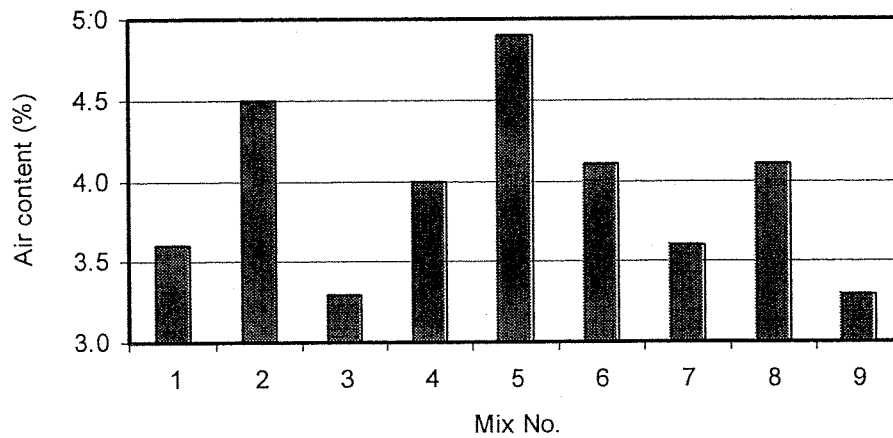


Fig. 3. Air Content of the Studied Concrete Mixtures.

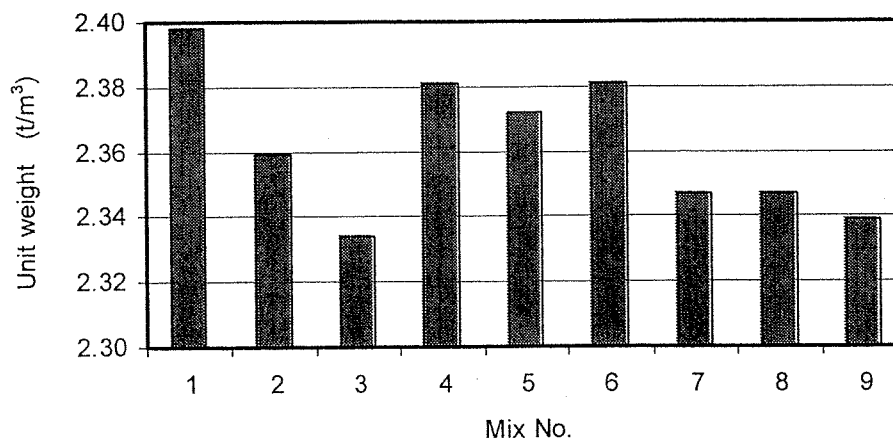


Fig. 4. Unit Weight of the Studied Concrete Mixtures.

PROPERTIES OF HARDENED CONCRETE

The obtained results of compressive strength of the studied concrete mixtures at ages of 3, 7, 28, and 90 days are shown in Fig. 5. The compressive strengths of silica fume concrete (Mixes 4 & 5) are higher than those of all studied mixes at all ages. The control mix (OPC) shows higher strengths than those of Mix 2 (15% FA) at ages 3 and 7 days. While, the results of 28 and 90 of Mix 2 (15 FA) indicate an equivalent compressive strength to the control mix. Mix 3 of fly ash show lower compressive strengths than those of the control concrete at all ages due to the effect of high replacement percent (25%) of fly ash. The mixes of ternary systems show lower compressive strength than those of OPC mix (control mix) at ages 3 and 7 days and they indicate an equivalent compressive strength to the control mix at ages 28 and 90 days.

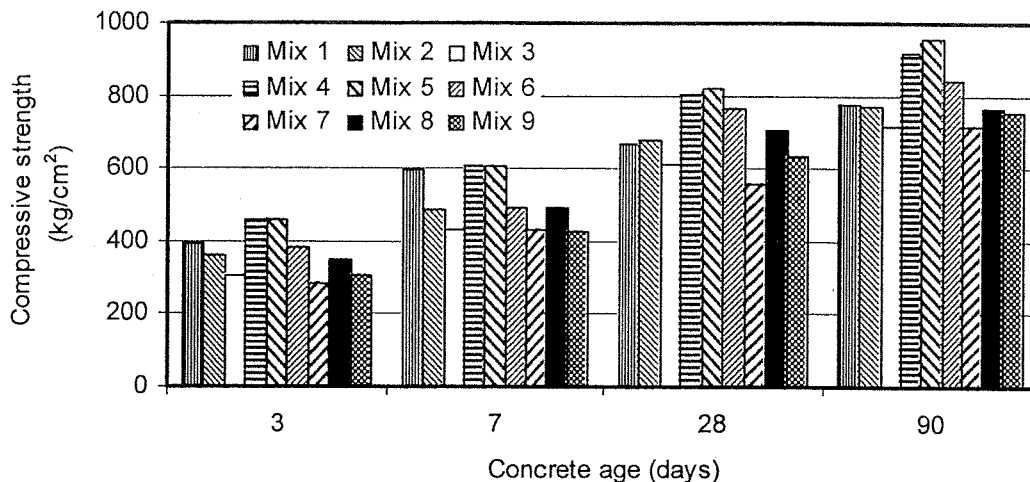


Fig. 5. Compressive Strength of The Studied Concretes.

Table 5. Rate of Compressive Strength Development For The Studied Concretes

Mix No.	Rate of strength gain (kg/cm ² /day)			
	(0~3) days	(3~7) days	(7~28) days	(28~90) days
1	132	49.3	3.6	1.74
2	120.7	30.5	9.2	1.52
3	102.7	31.5	8.5	1.68
4	152.3	36.8	10.7	1.84
5	152.7	37.5	11.6	2.24
6	127.0	28.0	12.9	1.24
7	95.3	35.8	6.24	2.55
8	117.0	35.0	10.1	0.98
9	101.3	30.5	9.81	1.98

The rates of the compressive strength development up to age of 90 days of concrete mixes with various combinations of Portland cement, fly ash, and silica fume are listed in Table 5. The obtained results are confirmed with Thomas [18] who reported that the combination of Portland cement, silica fume and fly ash in a ternary cement system should result in a number of synergistic effects, some of which are obvious or intuitive. Also, the results comply with the finding of Lane [19] who indicated that the use of ternary blends incorporating small amounts of silica fume with smaller amounts of fly ash or slag was shown to be a viable approach to counteract the negative impact of higher replacement levels of fly ash and slag on early strength. The obtained data show that binary cementitious blends of Portland cement and silica fume offer significant advantages over plain Portland cement. Moreover, ternary cementitious systems of Portland cement, silica fume (5 to 10%), and fly ash (15 to 25%) indicate satisfactory compressive strength especially at ages of 28 and 90 days.

From data of Fig. 5, the early age compressive strength of binary systems of OPC and FA concretes is lower than the control concrete, because of FA acts as filler in concrete and does not contribute to the strength development. Further, the hydration reaction of FA mixes is somewhat slower due to the lower cement content of the mix (due to the fact that part of cement is being replaced by FA). Contrary, the early age compressive strength of binary systems of OPC and SF is higher than the control mix. The compressive strength results of the ternary cementitious systems of OPC, SF and FA show almost an equivalent values to the control mix.

Direct comparison of the compressive strength values between mixes can be driven if the water/cementitious materials ratio, air content and slump of mixes are constants. However, a comparison of the results in Fig. 5 provides an indication of the individual contributions of the FA and SF in the ternary blend. Using SF increases the strength of concrete at all ages, but it is apparent that much of the increase is realized at early ages and the rate of strength development at later ages is similar for SF concrete and OPC concrete. FA has the opposite effect, contributing little to strength at early ages, but significantly enhancing strength at later ages. The combination of SF and FA results in concrete with improved early age and long-term strength development.

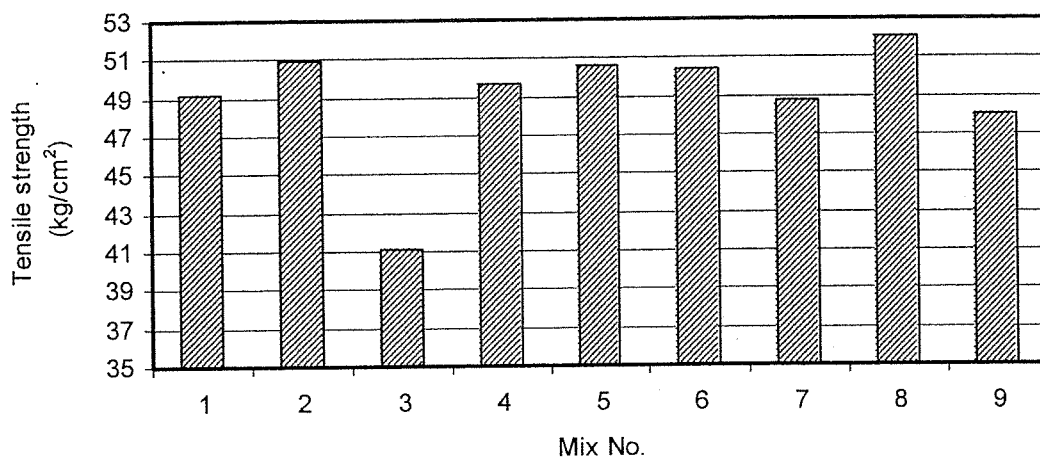


Fig. 6. Tensile Strength of the Studied Concretes.

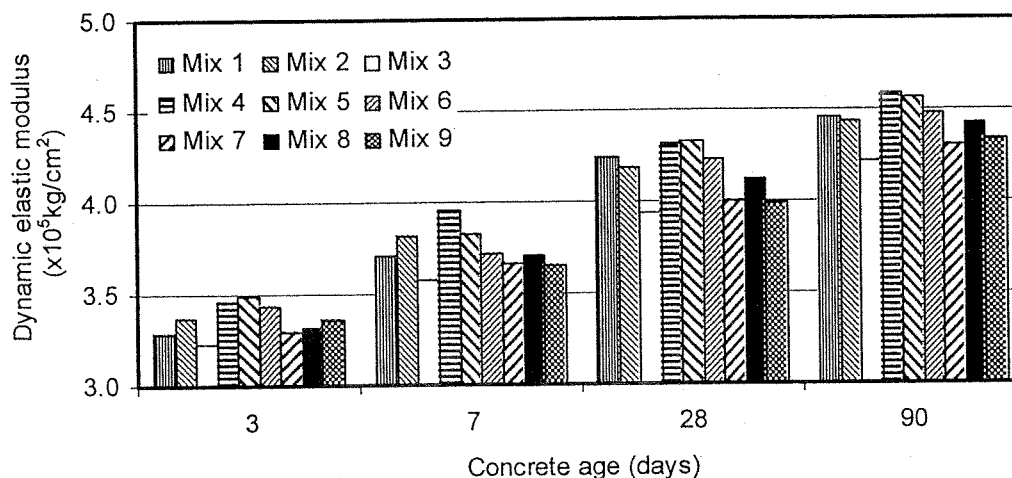


Fig. 7. Dynamic Elastic Modulus of The Studied Concretes.

Results of the tensile strength of tested concrete mixtures after 28 days of curing are listed in Table 6 and represented in Fig. 6. The tensile strength results show approximately the same trend as the compressive strength at 28 days. From data of Table 6, Mix 3 shows the minimum tensile strength due to the effect of using large replacement percent of FA. While, Mix 8 shows the maximum tensile strength due to using the combination of FA and SF with reasonable replacement percents. The results of the tensile strength indicate that the binary and ternary cementitious systems of silica fume mixes show an equivalent tensile strength to the control mix. Tensile strength results reveal that the using of binary and ternary cementitious systems of Portland cement, fly ash and silica fume does not significantly affect the tensile strength of concrete. Approximately similar tensile strength was observed for the control, binary and ternary cementitious systems concrete mixes (except Mix 8 shows higher tensile strength than that of control mix and Mix 3 shows lower tensile strength than that of control mix) as shown in Fig. 6.

It should be noted that the dynamic elastic modulus is different from the Young's modulus (or static elastic modulus) commonly determined by a static unidirectional compression test of a concrete specimen. The dynamic elastic modulus is defined as a linear ratio between the uniaxial stress and the strain of a material at low strain level. Generally speaking, the ratio of dynamic modulus to the static modulus of elasticity is more than 1 and its value varies with the mix proportion of concrete [20]. The obtained test results of dynamic elastic modulus for different concrete mixtures up to age of 90 days are shown in Fig. 7. While, the measured values of static elastic modulus are represented in Fig. 8.

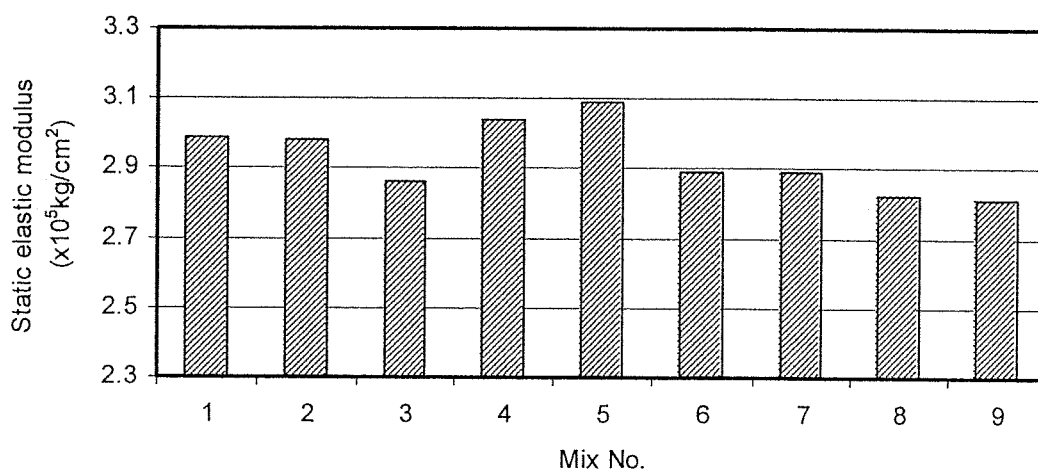


Fig.8. Static Elastic Modulus of the Studied Concretes.

The results of dynamic elastic modulus of tested concrete show approximately the same trend as the compressive strength and it is possible to use this test to compare or check the quality of concrete. The dynamic elastic modulus of tested concrete indicate slight differences due to change in the used of combination of the cementitious materials at all ages. Moreover, Fig. 7 shows that the binary or ternary cementitious materials show approximately similar values of dynamic elastic modulus as the control mix except Mix 3 (25% FA) which shows lower values than those of the control mix. The static Young's modulus results of the binary and ternary cementitious systems of Portland cement, fly ash and silica fume mixes are approximately the same as the values of the control mix except Mixes 4 and 5 which show higher static Young's modulus than that of control mix. Moreover, Mix 3 shows lower static Young's modulus than that of control mix as shown in Fig. 8.

CONCLUSIONS

1. More attention must be given to the development of a new types of cements incorporating combination of the cementitious materials in binary and ternary cementitious systems. Results show that ternary cementitious blends of Portland cement, silica fume, and fly ash offer significant advantages over binary blends and plain Portland cement.
2. The combination of silica fume and fly ash is complementary: the silica fume improves the early age performance of concrete with the fly ash continuously refining the properties of the hardened concrete as it matures.
3. Combinations of 5 to 10% silica fume with 15 to 25% fly ash show satisfactory performance in both fresh and hardened concrete. Such combinations produce concrete with generally good properties and offset the problems associated with using fly ash or silica fume when these materials are used individually.

ACKNOWLEDGEMENT

The author is grateful to Prof. Koji Sakai, Department of Safety Systems Construction Engineering, Kagawa University, Japan, for his kind assistance and financial support to prepare this paper. The author would like to acknowledge the corporation of the Civil & Architectural Engineering Department, Shikoku Research Institute, Shikoku electric Power Company, Japan.

REFERENCES

1. Antiohos, S., Maganari, K., Tsimas, S. (2005), "Evaluation of Blends of High and Low Calcium Fly Ashes for Use as Supplementary Cementing Materials", *Cement and Concrete Composites*, Vol. 27, No. 3, pp. 349-356.
2. Mehta, P.K. (2004), "High-Performance, High-Volume Fly Ash Concrete for Sustainable Development", *Proceeding of the International Workshop on Sustainable Development and Concrete Technology*, Beijing, pp.3-14.
3. Wu, Z., Naik, T.R. (2002), "Properties of Concrete Produced from Multicomponent Blended Cements", *Cement and Concrete Research*, Vol. 32, No. 12, pp. 1937– 1942.
4. Naik, T.R., Singh, S.S. (1998), "Fly Ash Generation and Utilization—an Overview", in: A.K. Suri, A.B. Harapanahalli (Eds.), *Recent Trends in Fly Ash Utilization*, SOFEM Publisher, New Delhi, India, , pp. 1 –25.
5. Mehta, P.K (1994), "Mineral Admixtures for Concrete—an Overview of Recent Developments", in: M.W. Grutzeck, S.L. Sarkar (Eds.), *Advances in Cement and Concrete*, ASCE, New York, pp. 243–256.
6. Maltais, Y.M., Marchand, J. (1997), "Influence of Curing Temperature on Cement Hydration and Mechanical Strength Development of Fly Ash Mortars", *Cement and Concrete Research*, Vol. 27, No. 7, pp. 365– 1377.
7. Davidovits, J., (1994) "High-Alkali Cements for 21st Century Concretes", in: P.K. Mehta (Ed.), *Concrete Technology—Past, Present, and Future*, vol. SP-144, ACI, Farmington Hills, MI, pp. 385– 397.
8. Poon, C.S., Kou, S.C., Lam, L., Lin, Z.S., "Activation of Fly Ash/Cement Systems Using Calcium Sulfate Anhydrite (CaSO₄)", *Cement and Concrete Research*, Vol. 31, No. 6, 2001, pp. 873–881.
9. Mittal, P.K., Kumar, K., "Experience in Separate Grinding Systems for Blended Cement", *World Cement*, Palladian Publishing, Farnham, UK, 1996, pp. 42–44.
10. Osback, B., Smith, F.L. (1981), "Effect of Grinding on Properties of Fly Ash Cements", *Proceedings of Materials Research Society Annual Meeting*, MRS, Boston, MA, , pp. 281– 288.
11. Naik,T.R., Ramme, B. W. (1987), "Low Cement Content High Strength Concrete", *Cement and Concrete Research*, Vol. 17, No. 3, pp. 283– 294.

12. Malhotra, V.M. (1992), "CANMET Investigations Dealing with High-Volume Fly Ash Concrete", in: V.M. Malhotra (Ed.), *Advances in Concrete Technology*, CANMET, Ottawa, Canada, pp. 433–471.
13. Uchikawa, H., Okamura, T. (1993), "Binary and Ternary Components Blended Cement", in: S.L. Sarkar (Ed.), *Mineral Additives in Cement and Concrete*, ABI Books Private, New Delhi, India, pp. 1 – 79.
14. E.E. Berry, E.E. (1980), "Strength Development of Some Blended Cement Mortars", *Cement and Concrete Research*, Vol. 10, No. 1, pp.1 – 11.
15. Nehdi, M. (2001), "Ternary and Quaternary Cements for Sustainable Development", *Concrete International*, Vol. 23, No. 4, pp. 35–42.
16. Popovics, S. (1993), "Portland Cement –Fly-Ash –Silica –Fume System in Concrete", *Advanced Cement Based Material*, Vol. 1, No. 2, pp. 83– 91.
17. Regourd, M., Mortureux, B., Hornain, H. (1983), "Use of Condensed Silica Fume as Filler in Blended Cement", in: V.M. Malhotra (Ed.), *Proceedings of First CANMET/ACI International Conference on Use of Fly Ash, Silica Fume, Slag and Other Mineral By-Products in Concrete*, Montebello, Canada, vol. SP-79, ACI, Farmington Hills, MI, pp. 847– 865.
18. Thomas, M.D.A., Shehata, M.H., Shashiprakash, S.G., Hopkins, D.S., Cail, K. (1999), "Use of Ternary Cementitious Systems Containing Silica Fume and Fly ash in Concrete", *Cement and Concrete Research*, Vol. 29, No. 8, pp. 1207 – 1214.
19. Lane, D.S., Ozyildirim, C. (1999), "Combinations of Pozzolans and Ground, Granulated, Blast Furnace Slag for Durable Hydraulic Cement Concrete", Final Report, Virginia Department of Transportation, University of Virginia, Charlottesville, Virginia, Aug., VTRC 00-R1.
20. Lin, Y., Lai, C., and Yen, T. (2003), "Prediction of Ultrasonic Pulse Velocity (UPV) in Concrete", *ACI Materials Journal*, Vol. 100, No. 11, pp. 21-28.

EVALUATION OF CONCRETE PROPERTIES BY USING DEMOLISHED AGGREGATES

ZEINAB SALAH ELL DIN HOUSSEEN

Researcher at the Housing and Building National Research Center

ABSTRACT

It is an economic concept to get rid of any demolished type by using in constructions, so, in Egypt; there are many activities in the field of recycled aggregate for using in different ways. This study aims to identify the properties for concrete of demolished aggregates as coarse and fine aggregates. Local aggregates such as siliceous, limestone, basalt as coarse aggregates and siliceous sand as fine aggregate and air cooled slag (course and fine) were used to study their physical and mechanical properties. In addition, concrete mixes of the used aggregates were prepared to investigate the effect of using demolished aggregates with every type of the local aggregates separately at the percentages (25, 50, 75) %. Concrete mixes properties were investigated for fresh and hardened states. Those properties were slump, and density in fresh state, compressive, flexural, tensile strengths, and drying shrinkage in hardened state.

Key words: Demolished aggregates, natural aggregates, recycled concrete, compressive, flexural, tensile strengths, drying shrinkage.

INTRODUCTION

There are many activities in the field of demolished aggregates ,in February 2002 there was a conference to show the importance of the of the demolished aggregates in concrete works for both roads and building⁽¹⁾. In France ,concrete made of demolished aggregates has been studied for about 10 years⁽²⁾. In Germany ,there are many projects in the field of demolished aggregates. In Copenhagen, reconstruction of run way was made with demolished aggregates⁽³⁾. In Vienna, a good case for recycling since large quantities of a well defined materials are available, recycling of concrete is also a practice already well established⁽⁴⁾. In Japan the main concept about recycling is to raise the strength of concrete that produced in the near future is directly connected with circulating reuse of demolition concrete as aggregate resources by raising the compressive strength to be higher than those concrete of traditional one⁽⁵⁾. In England ,using of reuse demolition materials in the recommendation of civil engineering works⁽⁶⁾. In the United States and the European countries the recycled aggregates from old concrete paving has been used as materials for pavement⁽⁷⁾. A study was made to investigate the applicability of recycled aggregates as concrete aggregates for paving concrete or lean concrete base course. The strengths, fatigue, flexural strength, drying shrinkage, and freezing-thawing of concrete made with recycled aggregates were investigated. Some properties of fresh and hardened high fly ash lean concrete made with recycled reconstruction⁽⁸⁾ of roadways.

EXPERIMENTAL DETAILS

Materials

Cement

Ordinary Portland cement was used and its properties are within the E. S.S

Aggregate

Five different types of local aggregates types were used in this study (siliceous aggregate, basalt lime stone as natural types, demolished aggregates a (coarse and fine) and, air cooled slag(coarse and fine) as artificial one.

The Demolished Aggregates

were crushed by jaw crusher and screened to divide into coarse and fine adjusted to 25 mm, then the crushed original aggregate were screened and classified according the particle size into coarse and fine aggregates. The coarse aggregates are above sieve 4.67 mm and the fine aggregate particle passed sieve 4.67mm.

Physical Properties

Main physical properties of various types of the used aggregates are shown in Table(1).

Finesse modulus

Demolished coarse aggregates showed the highest values than the other aggregate types .

Specific gravity

Specific gravity in dry condition of demolished aggregates is (2.7) g/cm³ these value was the highest value comparing with the others.

Absorption

Absorption of demolished aggregates is the largest value(3.25%) comparing with the others.

Void ratio

The value for the demolished aggregates is the smallest value 25% comparing with the others.

Unit weight

Value for the demolished aggregates is the smallest value (1.5) kg/cm³ comparing with the others.

Mechanical Properties

Main mechanical properties of various types of the used aggregates are shown in Table (2).

Abrasion

value for the demolished aggregates are higher (21%),so it is harder than the natural aggregate but the best aggregate type is air cooled slag (artificial aggregates) has value(15.5%) .So,it is the hardest one.

Crushing

Value for the demolished aggregates is 23% and higher than the air cooled slag abrasion value (16) % .So, it is the hardest one (air cooled slag).

Impact

Value for the demolished aggregates is 18% and higher than the air cooled slag aggregate impact value (11%).So, it is the hardest one(air cooled slag).

MIXING, CASTING, CURING AND TESTING.

The examination items as specimen and curing method were shown in table (3). Concrete mixes The mixes proportions of concretes are shown in Table (4) are designed according to ACI(1) . Slump, and wet density, tests were according to ACI Specification as fresh tests for concrete. Table (5) illustrates the results of the mechanical properties for hardened concrete compressive, tensile, flexural strengths and drying shrinkage was tested for hardened concrete according to

ASTM. Specimens were demoulded about 24 hrs .after casting and were cured in water for 28 days until the date of test. .All specimens were tested at 3, 7, and28 days.

Table 1: Physical Properties of the Used Aggregates

Type of Aggregate	Specific gravity	Absorption (%)	Silt & Clay (%)	Unit Weight (t/m ³)	
Siliceous + Sand	2.56	0.80	1.60	1.70	32
Air cooled slag	2.74	1.0	0.0	1.9	28
Basalt + Sand	2.56	2.10	0.32	1.76	32
Crushed concrete	2.74	3.25	0.30	1.50	25
Limestone	2.60	3.20	1.00	1.60	28

Table 2: Mechanical Properties of the used Aggregate

Type of Aggregate	Abrasion (%)	Crushing (%)	Impact
Siliceous + Sand	25	18.80	10.30
Air cooled slag	15.5	16.0	11.0
Basalt + Sand	22	18	19
Crushed concrete	21	23	18
Limestone	26	29	11.60

Table3: Examination Items, Specimens and Curing Method

Items		Shape and size	Curing method
Strength	Compression	Cylinder 15x30cm	Cured in water through all ages
	Tensile	Cylinder 15x30cm	
	Flexural	10×10× Prisms 70 cm	
Shrinkage		Prisms7x7x28	
Modulus of Elasticity		Cylinder 15x30cm	

Table 4: Concrete Mixes Proportions

Type of Concrete	Mix Prop.	Aggregate		Cement (Kg)	W/C	Wet Density (Kg/m ³)
		C.A. (Kg)	F.A (Kg)			
Siliceous + Sand		1300	700	350	0.40	2350
Air cold slag		1350	730	350	0.42	2500
Basalt + Sand		1400	700	350	0.45	2400
Crushed concrete		1280	685	350	0.55	2300
Limestone		1250	700	350	0.50	2450

Type of concrete Mixes

17 concrete mixes were casted .In addition every test result for any sample was the average of three specimens , therefore every mix had 27 prisms for testing compressive ,tensile strengths, and10x10x70 for testing flexural strength, at ages 3,7 and 28 days, and three prisms for testing drying shrinkage7x7x28.

Table (4) summaries the concrete mixes proportions. The basic aggregate type was recycled aggregate, it used at the percentages 25, 50, 75%. With all aggregate types separately So, the concrete mixes were divided into four series according to the aggregate type. Series (I)consists of recycled aggregate replacement by siliceous aggregate at 25,50 and 75%.Series(II) consists of demolished aggregates replacement by air cooled slag aggregates(coarse+fine) at 25,50 and 75%.. Series (III) consists of demolished aggregate replacement by basaltl aggregates at 25, 50 and 75%. Series (IV) consists of demolished aggregate replacement by limestone aggregates at 25, 50 and 75%.

Properties of fresh concrete

Slump: it ranged from 5-7cm for all concrete mixes. Fresh Density of the demolished concrete was less than for the natural one. In addition, It gradually decreased as the replacement ratio by demolished increased with traditional aggregates at the percentages 25, 50 and 75%.

Properties of hardened concrete

Table (5) shows the test results of mechanical properties of reference concrete mixes and table (6) shows the test results of mechanical properties of concrete mixes(aggregate mixes), after 3,7,28. In Fig 1 shows the development of compressive, tensile and flexural for series (I). Fig. (2) shows the development of compressive, flexural and tensile for series II. Fig. (3) shows the development of compressive, flexural and tensile for series III Fig. (4)shows the development of compressive, flexural and tensile for series III,figs. (5,6,7 and 8) show the development of shrinkage for concrete mixes of series I, II, III and IV.

Table 5: Mechanical Properties of Reference Hardened Concrete

Tests Age (days) Type of Concrete	Compressive strength(Kg/cm ²)			Tensile strength (Kg/cm ²)			Flexural strength (Kg/cm ²)		
	3	7	28	3	7	28	3	7	28
Siliceous + Sand	220	250	300	24	28	33	44	50	60
Air cooeld slag	260	370	400	29	41	44	52	74	80
Basalt + Sand	180	210	280	20	23	31	36	42	56
Crushed concrete	200	225	270	22	25	30	42	45	54
Limestone	210	260	290	23	29	32	40	48	58

Compressive strength.

Using 25% recycle aggregate and 75% air cooled slag aggregate, the compressive strength reached 368.kg/ cm² after 28 days water curing. In addition, that mix is the highest compressive strength and is the most economic one in series II. In series III the best mix is 25% recycled aggregate and 75% basaltic .aggregates, it gives 278 kg/ cm²compressive strength after 28 days water curing. In series IV the best mix is 25% recycled aggregate and 75% limestone aggregates, it gives 285 kg/cm² compressive strength after 28 days water curing.

Table 6: Test Results of Mechanical Properties for Concrete Mixes

Concrete Type		Compressive Strength			Flexural Strength			Tensile Strength		
		3	7	28	3	7	28	3	7	28
S1		220	250	300	44	50	60	24	28	33
D1		200	225	270	40	45	54	22	25	30
75%D1+25%S1		213	231	278	41	46	56	22.5	26	30
50%D1+50%S1		210	238	335	42	46.5	59	23	26.5	30
25%D1+75%S1		215	243	293	43	48	59	23.5	27	31
A1		260	370	400	52	74	80	29	41	44
D1		200	225	270	40	45	54	22	25	30
75%D1+25%A1		215	261	303	43	52	61	22.5	29	34
50%D1+50%A1		230	298	339	46	60	67	21.5	33	36
25%D1+75%A1		245	334	368	49	67	74	23.5	36	41
B1		180	210	280	39	42	56	20	23	31
D1		200	225	270	40	45	54	22	25	30
75%D1+25%B1		195	222	273	43	45	55	21.5	25	31
50%D1+50%B1		190	217	275	38	44	55	21	23	30
25%D1+75%B1		185	214	278	37	43	56	20.5	24	29
L1		210	260	290	42	52	58	23	29	32
D1		200	225	270	40	45	54	22	25	30
75%D1+25%L1		203	234	275	41	47	55	22.25	27	31
50%D1+50%L1		205	240	280	41	48	56	22.2	27	32
25%D1+75%L1		208	256	285	42	50	57	21	29	33

Tensile strength

Using 50% recycled aggregates and 50% siliceous aggregates in concrete mixes gave a tensile strength 31 kg/cm² after 28 days water curing. Using 25% demolished aggregate and 75% air cooled slag aggregate, the tensile strength reached 41 kg/cm² after 28 days water curing. In addition, that mix is the highest tensile strength and is the most economic one in series II. In series III the best mix is 25% demolished aggregate and 75% basaltic aggregates, it gives 31 kg/cm² tensile strength after 28 days water curing. In series IV the best mix is 25% demolished aggregate and 75% limestone aggregates, it gives 33 kg/cm² tensile strength after 28 days water curing.

Flexural strength

Using 50% demolished aggregates and 50% siliceous aggregates in concrete mixes gave a flexural strength 59 kg/cm². Using 25% siliceous aggregates with 75% demolished aggregates after 28 days water curing. So, it is economical to use 50% recycled with 50% siliceous aggregates in concrete mixes. Using 25% demolished aggregate and 75% air cooled slag aggregate, the flexural strength reached 74 kg/cm² after 28 days water curing. In addition, that mix is the highest flexural strength and is the most economic one in series II. In series III the best mix is 25% demolished aggregate and 75% basaltic aggregates, it gives 56 kg/cm² flexural strength after 28 days water curing. In series IV the best mix is 25% demolished aggregate and 75% limestone aggregates, it gives 57 kg/cm² flexural strength after 28 days water curing.

Shrinkage

Using 25% recycle aggregate and 75% air cooled slag aggregate, the drying shrinkage reached 5.25×10^{-4} after 28 days water curing. In series II. In series III the best mix is 25% recycled aggregate and 75% basaltic aggregates, it gives 4.75×10^{-4} drying shrinkage after 28 days

water curing In series IV the best mix is 25% recycled aggregate and 75% limestone aggregates, it gives 5.25×10^{-4} drying shrinkage after 28 days water curing.

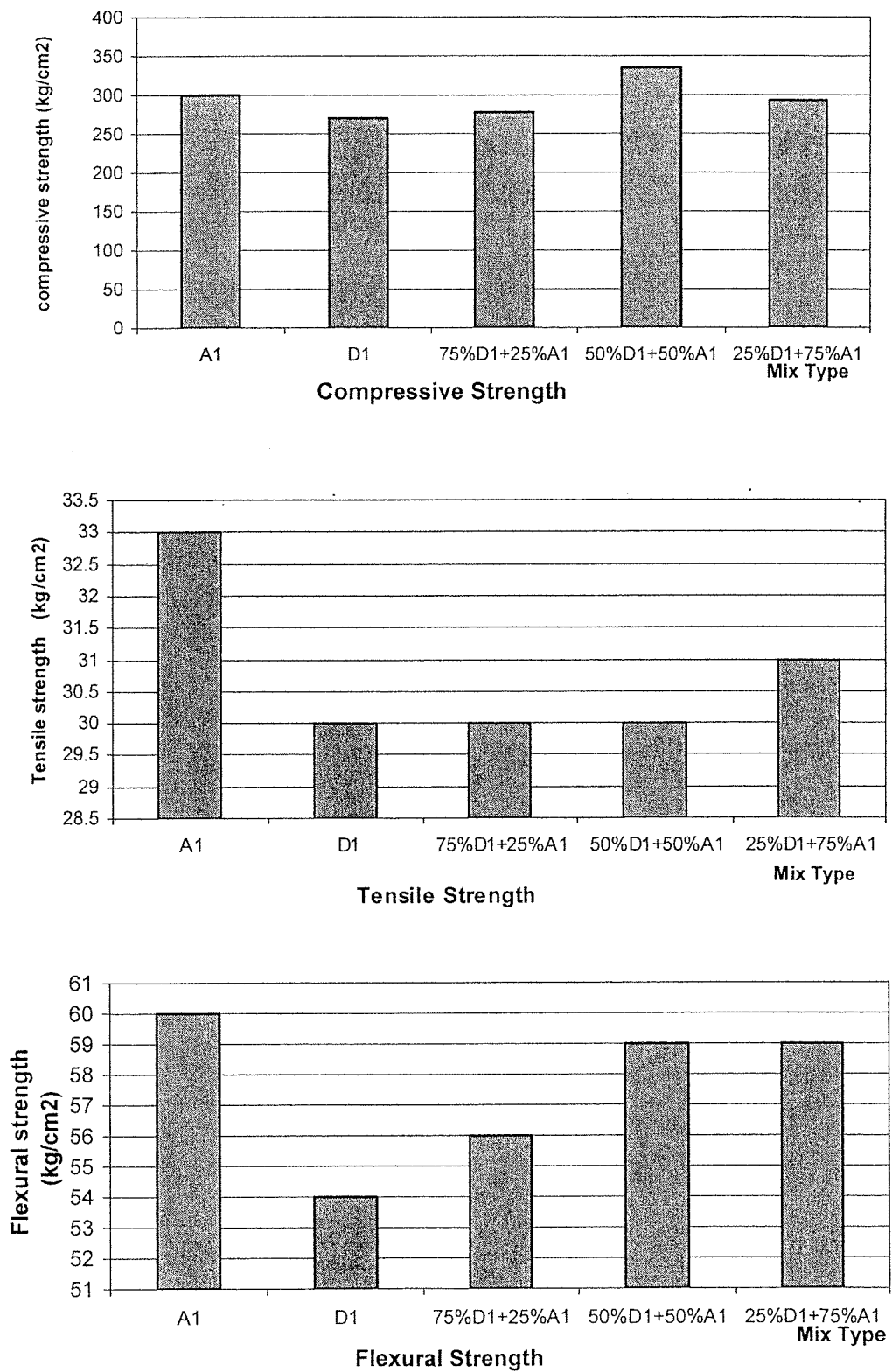


Fig. 1: Mechanical properties for concrete series I

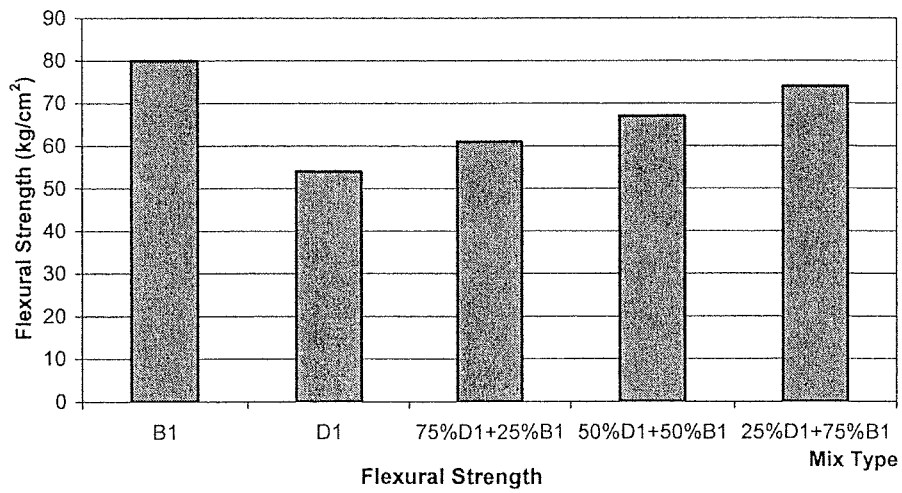
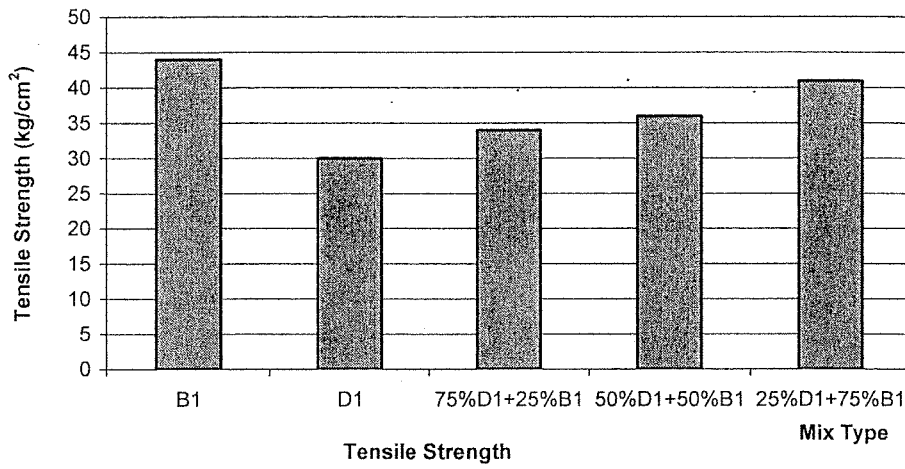
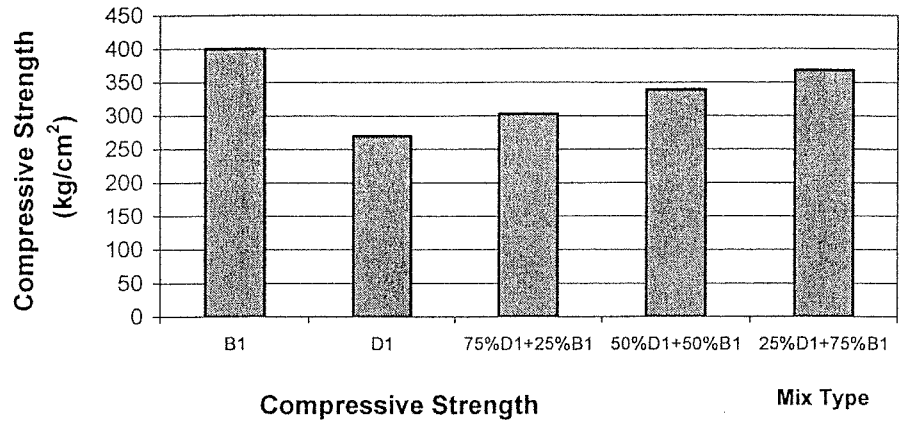


Fig. 2: Mechanical properties for concrete series II

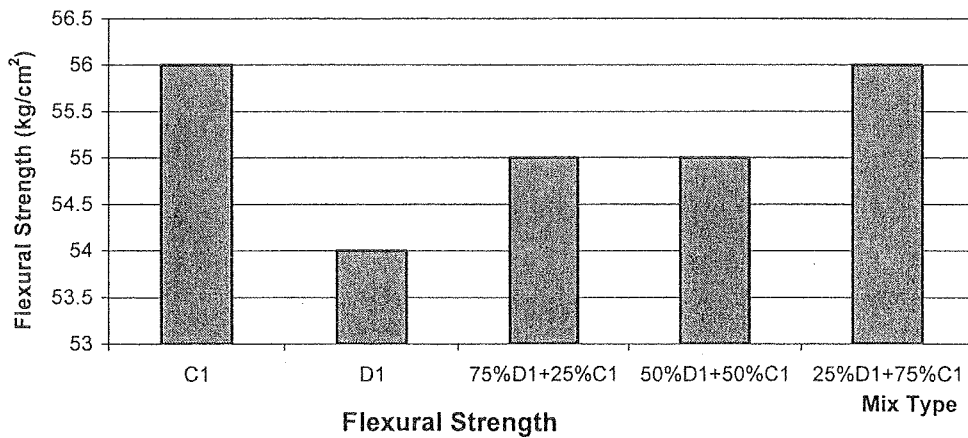
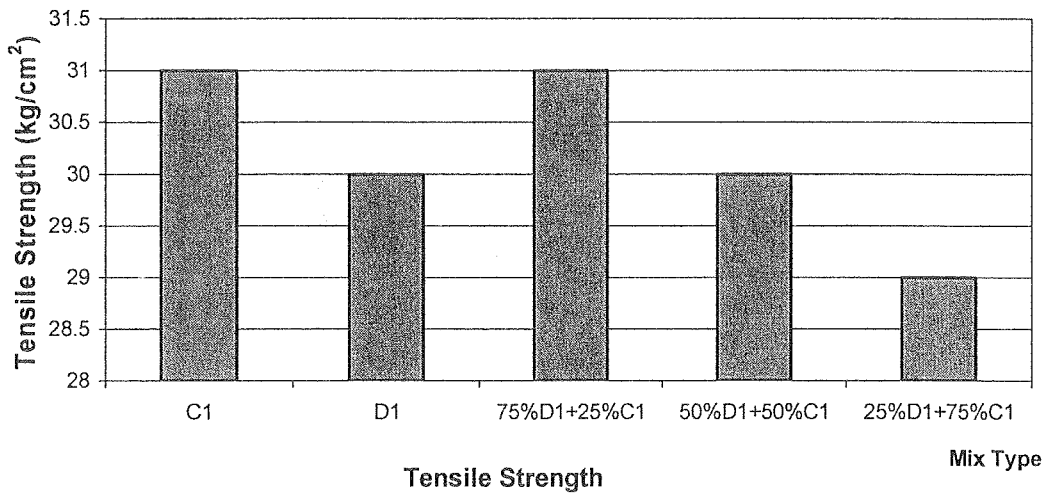
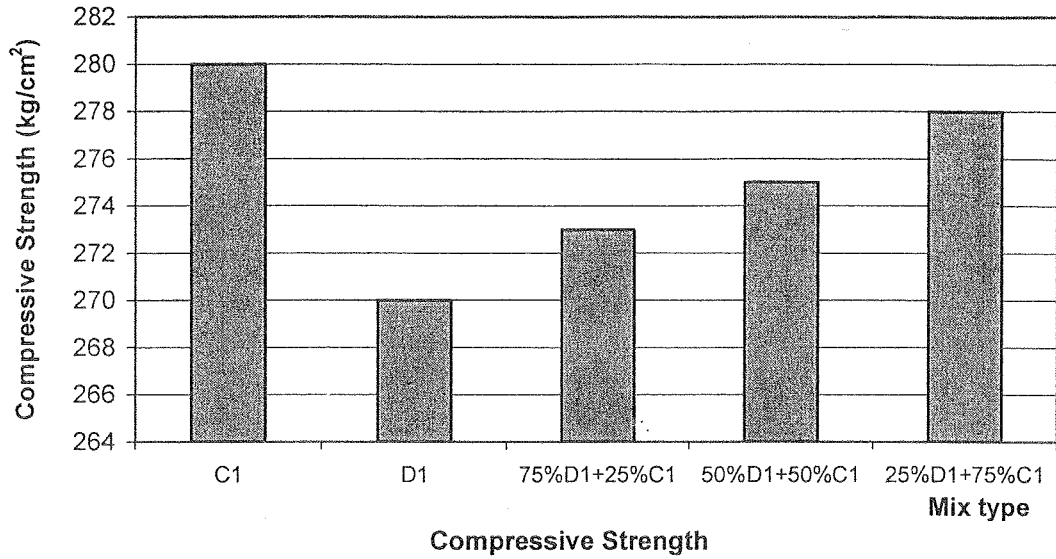


Fig. 3: Mechanical properties for concrete series III

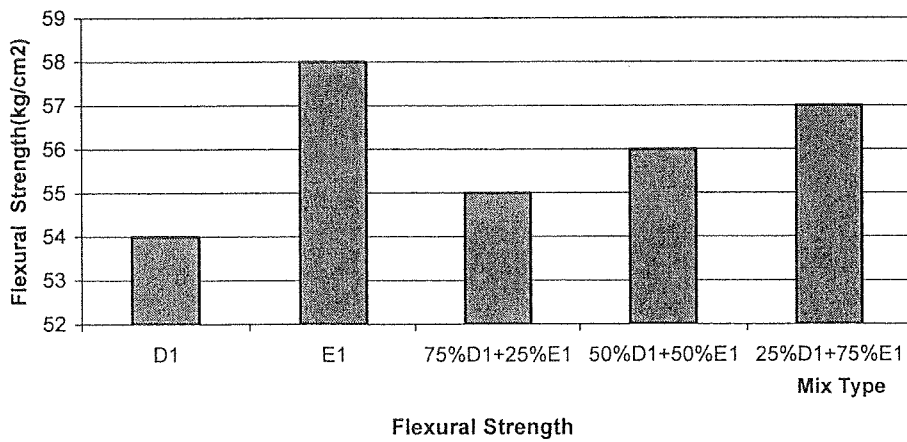
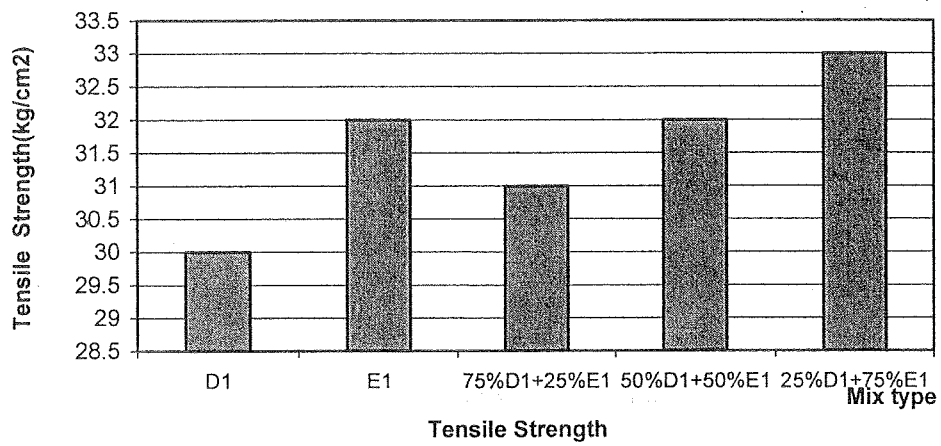
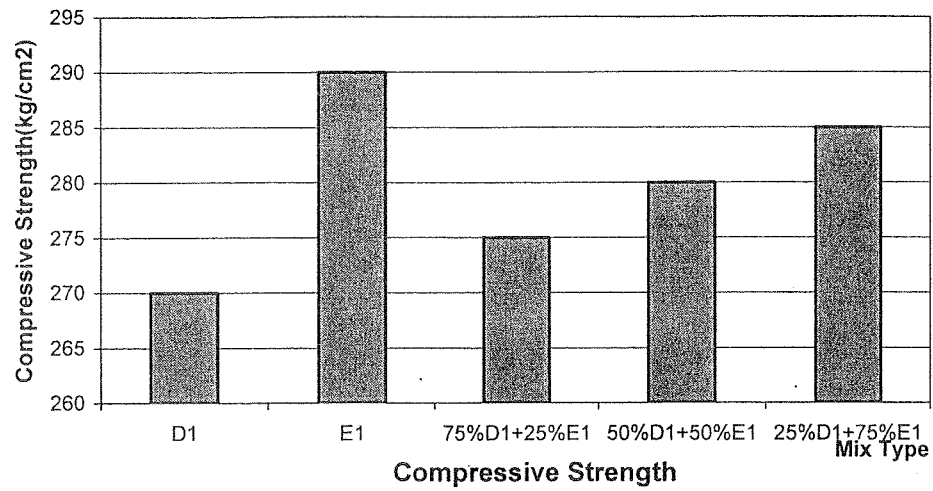


Fig. 4: Mechanical properties for concrete series IV

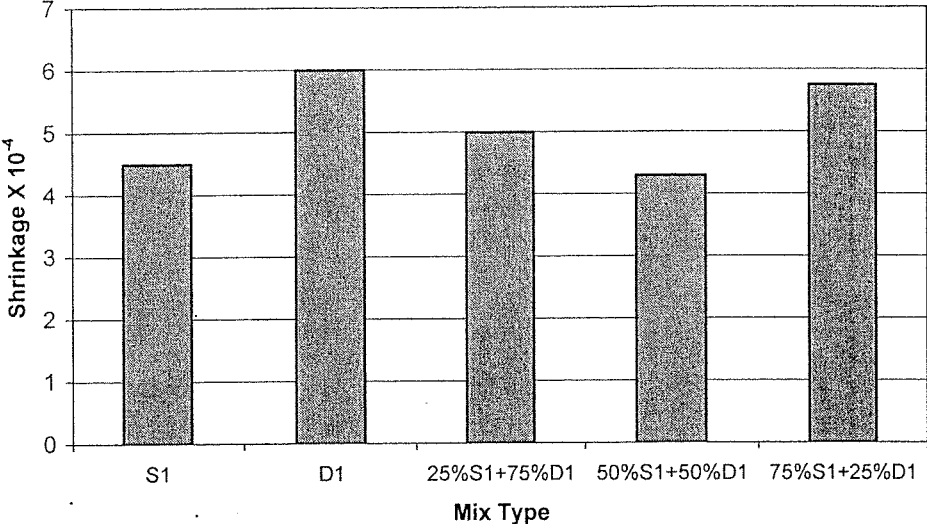


Fig. 5: Shrinkage for concrete series I

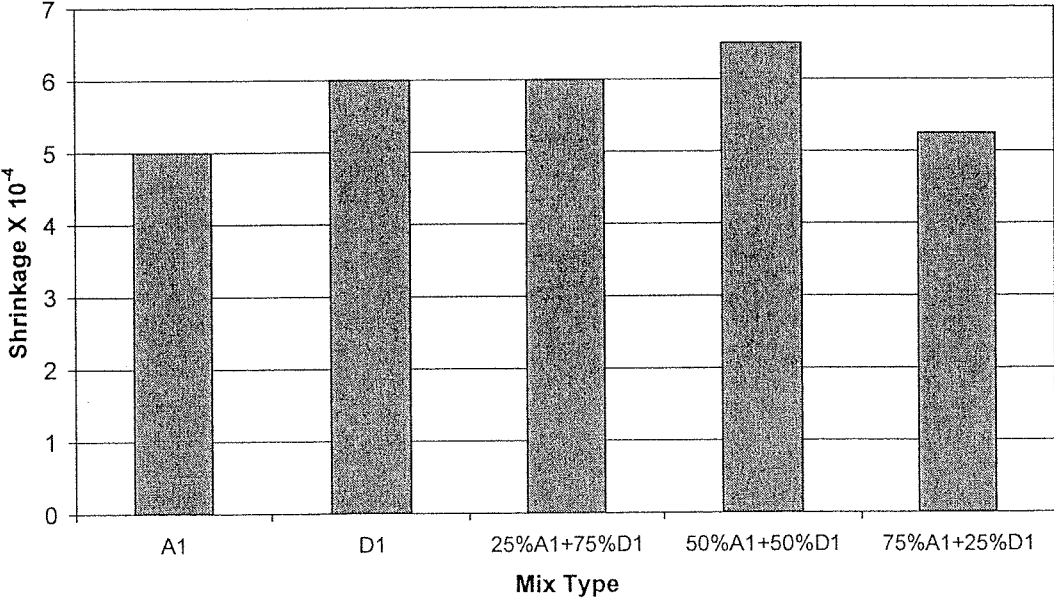


Fig. 6: Shrinkage for concrete series II

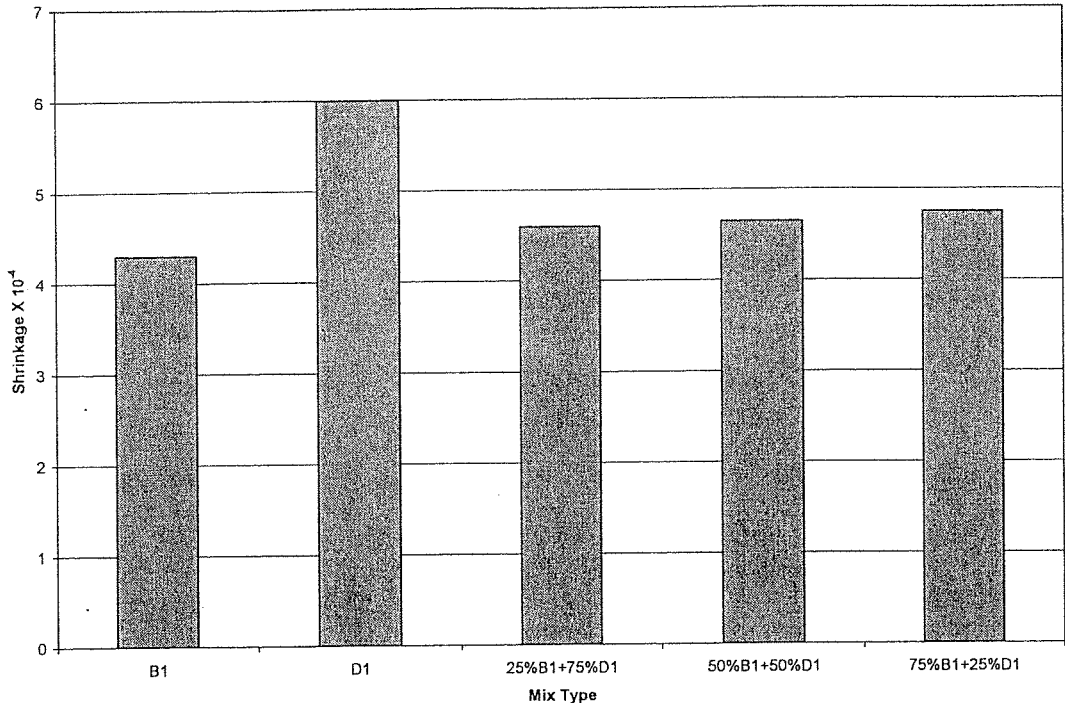


Fig. 7: Shrinkage for concrete series III

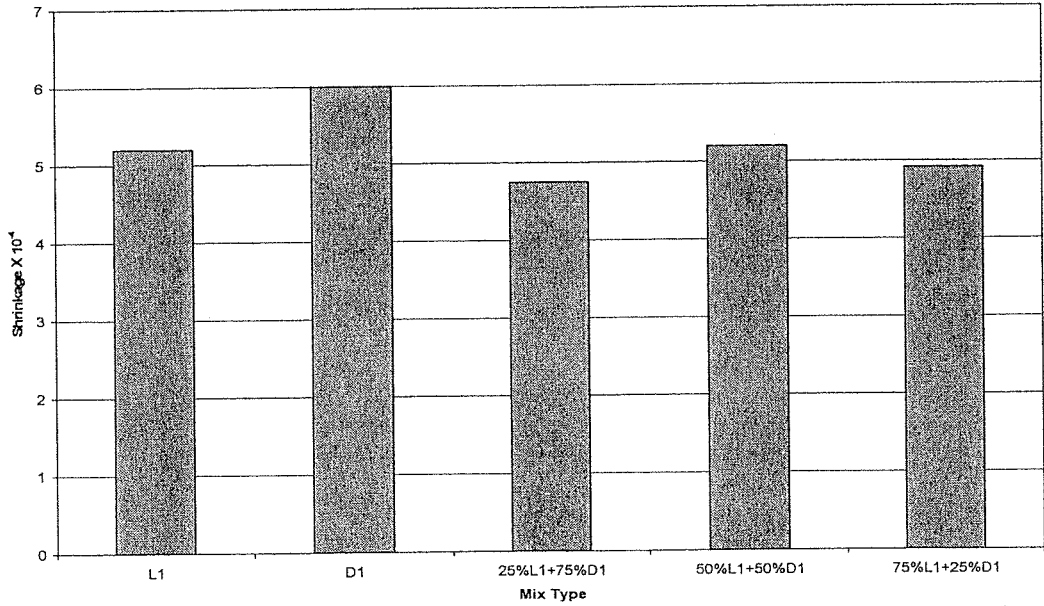


Fig. 8: Shrinkage for concrete series IV

CONCLUSION

The main conclusions from the present investigation on recycled aggregate and recycled concrete are summarized as follows:

1. Recycled aggregate have relatively higher fineness modulus than the other one.
2. High percentage absorption value is observed for the recycled aggregate comparing with the other aggregates.
3. Workability of recycled aggregate concrete is quite as all mixes but it enhance with increase in replacement ratio
4. Up to 50% of siliceous, basalt and lime stone are replaced with recycled aggregate concrete without seriously affecting the properties of concrete, both in fresh and the hardened states.
5. The values obtained for the mechanical properties of recycled aggregate concrete are lower than for natural aggregate ones. In addition their drying shrinkage is higher than for natural aggregate concretes.
6. The replacement ratio with recycled aggregate influenced on compressive, tensile and flexural strengths and on the drying shrinkage
7. Using air cooled slag aggregate (by product) as it is or using it replacing with recycled aggregate at 25, 50 and 75 % gave high result for compressive, tensile and flexural strengths.

REFERENCES

1. Mukai,Kikuchi (1988), "Properties of Reinforced Concrete Beam Containing Recycled Aggregate" Proceeding of Second International Symposium held by REILM., vol.2pp.670-679.
2. J.d MERLET and P.PIMIANTA (1999), "Mechanical Physico –Chemical Properties of Concrete Produced with Coarse and Fine Aggregates'CSTB,Paris ,France
3. Christian Busch (2000) " Crushed Concrete Used as Basecourse Material on Runway 04 R-22L.AT COPENHAGEN AIRPORT"Airport and Pavement Department ,Cowiconsult.
4. H. sommer (1998), "Recycling of Concrete for the Construction of the Concrete Pavement on the VIENNA –SALZBURG Motorway"Zementindustrie,VIENNA,AUSTRIS.
5. M.kikchi and Ayasunaga (2003), "The Total Evaluation of Recycled Aggregate and Recycled Concrete"Department of Architecture,Meiji University,Japan.
6. M. BAUCHARD (2001), "The Use in Road of Aggregate Made from Demolish Materials "Laboratories Regional de L Est Parisien ,le Bourget _France.
7. M.Kaeamura & K.torii (2000), " Reuse of Recycled Concrete Aggregate for Pavement "Department of Civil EngineeringKansawa University.
8. Ahmad, S.H.; Fisher, D.G.; Sackett, K.W. (1994), (1996), "Properties of concrete made with north carolina recycled coarse and fine aggregates". Final report.
9. Judy, S., (2002) "Recycling 1-70",The Journal of Mid West Contractor,June 1999,pp.8-13,Associated Construction Puplication

RECYCLING OF CEMENT KILN DUST AND WATERGLASS SLUDGE IN THE MANUFACTURE OF ACID RESISTANT MASONRY UNITS

Medhat S. El-Mahllawy and Tarek M. El-Sokkary

Housing and Building National Research Center, Cairo, Egypt

E-mail: medhatt225@yahoo.com

ABSTRACT

The objective of the reported paper is to study recycling of some Egyptian wastes with a clay raw material in the manufacture of acid resistant masonry units. These include acid resisting bricks for using in the sewage canals and tanks lining as well as in structures requiring low absorption and high resistance to chemical action. This is a dual target for economic benefit and environmental pollution protection. Accordingly, four batches composed of Kafr Homeid clay (KHC) and wastes of cement kiln dust (CKD) and waterglass sludge (WGS) were suggested for this investigation. Articles from each batch composition were prepared by pressing then firing them at temperatures ranging from 1075°C to 1150°C at 5°/m (firing rate) and 4 hours (soaking time). The CKD and WGS wastes were added in different percentages ranging from 25-40% and 10-25%, respectively. To assess the product properties the testing methods outlined in the ESS 41:1986 and ASTM C32-93 (2000) standards were applied. Consequently, the suitable mixtures design that fulfill these specifications were selected, taking into consideration the industrial economy and environmental protection factors. It was found that the most applicable articles which achieve the applied specifications were prepared from batch T3 after firing at 1125°C having 50% clay, 30% CKD and 20% WGS. Also, batch T3 successfully achieved comparable properties of water absorption, weight loss due to acid attack and compressive strength and deserve to be the most applicable and superior one from the industrial point of view.

INTRODUCTION

In Egypt, large quantities of industrial by-products are annually produced by various industries. The main goals of environmental protection organizations are to seek ways to minimize the dual problems of disposal and health hazards of these by-products. Waterglass sludge (WGS) and cement kiln dust (CKD) are examples for these by-products. Such wastes cause environmental and health impacts. The waste waterglass sludge has still limited useful applications. The most recent studies have been carried out for this purpose are Chanda et al. (1998), El Shafai (2000), Puertas et al. (2004), Palacios and Puertas (2005). The very fine cement kiln dust is produced by cement industry and emitted for several distances depending on its density and atmospheric events. Furthermore, the amount of CKD discards daily by cement factories in Egypt is estimated to be in the range of 200 to 300 tons (HCT, 1999) collected from exhausted gases of the cement kiln. It was found that due to its high alkalis content, it could not be recycled in the cement manufacture. Several studies have been reported on the possibility of reuse CKD in different industries. The most recent ones have been investigated by Elwan et al. (1999), Shoaib et al. (2000), Youssef (2002), Al-Harthy et al. (2003), El-Sherbiny et al. (2004), Al-Jabri et al. (2005) and others.

The production of the acid resisting bricks in large quantities is a demand due to the vast expansion of sewage systems in the new cities in Egypt. Both of the WGS and CKD wastes were not assessed before in manufacturing acid-resistant masonry units. Therefore, the aim of this work is to study the possibility of their application as additives in clay-based batches for producing acid-resisting bricks. This will lead to environmental protection as well as production cost reduction of these bricks.

MATERIALS AND METHODS

Materials

The materials used in this study are Kafr Homeid clay (KHC), waterglass sludge (WGS) and cement kiln dust (CKD). The KHC was previously obtained from Kafr Homeid clay deposits (Kafr Homeid area, Giza governorate). These deposits attain a thickness of about 40m as demonstrated in the geological section of Figure (1). The studied bed is mainly composed of grayish, compact and salty claystone. The waterglass sludge (WGS) was taken from the Egyptian Salt and Soda Company (Kafr El-Zayat city). Whereas, the cement kiln dust was supplied by Tora Cement Company (south of Cairo city).

The texture and nomenclature of KHC sample were described after determining their particle size distribution applying sieving and sedimentation processes (ASTM D422-63) as well as the adoption of Picard's method (1971) for graphical representation.

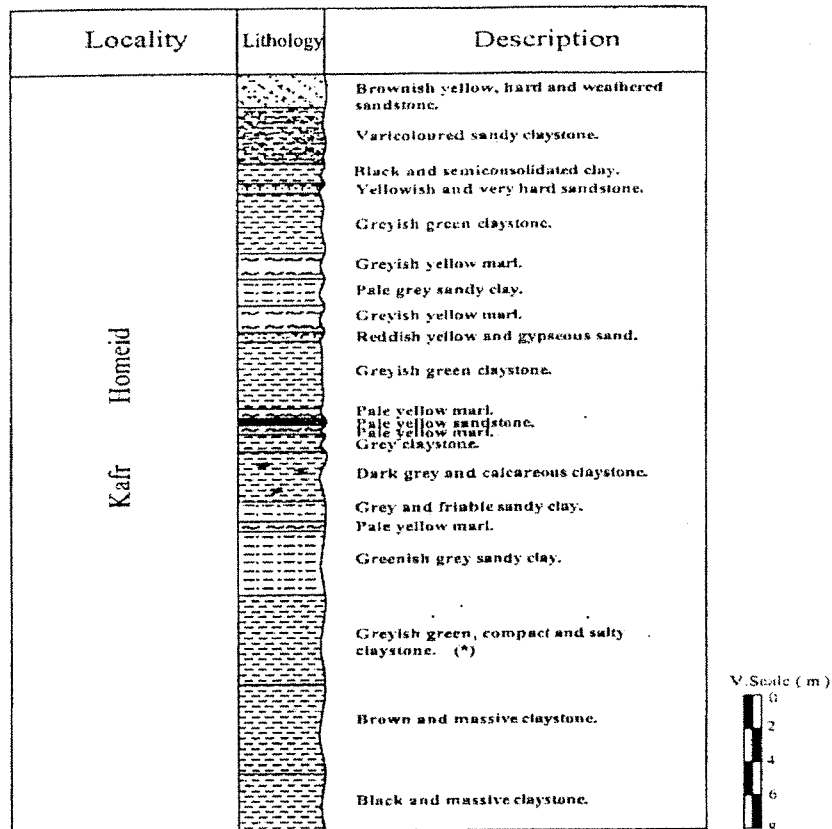
Methods

The chemical composition of the studied materials was determined by using a computerized X-ray fluorescence (Phillips, PW 1400 Spectrometer, Holland). The mineralogical composition was qualitatively identified by using X-ray diffraction technique (Phillips, PW 1373 Vertical Diffractometer, Holland) at 40 kV and 40mA using Cu K α radiation. The identification of minerals was achieved by MPDF (1998). Furthermore, the mineralogical and dehydration information of the studied clay sample were gained through differential thermal (DTA) and thermo-gravimetric (TGA) analyses by using the thermal analyzer: DT 50 (Schimadzu Co., Kyoto, Japan).

Batch Design and Article Preparation

Four batches, referred to as T1, T2, T3 & T4, were designed and prepared for this study. These batches are based on 50 weight % of KHC as well as addition of 10 up to 25% WGS at the expense of CKD, which gradually decreases from 40% in T1 to 25% in T4 as illustrated in Table 1. KHC and WGS materials were crushed, separately ground in a laboratory ball mill and screened to pass 90 μ m sieve. CKD is too fine and doesn't need more grinding.

The prepared batches were moulded into cubic articles of 5cm-side length by semi-dry pressing method under 225 kg/cm². Mixing of these mixtures was performed on dry basis and then moistened by spraying 5 wt% water before molding. The pressed articles were fired at temperatures of 1075°, 1100°, 1125° and 1150°C at 5°C/m firing rate and 4 hours soaking time. Physical and mechanical characteristics of the resultant fired articles were determined and assessed according to ESS 41:1986 and ASTM C32-93 (2000). Accordingly, the successful batch designs will be identified for using as acid resisting bricks.



(*) The selected clay deposit

Fig. 1. Geological Columnar Section at Kafr Homeid Site, Giza Governorate

Table 1. Batch Composition of the Four Mixtures

Symbol	Composition (%)		
	Kafr Homeid clay (KHC)	Cement kiln dust (CKD)	Waterglass sludge (WGS)
T1	50	40	10
T2	50	35	15
T3	50	30	20
T4	50	25	25

Table 2. Chemical Composition of the Used Materials on Dry Basis

Oxide content %	Clay sample (KHC)	Cement Kiln Dust (CKD)	Waterglass sludge (WGS)
SiO ₂	51.20	12.10	47.00
Al ₂ O ₃	16.80	3.30	4.08
Fe ₂ O ₃	7.40	2.80	1.07
CaO	0.38	48.50	7.84
MgO	3.71	1.60	1.10
Na ₂ O	2.60	2.50	20.18
K ₂ O	1.11	5.20	nil
SO ₃	0.13	4.80	0.30
Cl ⁻	2.80	4.30	nil
L.O.I	16.70	18.70	17.83

RESULTS AND DISCUSSION

Characteristics of the Starting Materials

Based on the particle size distribution of KHC sample it is considered as well-sorted and very fine claystone type. Also, it includes about 3.20% fine sand (500-63 μ m), 9.20% silt (63-2 μ m) and 87.60% clay (< 2 μ m).

Table 2 summarizes the chemical constitution of KHC as well as CKD and WGS samples. It is evident that KHC is of low-grade type. It contains high SiO₂ and Fe₂O₃ contents with low Al₂O₃ as well as minor MgO, Na₂O, K₂O and CaO in decreasing order of abundance. Also, it contains some SO₃ and high Cl⁻ ion. This is confirmed by the presence of halite (NaCl) mineral, as shown from the XRD patterns of KHC powder sample in Fig. (2). Furthermore, this pattern reflects the occurrence of quartz and feldspar as non-clay minerals. Also, XRD patterns of the untreated, glycolated and heated clay fraction of this sample indicate that it is mainly composed of montmorillonite, kaolinite and illite clay minerals in descending order of abundance. This clay mineral composition is characterized by an intense endothermic peak at 112°C due to the removal of its interlayer water as shown on the DTA curve of KHC sample in Fig. (3). This is followed by a weak endothermic peak at 272°C and intense one as endothermic reaction peak at ~ 515°C. These refer to the dehydration of goethite [FeO(OH)] mineral and to the dehydroxylation of clay minerals (Smykatz-Kloss, 1974). The small S-shaped endothermic-exothermic reaction peaks which take place at 849 and 908 °C are due the complete destruction of the clay mineral structure and its recrystallization. The latter peak is not accompanied by any loss in weight, since it is a structural peak as shown on the TGA curve (Fig.3).

The chemical and mineralogical composition of CKD and WGS waste samples are revealed from their chemical analysis data of Table 2 and XRD patterns of Fig. (4). It is found that CKD is predominately composed of portlandite [Ca(OH)₂] and calcite [CaCO₃] minerals as well as subsidiary minerals; namely, sylvite [KCl], halite [NaCl], quartz [SiO₂] and larnite [Ca₂SiO₄]. Hence, its chemical analysis data show CaO, SiO₂, K₂O, Al₂O₃, Fe₂O₃, Na₂O and MgO in descending order as well as too much contents of SO₃ (4.80%) and Cl⁻ (4.30%). On the other

hand, WGS sample is rich in SiO_2 , Na_2O and CaO with some Al_2O_3 , Fe_2O_3 and MgO . These oxides exist as major quartz [SiO_2] mineral in addition to minor phases of stilbite [$\text{Ca}_2\text{Al}_5\text{Si}_{13}\text{O}_{36}(14\text{H}_2\text{O})$], gonnardite [$\text{CaNa}_4\text{Si}_6\text{Al}_4\text{O}_{20}(7\text{H}_2\text{O})$] and ussingite [$\text{Na}_2\text{AlSi}_3\text{O}_8(\text{OH})$]. Furthermore, as clarified from the chemical composition of the materials used that the fired articles from the different batches may give constituents fall within the ternary phase diagram of SiO_2 - Al_2O_3 - CaO .

Mineralogical Composition of the Fired Articles

It is worthy to note here that T1 articles are densified on firing up to 1150°C , without any changes in their shapes due to partial melting. While, T2 as well as T3 articles are densified up to 1125°C and those of T4 up to only 1100°C . The shape of these articles (T2, T3 & T4) is changed above these temperatures due to their partial melting and over firing. This is mainly attributed to the high content of the alkali Na_2O and K_2O oxides in the fired T1-T4 batches (8.7-10.5%) as demonstrated in Table (3). From this table, it is also evident that with the increase of WGS from T1 to T4 batches at the expense of CKD content, Na_2O content is increased from 5.40 to 8.60% at the expense of K_2O decreasing from 3.30 to 1.90%. Thus, the total Na_2O and K_2O consequently increased from 8.70 to 10.50%. This construe the lowering of the partial melting temperature, i.e vitrification of the fired articles from batch T1 to T4. The intensive fluxing effect of Na_2O and K_2O is also responsible for reducing top temperature maturing (kingery).

Table (3) also illustrates the increase of SiO_2 content from 43.90 (T1) to 49.90% (T4) with simultaneous decrease of the CaO content from 25.50 to 17.70% due to the gradual increase of WGS addition at the cost of CKD from T1 to T4. Accordingly, the molar CaO/SiO_2 ratio, i.e. basicity of these batches is gradually decreased from 0.62 in T1 to 0.38 in T4. Meanwhile, the Al_2O_3 , Fe_2O_3 and MgO contents exist at more or less constant levels of 12.50, 6.00 and 3.20%, respectively. These data indicate that on increasing WGS at the expense of CKD from T1 to T4, gradual decreasing of C/S molar ratio and increasing of total alkali content occur.

Figures (5–8) exhibit the XRD patterns of the articles which didn't suffer from the partial melting and processed from the four bathes (T1 to T4) after firing between 1075° and 1150°C with an interval of 25°C . At 1075°C , all articles show α -wollastonite [CaSiO_3], gehlenite [$\text{Ca}_2\text{Al}_2\text{SiO}_7$], augite [$\text{Ca}(\text{Fe},\text{Mg})\text{Si}_2\text{O}_6$], merwinite [$\text{Ca}_3\text{Mg}(\text{SiO}_4)_2$] and residual of unreacted quartz [SiO_2]. These phases are consistent with the neomineralization of Jordan et al. (2001). On increasing firing temperature up to 1150°C in T1, up to 1125°C in T2 and T3 as well as up to 1100°C in T4, significant increase of the amount of augite, which has lower C/S molar ratio (0.50) occurs with gradual diminishing of the phases having higher C/S ratio; namely gehlenite (2.0), merwinite (1.50) and wollastonite (1.0). The coexistence of these phases together with some unreacted SiO_2 at 1075°C indicates that they are metastable phases formed at unequilibrium conditions (Gonzalez-Garcia et. al, 1990). Moreover, when the temperature increases to 800°C CaCO_3 decomposed to CaO and the latter reacts with quartz as well as Al_2O_3 and SiO_2 of the clay leading to formation wollastonite and metastable gehlenite (Tjerk, 1970). On further increase in temperature, gehlenite and merwinite contents diminish in intensities and augite appears (Jordan et. al, 2001). On rising firing temperature from 1100° to 1150°C with 4 hours soaking time, higher contents of liquid phases is expected to form in such batches containing high contents of alkali oxides and other fluxing oxides; namely, CaO , MgO , Fe_2O_3 . The existence of fluid phases enhances the reaction kinetics and increases the chemical communication between the reacting phases (Riccardi et al., 1999). Hence, this accelerates diffusion of all of the coexisting ions leading, on heating and/or cooling, to crystallize augite as a major phase at the cost of the metastable gehlenite, merwinite, wollastonite and quartz phases. The C/S ratio of augite (0.50) exists as intermediate value between those of the fired batches (0.38-0.62). Therefore, the amount of augite is intensively increased at the expense of gehlenite, merwinite, wollastonite and quartz phases which are greatly diminished on firing up to 1100° - 1150°C .

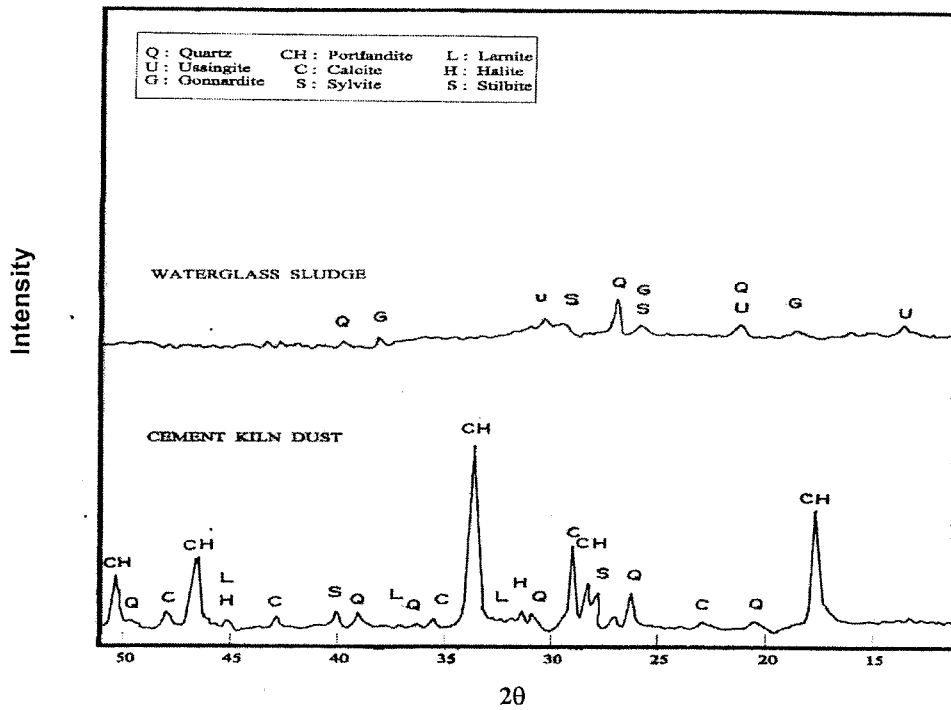


Fig. 4. X-Ray Diffraction Patterns of the Waterglass Sludge (WGS) and Cement Kiln Dust (CKD)

Table 3. Batch as Well as Chemical Composition of the Fired Batches on Calcined Basis

Batch	Batch composition, %			Chemical composition on calcined basis, %							
	KHC	CKD	WGS	SiO ₂	Al ₂ O ₃	Fe ₂ O ₃	CaO	MgO	Na ₂ O	K ₂ O	C/S m.ratio
T1	50	40	10	43.90	12.50	6.20	25.50	3.30	5.40	3.30	0.62
T2	50	35	15	45.90	12.50	6.00	22.90	3.20	6.50	3.00	0.54
T3	50	30	20	47.90	12.70	5.90	20.20	3.20	7.60	2.60	0.45
T4	50	25	25	49.90	12.60	5.80	17.70	3.10	8.60	1.90	0.38

Physical and Mechanical Properties of the Fired Articles

Figure (9) shows the effect of firing temperature on the properties of the fired articles by means of water absorption (WA), compressive strength (CS) and loss in weight (LIW) due to acid attack (%). It is clear that WA and LIW decrease with parallel increase of CS on rising firing temperature. This is mainly attributed to the increase of densification rate by the developed liquid phase. As the firing temperature increases, the liquid phase content is consequently increased leading to gradual closing of open-pore structure of the fired articles. The gradual decrease of open porosity also leads to decreasing the rate of attack on the articles by the absorbed acid with simultaneous increase of their CS (O'Farrel et. al, 2001). Therefore, minimum values of WA and LIW with maximum CS occur in all articles at their maximum firing temperatures. These temperatures are lowered from 1150°C in T1 to 1125°C in T2 & T3 and only 1100°C in T4. This is related to the increase of liquid phase formation from T1 to T4 due to the increase of their content of alkali oxides and other fluxing oxides in this direction. Too large proportion of fluxes, in the fired body, is one of the primary causes of increasing the fusibility and premature failure of some bricks at lower temperatures (Doremus, 2003).

Table 4 summarizes the minimum WA and LIW as well as maximum CS values obtained for the selected articles as determined according to the ESS 41:1986 and ASTM C32-93 (2000). These data are compared with the limits given by the applied standards. It is evident that there is a close agreement of the values of all properties determined according to the Egyptian (41:1986) and American (C32-93) Standards. It is also found that, the articles of T1, T3 & T4 fulfill the limits outlined by both of ESS 41:1986 and the ASTM C32-93 (grade SS) for water absorption, loss due to acid attack and compressive strength. Although, T4 articles have the privilege properties (least WA and LIW), but it considered a critical from industrial point of view. So, articles of batch T3 at 1125°C deserve to be the superior one.

QUALITY ASSESSMENT

As shown from the visual inspection of the successful fired articles which meet the applied Egyptian (ESS 41:86) American (ASTM C32-63) standard specifications that, they have a deep brown color, smooth surfaces and sharp ends and faces free from any type of cracks.

Table 5 demonstrates a debate between the properties obtained from the most congenial articles (T3) from our study with corresponding of other national and international products. This debate reveals that these articles, which were prepared from the most applicable batch (T3) at 1125°C, have distinctive properties values compared with the other types.

CONCLUSIONS

1. From the above findings, the following primer conclusions can be drawn:
2. Both of cement kiln dust and waterglass sludge can be recycled in the production of acid-resistant masonry units. The addition of 50% of these industrial wastes to 50% of a low-grade clay leads to obtain dense articles after firing up to 1100o-1150oC.
3. The addition of 10-25% waterglass sludge at the expense of cement kiln dust leads to increase the total alkali oxides content up to 10.50%. This decreases the temperature of densification by the developed liquid phase to 1100oC.
4. The fired articles are mainly composed of augite mineral show minimum water absorption & loss due to acid attack as well as maximum crushing strength. The values of these properties are superior to those of the nationally and internationally produced articles.
5. Utilization of the studied wastes in the production of high quality acid-resisting bricks achieves their environmentally safe disposal, production of useful products with high quality at low firing temperatures and saving the natural feldspar minerals, usually used as fluxing materials in such production.

6. Articles of batch T3 that fired at 1125°C is the most applicable and comparable one satisfying industrial aspects.

ACKNOWLEDGEMENT

The authors are indeed indebted to Dr. M. A. Serry professor of ceramics, refractories and building materials in the National Research Center (Cairo, Egypt) for his valuable comments and generous collaboration.

Fig. (2): X-ray diffraction patterns of the KH clay sample

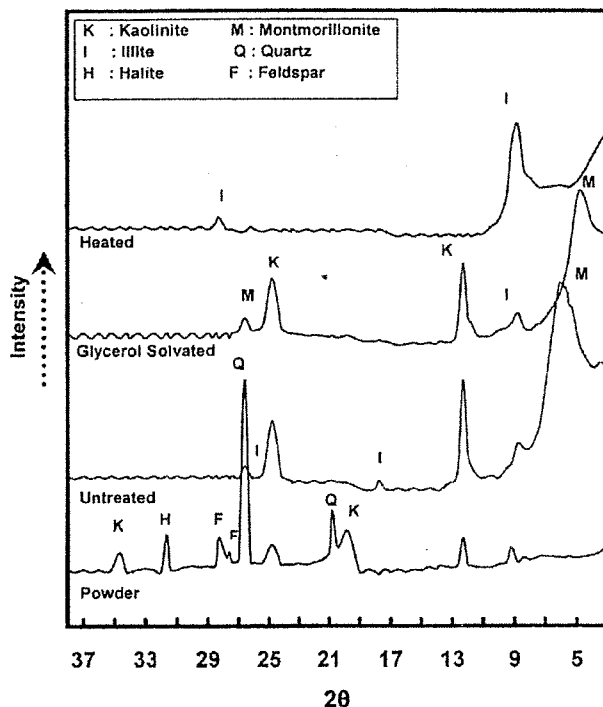
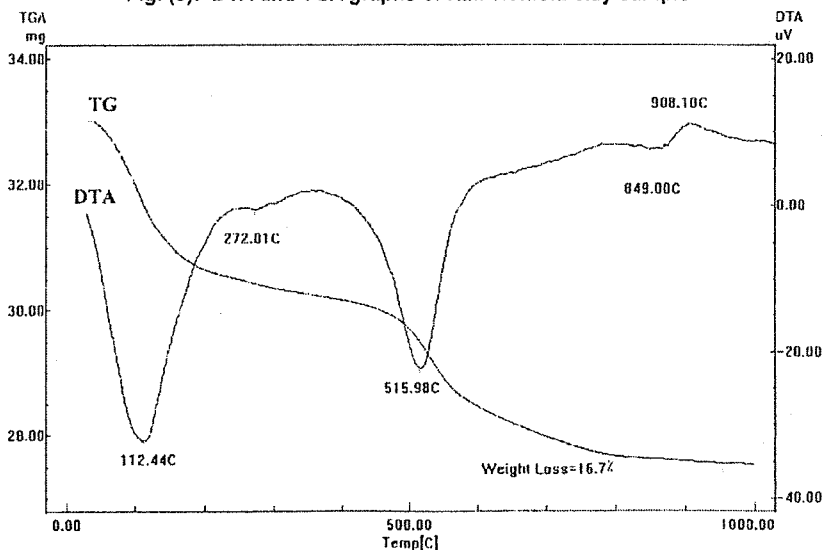


Fig. (3): DTA and TGA graphs of Kafr Homeid clay sample



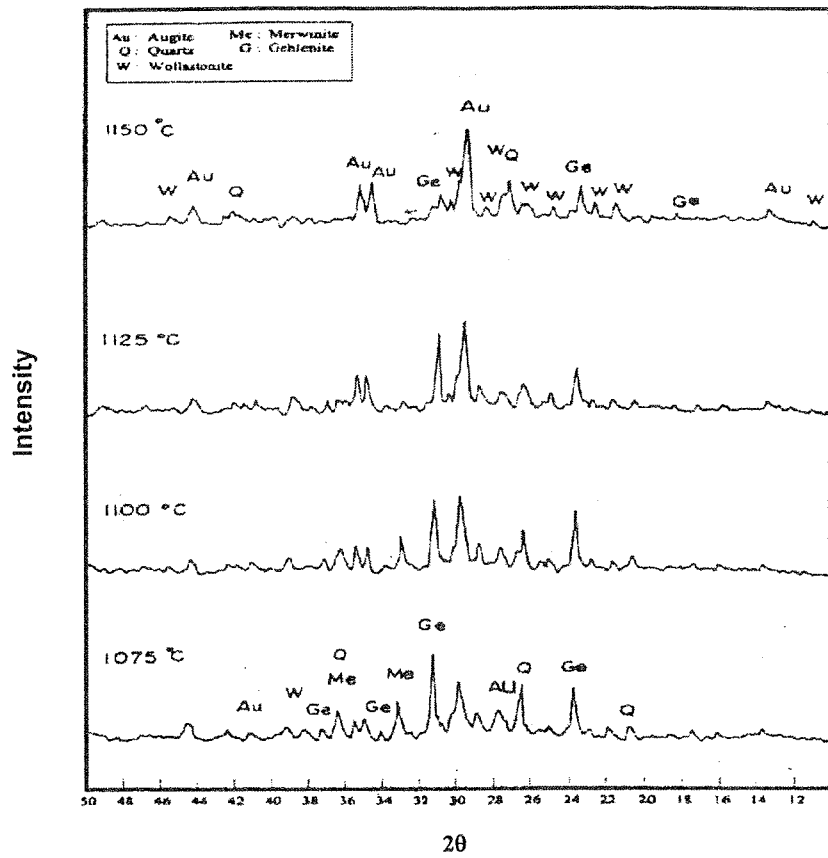


Fig. 5. X-Ray Diffraction Patterns of the Acid Resisting Articles of Mixture T1 and Fired at Different Firing Temperatures

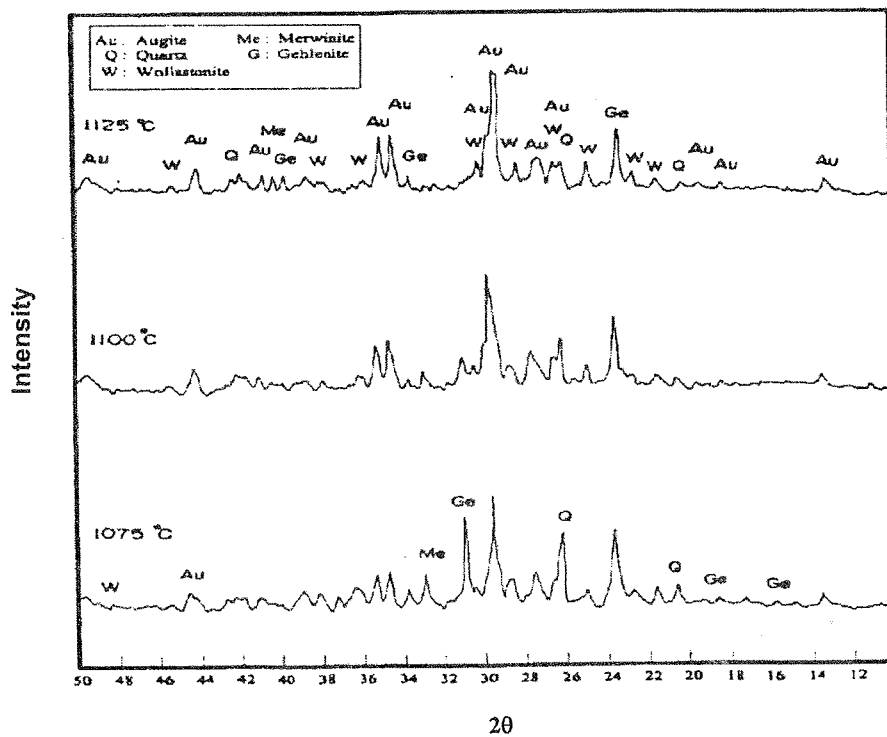


Fig. 6. X-Ray Diffraction Patterns of the Acid Resisting Articles of Mixture T2 and Fired at Different Firing Temperatures

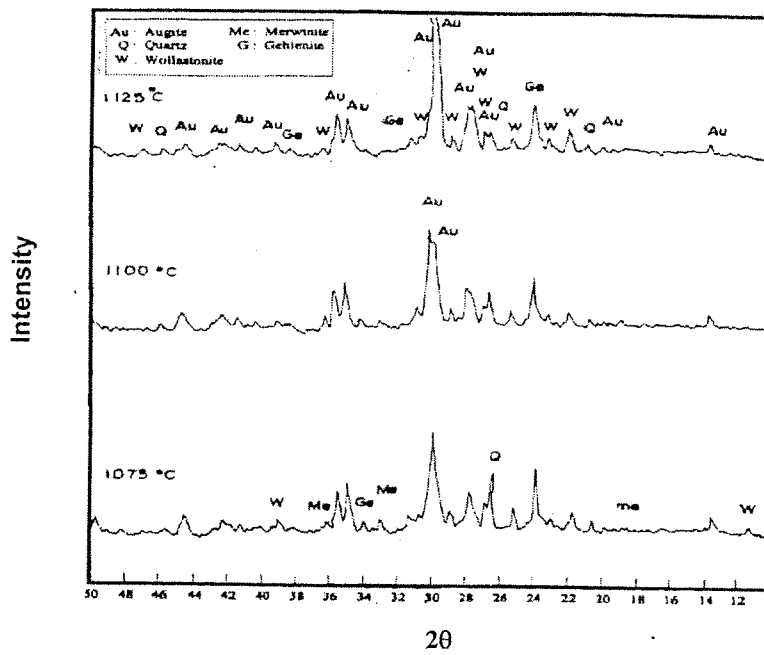


Fig. 7. X-Ray Diffraction of the Acid Resisting Particles of Mixture T3 and Fired at Different Firing Temperature

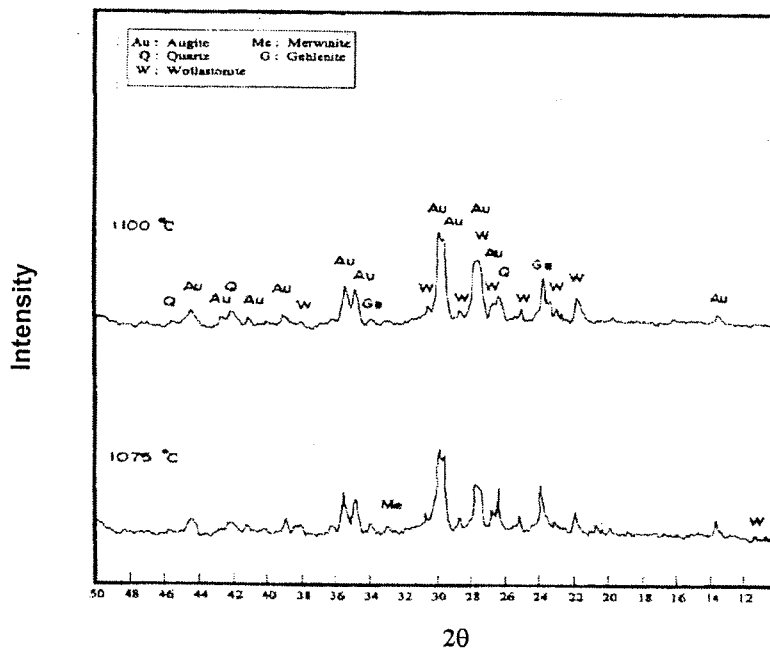


Fig. 8. X-Ray Diffraction Patterns of the Acid Resisting Articles Of Mixture T4 and Fired at Different Firing Temperatures

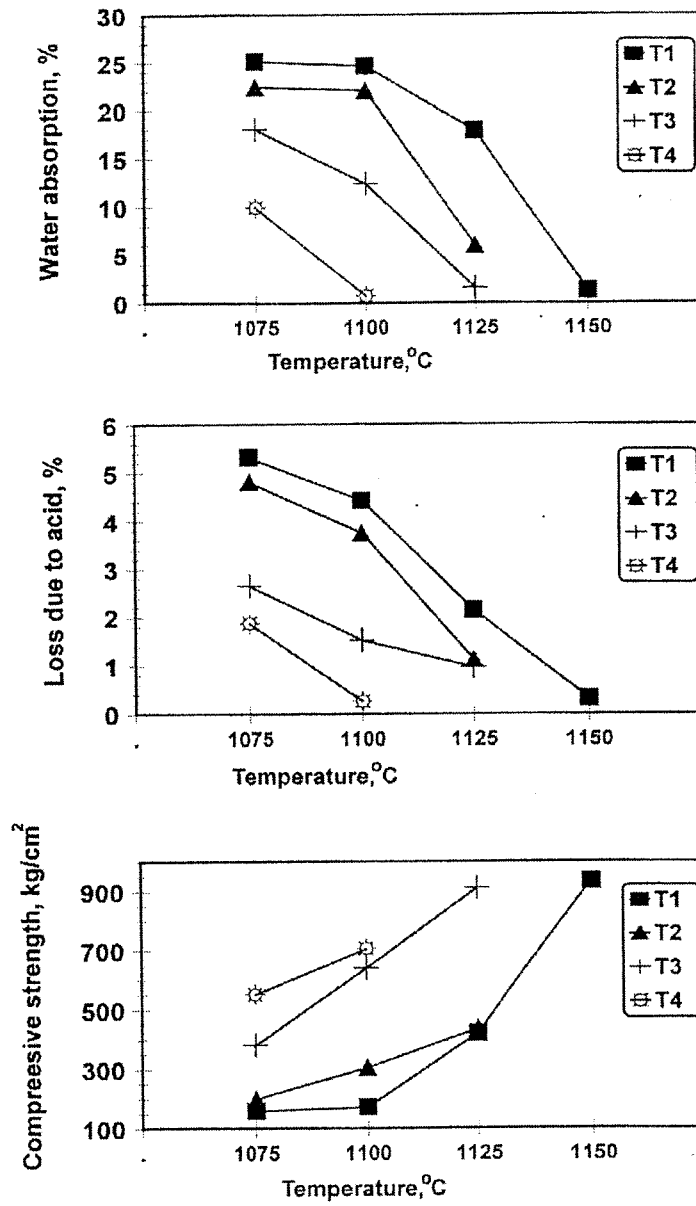


Fig. 9. Effect Of Firing Temperature on the Properties of Fired Articles of Batches T1 – T4

Table 4. Properties and Firing Temperature of the Selected Articles as Compared With the Limits Given by the Egyptian (Ess 41-1986) and American (ASTM C32-93) Standards

Article	Firing temperature °C	Water absorption		Weight loss due to acid attack		Compressive strength	
		%		%		Kg/cm ²	
		ESS	ASTM	ESS	ASTM	ESS	ASTM
T1	1150	1.31	1.22	0.32	0.38	936	936
T2	1125	6.00	6.05	1.12	1.22	435	435
T3	1125	1.59	1.62	0.96	1.15	910	910
T4	1100	0.73	0.76	0.26	0.32	705	705
ESS 41:1986		< 6.0		< 3.5		> 300	
ASTM C32-93 (grade SS)		< 6.0		---		> 550	

Table 5. A Comparison between Properties of Acid Resisting Bricks Produced Under Oxidizing Firing Condition and the Present Articles of the Most Applicable Batch (T3, 1125°C)

Produced by	Properties		
	Water absorption %	Weight loss by acid attack %	Compressive strength Kg/cm ²
KEPCO Co., 1996 (Egypt)	5.50	2.80	660.00
Sowelam Co., 2000 (Egypt)	4.20	3.00	350.00
Kundan Co., 2003, Class I, (India)	2.00	1.50	700
Gunatit Co., 2003, Class I, (India)	0.50 to 1.00	0.50 to 1.00	> 700
El-Mahllawy, 2004 (Egypt)	0.35	2.00	561.00
Present study, 2005 (Egypt)	1.59	0.96	910.00

REFERENCES

1. Al-Harthy, A. S.; Taha, R. and Al-Maamary, F. (2003), "Effect of cement kiln dust (CKD) on mortar and concrete mixtures," *Construction and Building materials*, 14, pp. 353-360.
2. Al-Jabri, K. S.; Taha, R. A.; Al-Hashmi, A. and Al-Harthy, A. S., "Effect of copper slag and cement by-pass dust addition on mechanical properties of concrete (2005)," *Construction and Building materials*, Article in Press, El-Sevier.
3. ASTM-Designation C32-93 (2000), "Standard specifications for sewer and manhole brick made from clay or shale," *Annual Book of ASTM Standards*, USA, 0405, pp.145-146.
4. ASTM-Designation D422-63 (1993), "Standard test method for particle size analysis of soil," *Standard Annual Book of ASTM Standards*, USA, 4, pp. 128-135.
5. Chanda, S. R. S.; Bandopadhyay, S. K. and Ghosh, S. N. (1998), " Investigation of Portland slag cement activated by waterglass," *Cement and Concrete Res.*, 28 (7), , pp. 1049-1056.
6. Doremus, R. H. (2003), "Melt viscosities of silicate glasses," *J. Am. Ceram. Soc.*, 82 (3), pp. 59-63.
7. Egyptian Standard Specification (ESS) 41 (1986), "Acid-resisting bricks for lining sewerages tunnels," pp.1-5.
8. El Shafai, M. M. (2000), "Effect of the addition of some industrial wastes and products on the geotechnical properties of a local soil," Ph.D. Thesis, Fac. Eng., Cairo Univ.
9. El-Sherbiny, S. A.; Youssef, N. F.; Ibrahim, O. A. and Abadir, M.F. (2004), " Use of cement kiln dust in the manufacture of vitrified sewer pipes," *Waste Management*, 34 (1), pp. 597-602.
10. Elwan, M.; Abdel Aziz, D. and El-Didamony, H. (1999), " Effect of by-pass cement dust on the properties of clay bricks," *Silicaty*, 43 (3), pp. 117-122.
11. Gonzalez-Garcia, F.; Romero-Acosta, V.; Garcia-Ramos, G. and Gonzalez-Rodriguez, M. (1990), "Firing transformation of mixtures of clays containing illite, kaolinite and calcium carbonate used by ornamental tile industries," *Appl. Clay Sci.*, 5 (4), pp. 361-375.
12. HCT (1999), "The scientific method of reusing the cement kiln by-pass dust (CKD) inside the cement companies in Helwan area," *Center of Technological Development for Researches and Studies, The act of first scientific seminar*, , Helwan Univ., Cairo, Egypt.
13. Jordan, M. M.; Sanfeliu, T. and Delafuente, C. (2001), " Firing transformations of Tertiary clays used in the manufacturing of ceramic tile bodies," *Appl. Clay Sci.*, 20, pp. 87-95.
14. 14-M P D F (1998)," *Mineral powder diffraction file data book*," Sets 1-42, ICCDD, Pennsylvania, USA.
15. O'Farrell, M.; Wild, S. and Sabir, B. B. (2004), "Pore size distribution and compressive strength of waste clay mortar," *Cement and Concrete composites*, " 23, pp. 81-91.
16. Palacios, M. and Puertas, F.(2005), "Effect of superplasticizer and shrinkage-reducing admixtures on alkali-activated slag pastes and mortars," *Article in press, corrected proof*, El-Sevier.
17. Picard, M. D., (1971), "Classification of fine-grained sedimentary rocks," *J. Sed. Prt.*, 41, pp.179-795.
18. Puertas, F.; Fernadez, A. and Blanco-Varela, M. T. (2004), "Pore solution in alkali-activated slag cement pastes, relation to the composition and structure of calcium silicate hydrated," *Cement and Concrete Research*, 34 (1), pp. 139-148.
19. Riccardi, M. P.; Messiga, B. and Duminuco, P. (1999), " An approach to the dynamics of clay firing," *Appl. Clay Sci.*, 15, pp. 393-409.
20. Shoaib, M. M.; Balaha, M. M. and Abdel-Rahman, A. G. (2000)," Influence of cement kiln dust substitution on the mechanical properties of concrete," *Cement and Concrete Research*. 30, pp.371-377.
21. Smykatz-Kloss, W. (1974), "Differential thermal analysis, application and results in mineralogy," *Springer-Verlag*, Berlin, Germany.
22. Tjerk, P. (1970), "Simple device to avoid orientation effect in X-ray diffractometer samples," *Nereko Rep.*, 17 (2), England, pp.23-24.
23. Youssef, N. F. (2002), "Utilization of cement kiln dust in the manufacture of wall tiles," *Industrial Ceramics*, 22 (1), pp. 1-8.

MODELING OF OPENINGS IN MASONRY INFILL PANELS IN R.C. FRAMES, 2D APPROACH

M. O. ElSeify

Civil Engineering Department, Faculty of Engineering, University of Calgary, Calgary, Canada

M. M. El-Attar, A. M. Ragab, O. A. Hodhod

Structural Engineering Department, Faculty of Engineering, Cairo University

ABSTRACT

In typical design procedures, structural engineers neglect the presence of masonry infill panels, and this is a result of the absence of an accurate and simple analytical model. One of the most important reasons that lead to the complexity of modeling the masonry infill panels is the usual presence of openings in these panels. The totally infilled frame with panels having no openings is a rare case, while the general case is the frame having panels with openings such as window, door and air conditions openings.

Neglecting the existence of openings in infill panels while determining the seismic capacity of R.C. framed structures will result in inaccurate estimation of lateral stiffness, strength, ductility and seismic capacity of buildings.

In this study the masonry infill panels are modeled using macro-modeling technique. In macro models, the infill panel is replaced by one or two diagonal struts (Holmes [1], Chrysotomou [2] and Stafford Smith [3]). Properties of the struts are determined based on experimental data or micro model (finite element) investigations. Macro models are computationally efficient and suitable to study the overall structural response of the building.

The objectives of this study are to propose a simple model for openings in masonry infill panels that can be used in two-dimensional analysis. Also to find out the influence of presence of openings in infill panels on the behaviour of R.C. frame buildings under seismic loading. So a probabilistic study was held to investigate the efficiency of the new proposed model for openings and to find out the influence of its presence on the lateral stiffness of masonry infill panels and subsequently on the seismic capacity of R.C. framed structures.

Keywords: Masonry, Infill, Seismic, Probabilistic, Openings, Model

CASE STUDY

Macro-Modeling of Masonry:

The model used for the masonry infill panels in this paper is a macro model. Macro-models are based on physical understanding of the behaviour of the infill panel as a whole. The macro-models are efficient computationally for the analysis of large buildings with numerous structural components. A macro-model can be implemented to simulate varying response effects resulting from different design and geometry of structural components by controlling the parameters of the model. The proposed analytical model assumes that the contribution of the masonry infill panel to the response of the infilled frame can be modeled by replacing the panel by a system of two diagonal masonry compression struts.

Stress-Strain Relationship for Masonry

The stress-strain relationship for masonry in compression can be idealized as an increasing polynomial function (Mander et al. [4]) until the peak stress (f_m') is reached for a given strain. Then this is followed by a sudden drop of the stress value by increasing the strain representing the brittle behaviour of masonry. After these stages the stress remains almost constant at this value. The assumed constitutive model for the masonry struts is shown in Fig. 1.. Since the tensile strength of masonry is negligible, the individual masonry struts are considered to be ineffective in tension. However, the combination of both diagonal struts provides a lateral load resisting mechanism for positive as well as negative directions of loading.

Lateral force Deformation Relationship

The lateral force-deformation relationship for the structural masonry infill panel (Saneinejad and Hobbs [5]) is a smooth curve bounded by bilinear strength envelope with an initial elastic stiffness (K_0) till the yield force (V_y) and then a post-yield degraded stiffness (αK_0) until the maximum force (V_m). The corresponding lateral displacement values are denoted as (U_y) and (U_m) respectively. The monotonic lateral force deformation relation ship assumed for the system of diagonal compression struts is shown in Fig. 2..

Probabilistic Study

The response of the building is calculated using the nonlinear analysis program IDARC2D version 4.0 developed for reinforced concrete frame structures by Valles et al. [6]. However, since both the ground motion and structural capacity are random in nature, a probabilistic approach is more realistic for this problem. To determine the statistical characteristics of the building response, the Monte Carlo simulation method is selected.

Building Configurations and Design

A twelve story building is selected for this analysis as a sample for high-rise building. In order to study the effect of presence of openings in masonry infill panels on the seismic capacity of R.C. framed structures, three various cases are considered. The cases considered are shown in Fig. 3..

Building is 20 x 25 m in plan with columns and beams spaced every 5 meters. A typical frame in the building is designed according to the provisions of the Egyptian Code for design and construction of concrete structures (2001). Concrete strength considered is 300 kg/cm² and steel yield strength is 4000 kg/cm².

MODELING OF OPENINGS

As it was mentioned before, the dynamic analysis is performed using IDARC2D version 4.0 which is a computer software package specific for the inelastic damage analysis of two dimensional buildings. Previous researches carried on infilled frames using similar 2D software packages modeled openings in infill panels using the concept of changing the assumed hysteretic model for infill panels by decreasing its thickness or compressive strength for example. This way of modeling is unrealistic somehow as it is built on assumptions that can not be easily proved. The influence of presence of openings on the lateral stiffness of the infill panels is controlled by so many parameters such as location, size and shape of the opening that can not be controlled by introducing one reduction factor to the strength or the thickness of the masonry.

In this study, the assumed hysteresis model used in the IDARC2D was not altered but the modeling is carried out using another and more realistic way. The openings were modeled by creating real openings in the infill panels in the input files using the capabilities of IDARC2D which enable the creation of real openings with their real dimensions, shape and location in the infill panels.

Modeling Procedure

In this model (ElSeify, M.O. [7]), creating real openings in the infill panels depends on using the capabilities of the IDARC2D version 4.0 such as the ability to introduce both real and virtual column lines, to control the beam connectivity and to control the infill panel connectivity.

As shown in Fig. 3., it can be noticed that frame F2 (Totally infilled with no openings) has only 5 column lines (J=1, 2, 3, 4 & 5) and all of these column lines have real columns. While frame F3 (Totally infilled with door openings) has 13 column lines (J=1 to 13) of which five column lines have real columns and the other eight lines are just virtual column lines having no columns and will be used to divide the infill panels into three portions.

In Frame F3 column lines 1, 4, 7, 10 and 13 are real column lines spaced by 5 meters. While column lines 2, 3, 5, 6, 8, 9, 11 and 12 are virtual column lines having no columns and will be used to divide the infill panels situated between any 2 columns into 3 portions. This technique enables creation of openings in the infill panels by removing one of the three portions.

During the beam connectivity procedure, any beam will be connected between the real column lines which represent the columns (1, 4, 7, 10 & 13), so the bay between any two real columns contains 1 beam. While during the infill panel connectivity procedure, the infill panels are connected between any two successive column lines (1 to 13) even though they are real columns or virtual column lines, the bay between any two real columns contain one infill panel which is divided into three portions.

So for example the bay between the two columns lines 1 & 4 at the first floor has the following:
2 columns on the column lines 1 and 4.

1 beam connecting between the 2 columns.

1 infill panel divided into 3 portions, the first portion is between column lines 1 and 2, the second portion is between column lines 2 and 3 and the third portion is between column line 3 and 4.

A door opening in the infill panel which was created by removing the second (middle) portion of the panel which is situated between column lines 2 and 3.

The width of the openings can be controlled by changing the distances between the virtual column lines, while the height can be controlled by introducing virtual beam lines having no beams.

Verification of the Model

The model was verified by creating two files. In the first file, there were 13 column lines. The infill panel was not divided into portions and was connected between the column lines having real columns (1, 4, 7, 10 & 13). So the panel between any two columns contains 4 column lines, 2 columns (left and right), 2 beams (up and down) and 1 masonry infill panels not divided into portions. This is the case which exists in reality, as the infill panel is not divided into portions.

While in the second file, there were 13 column lines. The infill panel was divided into 3 portions and was connected between all column lines, the ones having real columns (1, 4, 7, 10 & 13) and the other virtual column lines having no columns (2, 3, 5, 6, 8, 9, 11 & 12). So the panel between any two columns contains 4 column lines, 2 columns (left and right), 2 beams (up and down) and 1 masonry infill panels but divided into 3 portions. This is the case which helped in creating openings in the infill panels and which needs to be verified.

Here in this procedure both buildings are totally infilled, the aim is to verify that introducing virtual column lines and dividing each infill panel into 3 portions will not influence the seismic behaviour of the frame F3.

The results which were represented in terms of overall damage index of the buildings and inter story drift were compared for the above two mentioned cases. The result of this comparison showed 100% compatibility between the two cases.

ANALYSIS PROCEDURE

The performance of the structure is evaluated in terms of inter-story drift and damage index. To predict the nonlinear dynamic structural response, the computer program IDARC2D Version 4.0 developed by Valles et al. [6] is used. The state of damage in the structure is predicted with the

use of a damage index procedure. The Park and Ang [8] damage index which is already implemented in the program is used in this study. Park and Ang damage index evaluates damage in terms of energy dissipated and maximum drift. Value of the damage index is calibrated using damage states from recent earthquakes. Table 1. shows the relation between value of damage index and various damage states.

The use of actual earthquake records involves a number of difficulties because many of available records are not free field time histories. Therefore in this analysis, an artificially generated set of ground motion records is used to evaluate the response of the buildings.

Uncertainties in structural capacities are also considered through consideration of variability of concrete compressive strength, steel yield strength and dimensions.

Generation of Artificial Ground Motion Records:

The artificial ground motion time history is generated using the Clough and Penzien [9] power spectral density function for the ground acceleration.

$$S_g(\omega) = S_0 \frac{1 + 4\zeta_g^2 \left(\frac{\omega}{\omega_g}\right)^2}{\left[1 - \left(\frac{\omega}{\omega_g}\right)^2\right]^2 + 4\zeta_g^2 \left(\frac{\omega}{\omega_g}\right)^2} \frac{\left(\frac{\omega}{\omega_f}\right)^2}{\left[1 - \left(\frac{\omega}{\omega_f}\right)^2\right]^2 + 4\zeta_f^2 \left(\frac{\omega}{\omega_f}\right)^2} \quad (1)$$

Where S_0 is the amplitude of the white noise bedrock excitation; ω_g and ω_f are the frequencies of the first and second filters, respectively. Finally, ζ_g and ζ_f are the damping of the first and second filters, respectively. Table 2. represents the values for the mean and coefficient of variation of ω_g and ζ_g proposed by Lai [10]. The value of ω_f is taken equal to $0.1\omega_g$ and ζ_f is considered equal to ζ_g . Creating the artificial ground motion records is based on generating random numbers representing ω_g and ζ_g using mean, standard deviation and probability distribution for each parameter. Using these sets of random numbers, power spectral density functions are generated using Eq. 1. Then, the stationary acceleration time history is generated based on the work developed by Shinzouka [11]. Finally, the time varying intensity of the earthquake is modeled by multiplying the stationary acceleration time history by a suitable envelope function.

This set of ground motion records represents the soil site condition, and it contains 1000 ground motion records scaled to different values of peak ground acceleration (PGA) (0.2g, 0.3g & 0.4g).

Uncertainties in Member Capacity:

The main sources of uncertainties in the member capacity are the variation between the specified and the actual material strength and between the actual and design member dimensions.

To consider the variability in the material strength, the approach of Mirza et al. [12] had been followed. Mirza et al. proposed the use of normal distribution to model the concrete compressive strength with a coefficient of variation 0.15 and a mean value given by:

$$f_m = 0.675 f'_c + 7.59 \leq 1.15 f'_c \quad (MPa) \quad (2)$$

Where f'_c is the nominal concrete compressive strength. The variability of steel yield strength is modeled by a lognormal distribution with a mean value equal to 1.22 times the specified yield strength and a coefficient of variation 0.107.

Uncertainties in member dimensions depend on the level of quality control during construction. In order to take the uncertainties in member dimensions into consideration, the results of Mirza et al. [12] and Tso and Zelman [13] which are summarized in table 3. will be used.

Summary of the Analysis Procedure

The analysis procedure in this paper is based on generation of 1000 artificial earthquakes as shown in section (4.1). The uncertainties in earthquake ground motion were taken into consideration. Also the uncertainties in structural capacity were taken into consideration by preparation of various values for the random variables representing the material strength and the cross-sectional dimensions. To determine the statistical characteristics of the building response, the Monte Carlo simulation method was selected to combine various ground motion records with various other random variables representing the structural capacity. The ground acceleration time histories are scaled to different values of peak ground acceleration (PGA) 0.2g, 0.3g & 0.4g. Each frame (F1, F2 & F3) is subjected to the different generated earthquakes (1000 run with PGA=0.2g, 1000 run with PGA=0.3g and 1000 run with PGA=0.4g) scaled to various PGA considering in the same time the various values of concrete compressive strength and steel yield strength. The performance of the structure is evaluated in terms of inter-story drift, damage index and probability of exceedence which demonstrates the percentage of slight, minor, moderate, severe and collapse cases for each type of buildings.

ANALYSIS RESULTS

The results in this study were presented in terms of inter-story drift, damage index and probability of exceedence which demonstrates the percentage of different damage categories that occur for each building configuration.

Damage Index

Fig.4. compares the damage indices of the frames F1, F2 and F3. This comparison emphasizes that at PGA 0.3g, the damage index was reduced from 1 in case of no infill (F1) to 0.6 and 0.5 in the cases considering openings (F3) and totally infilled frame (F2) respectively.

So the reduction was 40% and 50% for the cases of frame F3 and frame F2 respectively. So it is obvious that the presence of openings increased the damage index by 10% more than frame F3 (totally infilled).

5.2. Inter-Story Drift:

Fig.5. compares the inter-story drifts of the frames F1, F2 and F3. This comparison shows that, the inter-story drift was reduced from 15 in case of frame F1 to 5.2 and 4.2 in case of frames F3 and F2 respectively. So there were large reductions in the inter-story drifts corresponding to 65.33% and 72% in case of frames F3 and F2 respectively. It can be concluded that the presence of openings in the masonry infill panels reduced the strength of the panels in bracing the different types of buildings and this leads to the increase in the inter-story drift in case of frame F3 by 6.67% more than frame F2.

Probability of Exceedence:

Fig.6. represents the results of the probability of exceedence analysis for ground motion records scaled to PGA 0.3g. These results demonstrate that the percentage of buildings that collapsed was 18% in frames F1, 8% in frames F3 and 5% in frames F2. The percentage of severe damage was the highest in frames with no infill (82%), and it drops to 13% in frames with openings and to 3% in totally infilled frames. Comparing the percentage of moderate damage in both frames F2 and F3 gave an evidence for the influence of openings on decreasing the lateral stiffness. 90% of totally infilled frames were moderate damage and this percentage dropped to 73% in frames with openings, and it nearly vanishes in non infilled frames.

Table 1. Relation between Park and Ang Damage Index and Various Damage States

Range of Damage Index	Damage State	Appearance
0.0	No Damage	Undeformed / Uncracked
0.0 – 0.2	Slight Damage	Moderate Cracking
0.2 – 0.5	Minor Damage	Severe Cracking
0.5 – 0.6	Moderate Damage	Spalling of Concrete Cover
0.6 – 1.0	Severe Damage	Buckled Bars – Exposed Core
> 1.0	Collapse	Loss of Shear / Axial Capacity

Table 2. Values Proposed by Lai [10] for the Mean and Coefficient of Variation of ω_g and ζ_g

Ground condition	ω_g (hz)		ζ_g	
	Mean	Co-efficient of variation	Mean	Co-efficient of variation
Rock	4.25	0.398	0.35	0.391
Soil	3.04	0.425	0.32	0.426

Table 3. Characteristics of Random Variables

Random Variables	Distribution	Coefficient of Variation
Concrete compressive strength	Normal	0.15
Steel yield strength	Lognormal	0.093 – 0.17
Reinforcement area	Normal	0.04
Beam height	Normal	0.01
Beam width	Normal	0.02
Beam depth	Normal	0.02
Column dimension	Normal	0.02

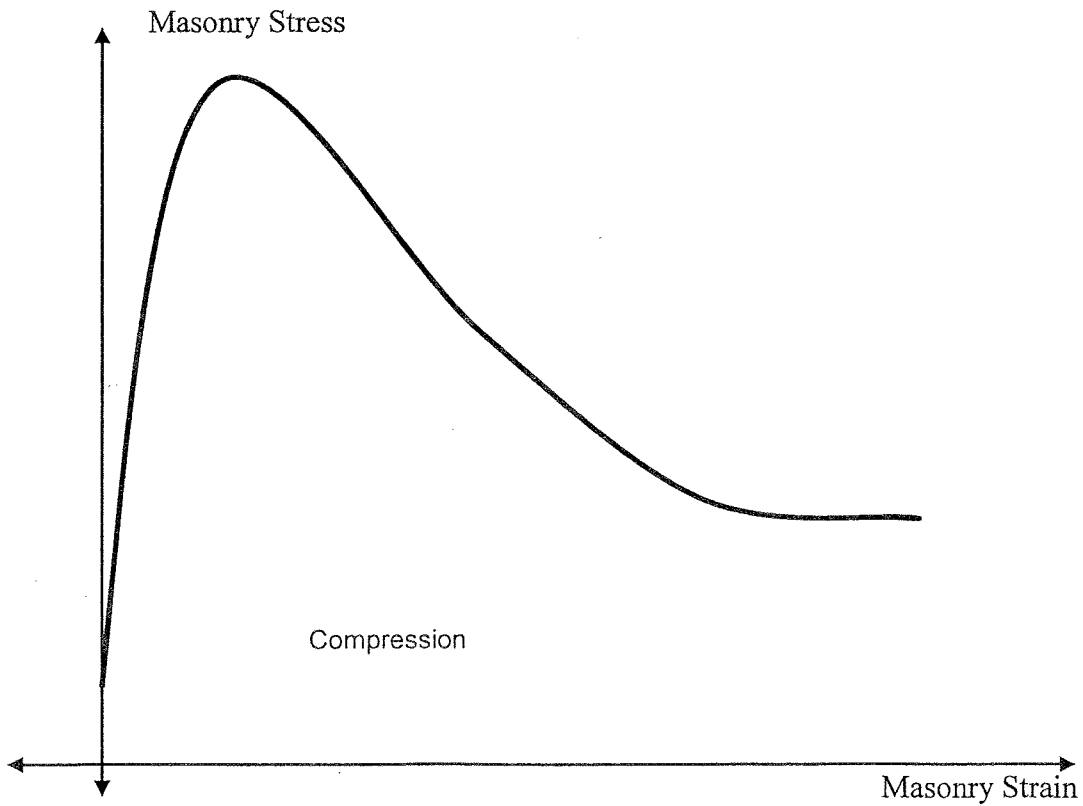


Fig. 1. Constitutive Model for Masonry (Mander et al. [4])

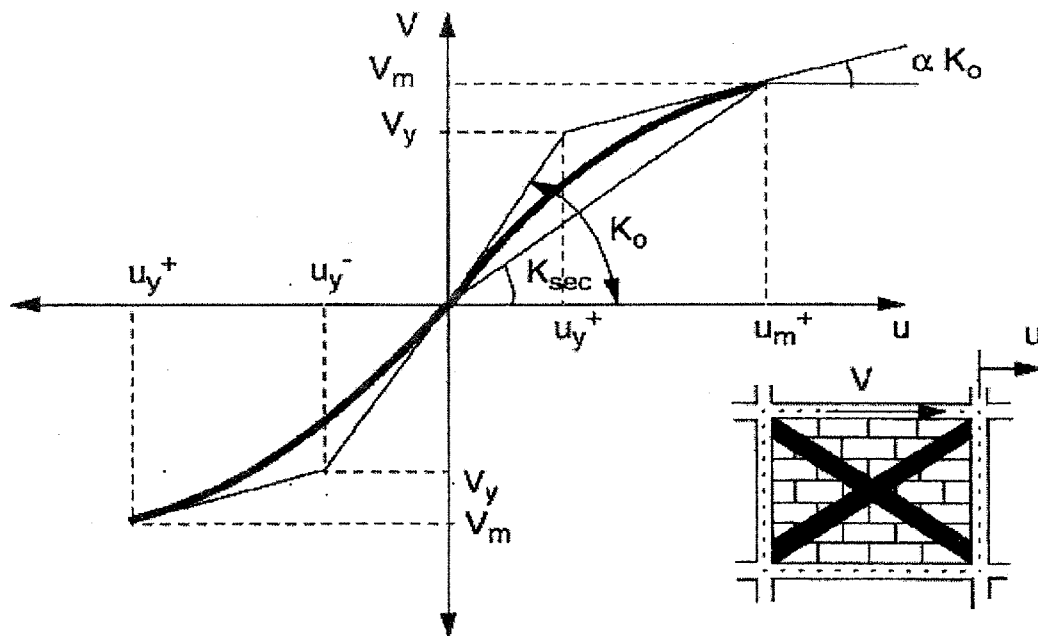
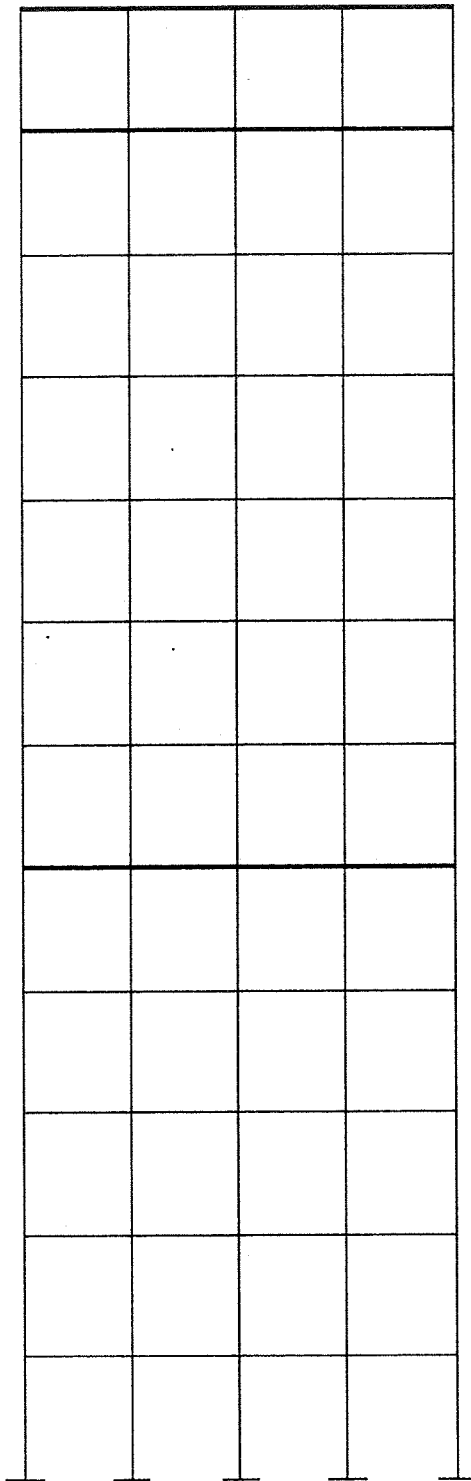
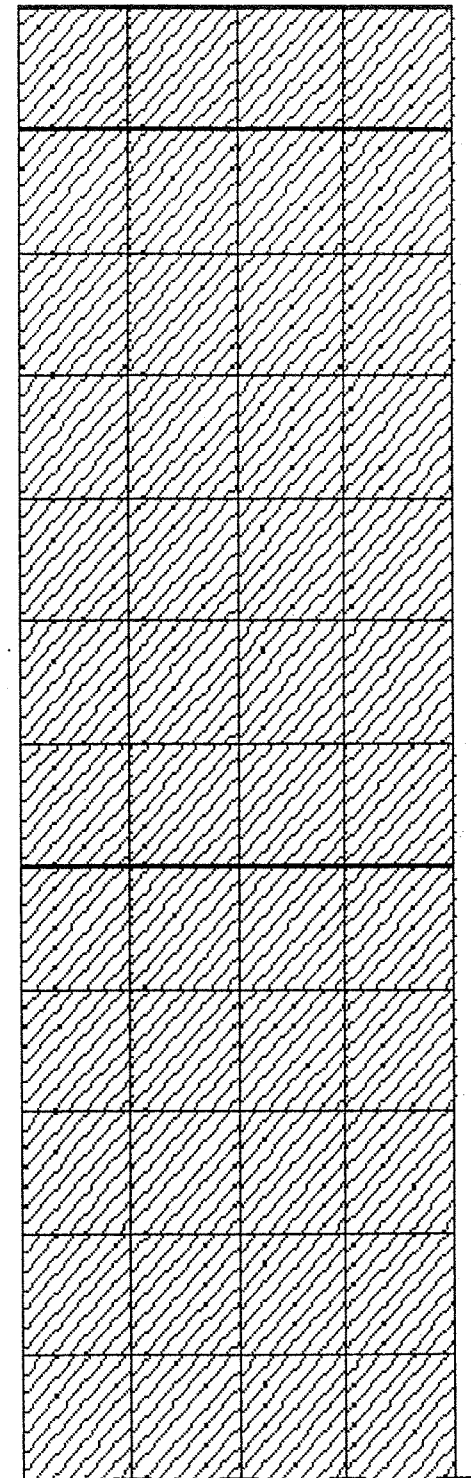


Fig. 2. Strength Envelope for Masonry Infill Panel (Saneinejad and Hobbs [5])



Frame (F1)



Frame (F2)

Fig. 3. Various Building Configurations

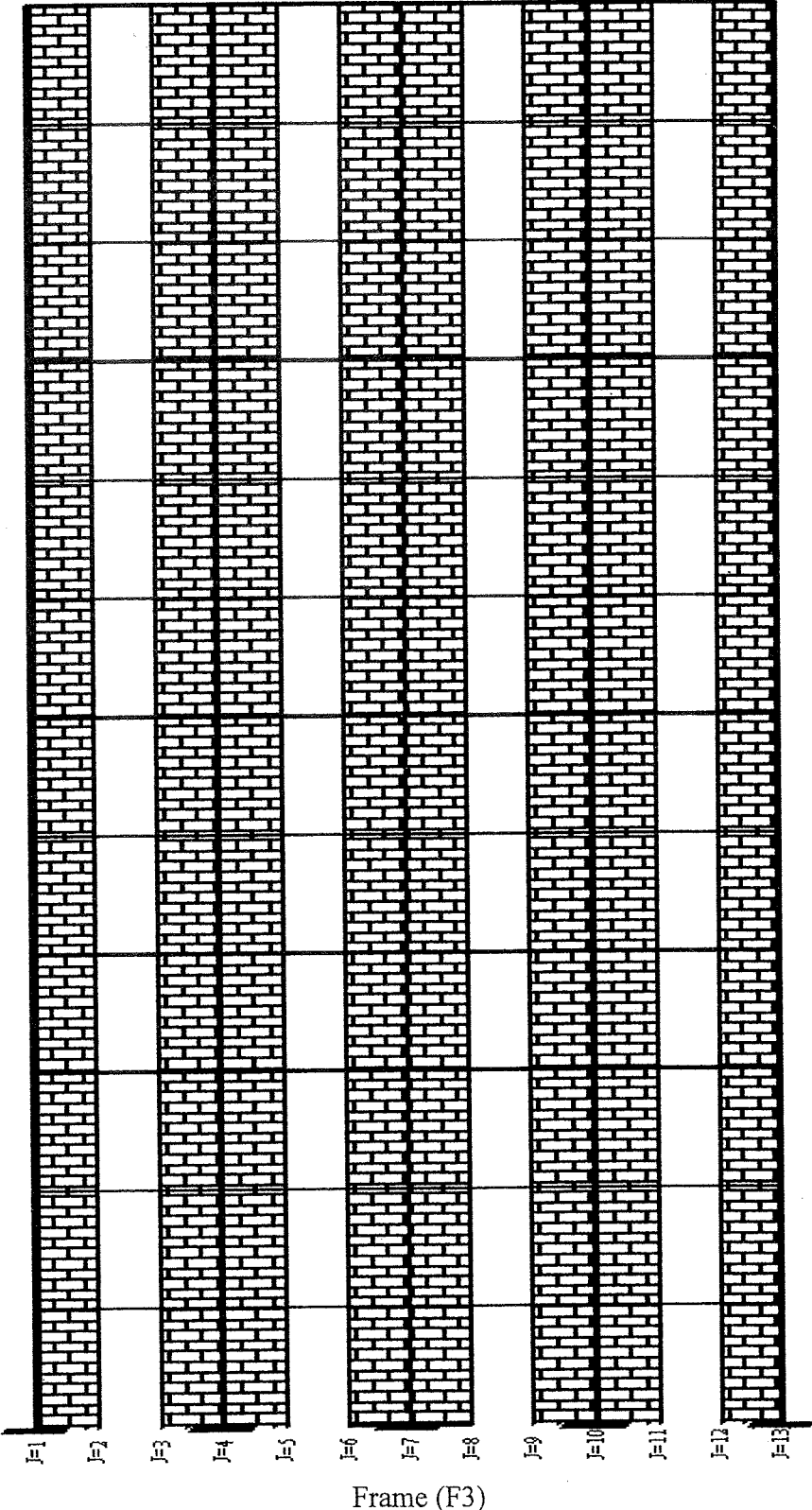


Fig. 3. Various Building Configurations (continue)

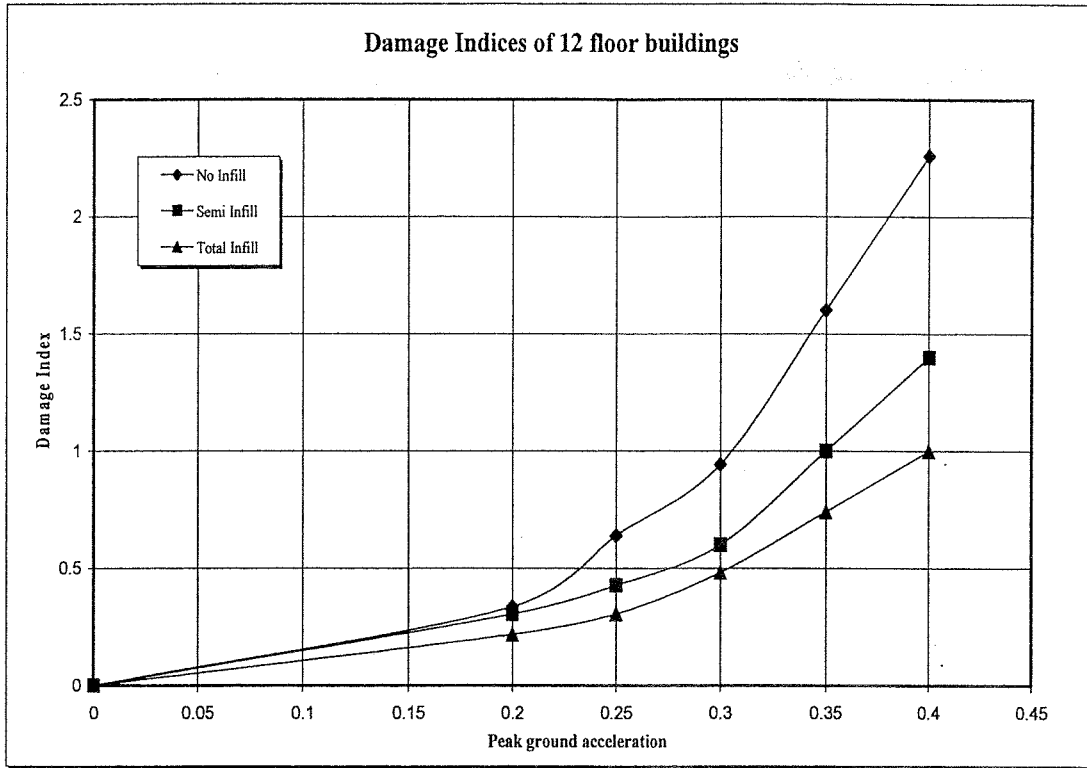


Fig. 4. Relation between PGA and Damage Indices

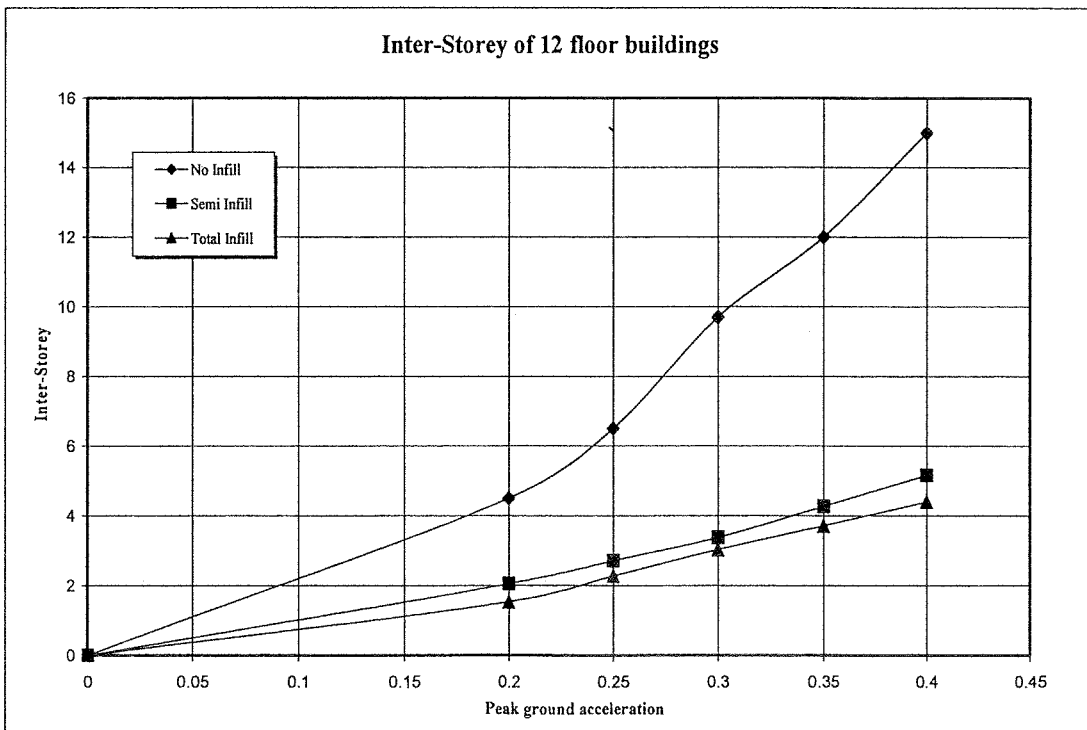


Fig. 5. Relation between PGA and Inter-Storey Drift

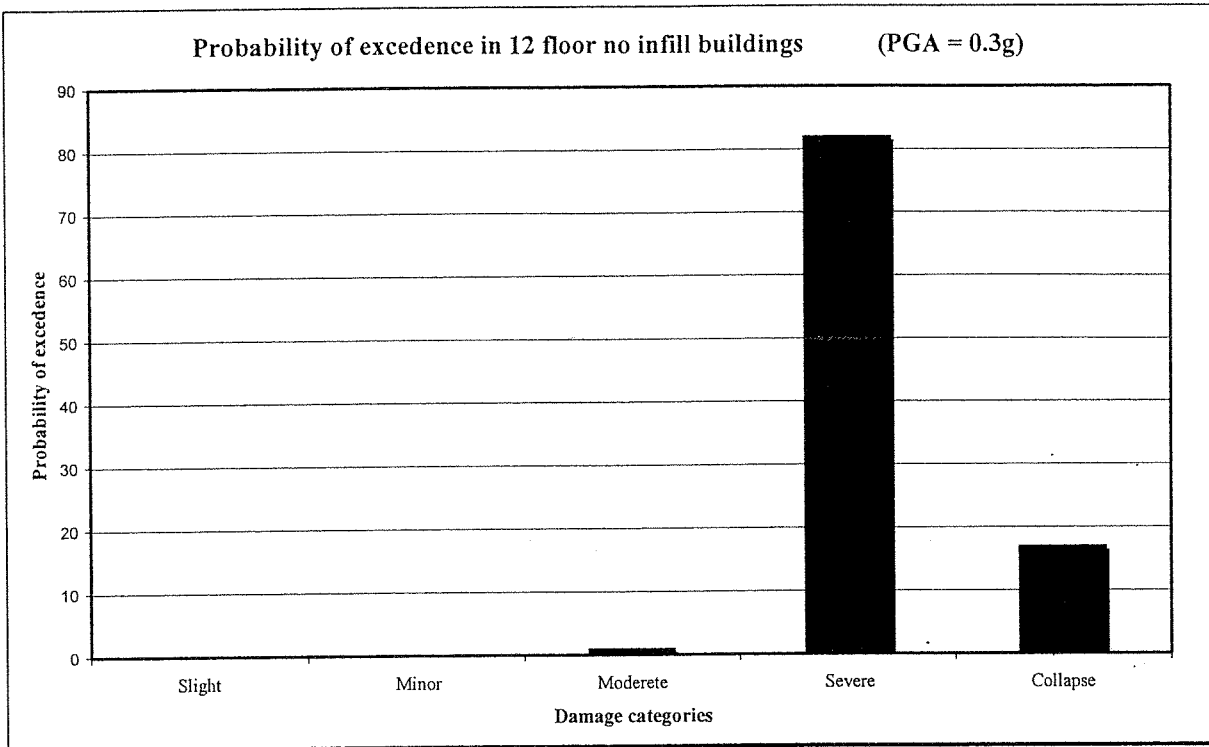


Fig. 6a. Probability of Exceedence for Frame F1

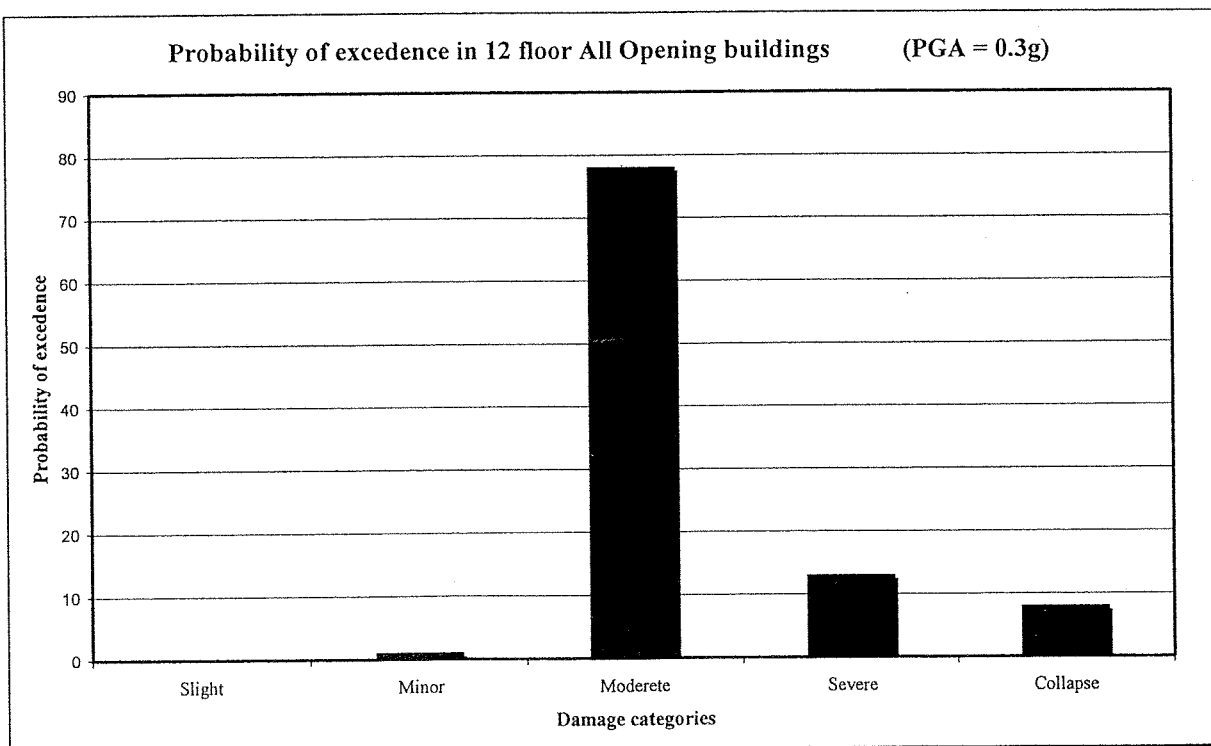


Fig. 6b. Probability of Exceedence for Frame F3

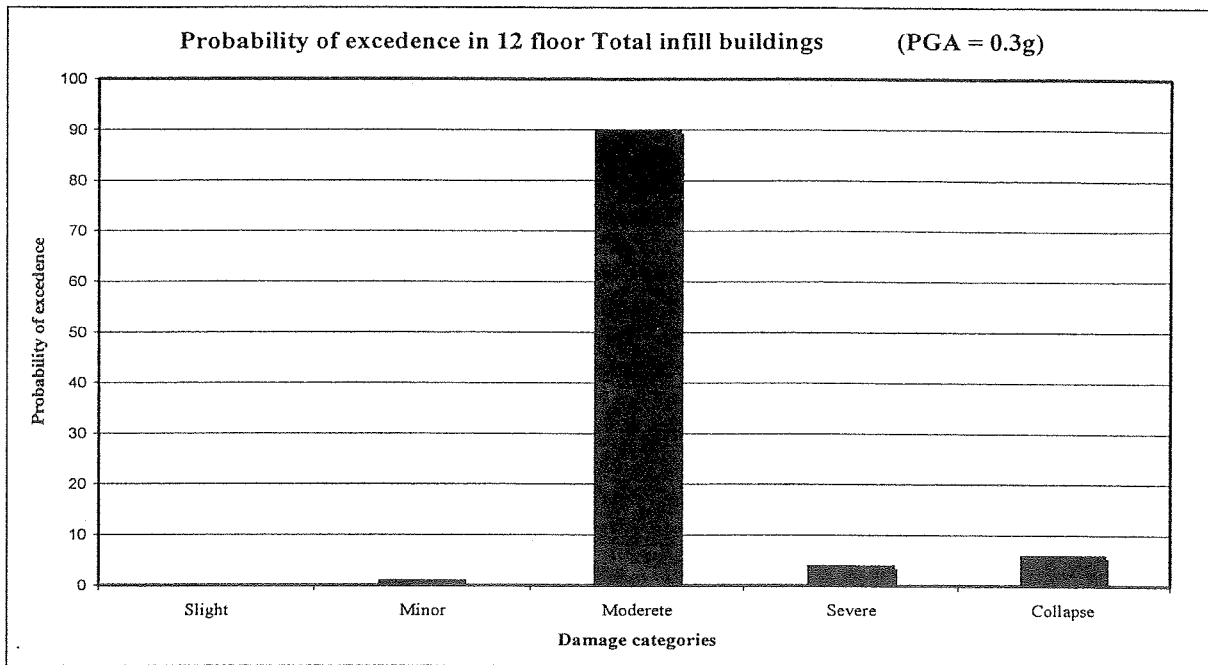


Fig. 6c. Probability of Exceedence for Frame F(2)

CONCLUSION

Since both the ground motion and the structural capacity are random in nature, a probabilistic study was conducted to study the presence of openings in the masonry infill panels on the lateral stiffness of the panels and subsequently on the seismic capacity of R.C. framed structures using nonlinear dynamic analysis. Different performance levels are defined for the structure in terms of damage level. The structure response from the dynamic analysis is related to the damage index, inter-story drift and probability of exceedence.

A new model for openings in masonry infill panels in the two dimensional analyses using macro-modeling was introduced and verified in this study. This model achieved high accuracy by not changing the hysteretic model of the masonry by proposing empirically reduction factors to the strength or thickness of masonry as was done in previous researches. This model is based on creating a real opening in the panel creating a real discontinuity at the real location of the opening and with the same size and shape.

The influence of presence of openings in masonry infill panels was shown clearly in this study, as presence of openings decreases the lateral stiffness of these panels which successively reduces the seismic capacity of the R.C. frame. The position of the openings plays a big role in decreasing the lateral stiffness of the infill panels, as positioning the opening in the middle of the panels gives worst results. Also the size of the opening is very important factor in determining the lateral stiffness of the infill panel, as the increase in the opening size leads to a clear decrease in the lateral stiffness of the infill panel.

Finally, the presence of openings in masonry infill panels can not be neglected as they have clear effect on the seismic capacity of R.C. framed structures as shown in this study.

REFERENCES

1. Holmes, M., "Steel Frames with Brick Work and Concrete Infilling", Proceedings of Institute of Civil Engineers, London, England, Part 2, 1961, Vol. 73, pp. 473-478.
2. Chrysotomou, C.Z., "Non Linear Seismic Response of Infilled Steel Frames", Proc. 10th World Conference on Earthquake Engineering, Madrid, 1992.

3. Stafford Smith, B., "Behaviour of Square Infilled Frames", Journal of Structural Eng., ASCE, Vol. 92, pp.381-403, 1969.
4. Mander, J.B., Priestly, M.J.N. and Park, R., "Theoretical Stress-Strain Behaviour of Confined Concrete" Journal of Structures Division, ASCE, Vol. 114, No. 8, pp.1827-1849, Aug. 1988.
5. Saneinejad, A. and Hobbs, B., "Inelastic Design of Infilled Frames", Journal of Structural Engineering, Vol. 121, No. 4, pp. 634-650, April 1995.
6. Valles, R.E., Reinhorn, A.M., Kunath, S.K., Li, C. and Madan, A., "IDARC2 Version 4.0: A Computer Program for the Inelastic Analysis of Buildings", Technical Report NCEER-96-0010, 1996, State University of New York at Buffalo, N.Y.
7. ElSeify, M.O., "Seismic Analysis of Infilled Frames", Thesis submitted in partial fulfillment of the requirements for a Master of Science in civil engineering, Cairo University, 2003.
8. Park, Y.J., Ang, A.H., Wen, Y.K., "Seismic Damage Analysis and Damage-Limiting Design of R.C. buildings", Civil Engineering Studies, Technical report No. SRS516, University of Illinois, Urbana, 1984.
9. Clough, R.W. and Penzien, J., "Dynamics of Structures", McGraw-Hill, 1975, New York.
10. Lai, S.-S.P., "Statistical Characterization of Strong Ground Motion Using Power Spectral Density Function", Bulletin Seismol. Society, 1982, Am 72, pp. 259-274.
11. Shinzouka, M., "Digital Simulation of Random Process in Engineering Mechanisms With Aids of FFT Technique", in Stochastic Problems in Mechanics, Eds. S.T., Ariaratnam and H.E.E. Liepholz, 1974, University of Waterloo press, Waterloo, Canada.
12. Mirza, S.A., Hatzinikolas, M., McGregor, J.G., "Statistical Descriptions of Strength of Concrete", Journal of Structural Engineering, ASCE, 1979, Vol. 105, pp. 1021-1036.
13. Tso, W.K. and Zelman, I.M., "Concrete Strength Variation in Actual Structures", ACI Journal, Vol. 87, pp. 981-988, 1970.

EFFECT OF STEEL FIBER (SF) CONTENT ON BEHAVIOR OF HIGH STRENGTH REINFORCED CONCRETE CIRCULAR COLUMNS

Samy S. Yousef, Hazem M. Abd El-Latif and Heba H. Bahnasawy
Housing and Building National Research Center Egypt

Mahmoud A. Metawea
El-Azhar University, Naser city, Egypt

ABSTRACT

This paper investigates the effect of steel fiber (SF) on the behavior of high strength fiber reinforced concrete (HSFRC) circular columns confined by spiral and subjected to monotonically concentric axial load. Effects of key variables such as fiber content and concrete compressive strength were studied. An experimental program was conducted to achieve the required objectives. Six columns with circular cross sections were tested under axial loads. They were divided as follows: one column without fiber as a reference column, three columns were cast to study the effect of fiber content and two columns were cast to study the effect of concrete compressive strength. This paper highlights the effect of the studied variables on the gain of core strength, confinement factor, (cracking, ultimate) load and ductility.

It was found that, Content of fibres has great effect on improving the behavior of (HSFRC) circular columns. Steel fibres optimum content that affects most of the characteristics of (HSFRC) circular columns is (0.5%).

Keywords: High Strength Concrete; Steel Fiber; Column; Ductility; Confinement.

INTRODUCTION

Technology of (HSC) has rapidly improved in as much as its significance but its known that (HSC) is a brittle material and there is an adverse relation between strength and ductility. To overcome this problem, fibers are used. This is due to its effect in delaying and controlling the crack propagation, subsequently ductility will be increased.

Wafa, F. F and Ashour, S. A., (1) studied the mechanical properties of high-strength fiber reinforced concrete using hooked-end steel fiber. It has been found that addition of 1.5 percent by volume of hooked end steel fiber resulted in a small increase (4.6 percent) in compressive strength. Hsu, L. S. and thomas Hsu, C. T. (2) studied the stress-strain behavior of steel fiber high-strength concrete (HSC) under compression test. Empirical equations were proposed to represent the complete stress-strain relationships for high-strength steel fiber concrete with compressive strength exceeding 10000 psi (70 MPa).

Taerwe, L. R., (3) discussed the results of loading tests on normal, medium and high-strength concrete (HSC) cylinders under axial compression. Special attention is paid to the descending part of stress-strain curve, which is known to be very steep for high-strength concrete (HSC). Adding steel fiber leads to a beneficial effect on strain-softening behavior and significantly increases toughness, which is measured by the area under the stress strain curve.

Hassan, A. A., (4), studied the behavior of high-strength fiber concrete columns under concentric loads and investigated the mechanical properties for fiber high-strength concrete (HSC) specimens. Sixteen square column specimens were tested under axial loads. It has been

concluded that the increase of fiber content led to an improvement in compressive strength up to 9.75%.

Therefore, this paper highlights the behavior of (HSFRC) circular columns by using steel fiber.

MATERIALS

Local materials were used in concrete mixes and tested according to Egyptian Standard Specifications (ESS) and American Standard of Testing Materials (ASTM).

Crushed dolomite as coarse aggregate was used with maximum size 19 mm, and the particle shape is angular. Fine aggregate used in this research was natural sand and it composed mainly of siliceous material. Ordinary Portland cement was tested to assure its compliance with ESS 373-1991. Silica fume is an extreme fine pozzolanic material, also it was added to the cement content to produce workable and high strength concrete. Also, super-plasticizer was added, it is a powerful water reducing agent, it makes the possibility to produce self-leveling concrete with the water content necessary to fully hydrate the cement particles. (SF) used in this study is produced by cutting cold drawn high tensile deformed steel wire. The wire is of 25 mm length with crimped shape to have more contact surface (average crimped height 2.4 mm) and circular cross section (1.0 mm diameter). It is suitable for concrete composite because of its higher strength characteristics, also it complies with ASTM A820. High steel deformed type of 16mm diameter for main steel and mild smooth steel type of 6 mm for stirrups were used.

CONCRETE MIXES PROPORTION

Six mixes were used as follows, one mix without fiber as a control mix, three mixes with different contents of (SF) to achieve target cubic strength 70 MPa to study the effect of fiber content on the behavior of (HSFRC) circular columns, and also to get the optimum content of fiber.

These mixes are identical except for the volume percentage of fiber. For these mixes, the cement content was 475 kg/m³ and the water cement ratio 0.31 by weight, 10% of silica fume by weight of cement and 18.75 lit. super-plasticizer per cubic meter were also used.

Also two mixes were used to achieve target concrete compressive strength 55 and 85 MPa by using 0% and 15% of silica fume, to study the effect of concrete compressive strength on the behavior of (HSFRC) circular columns.

Table 1. Concrete Mixes Proportion

Mix No.	Cement (kg)	Silica Fume %	Fibres Content (Vf)%	Dolomite (kg)	Sand (kg)	Water (lit)	Super Plast. (lit)
M 1	475	10%	0	1225	612.5	143	18.75
M 7	475	10%	0.25%	1225	612.5	143	18.75
M 8	475	10%	0.50%	1225	612.5	143	18.75
M 9	475	10%	1%	1225	612.5	143	18.75
M 10	450	0%	0.25%	1244	622	162	14
M 11	475	15%	0.50%	1225	612.5	143	18.75

* Sand / Dolomite = 1/2

* Water / (Cement + Silica Fume) = 0.31

DESCRIPTION OF TESTED COLUMNS

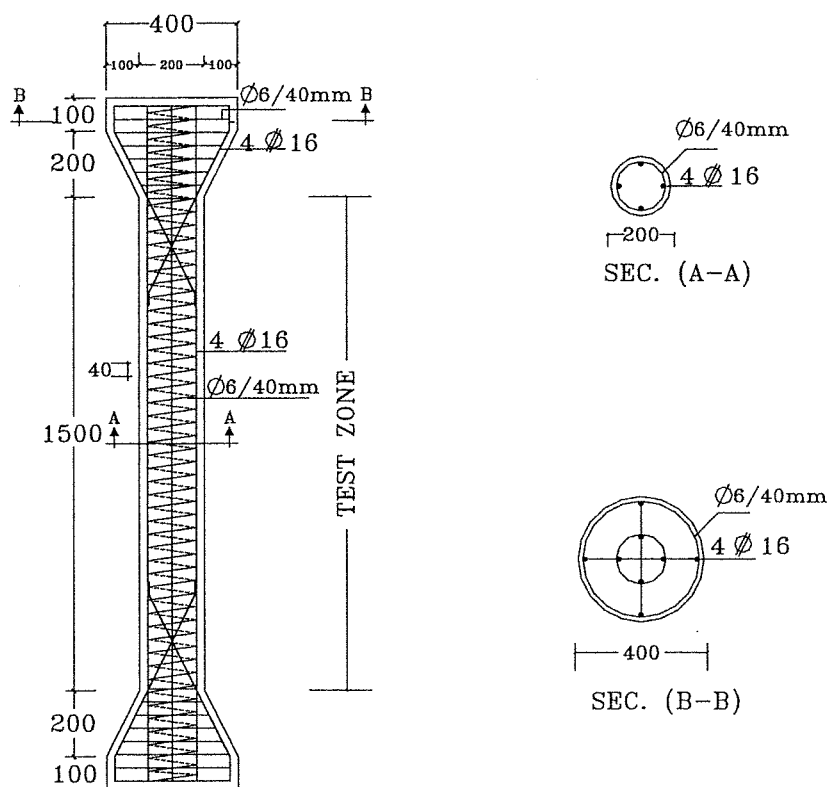
All columns were 200 mm in diameter and 1500 mm in length; the reinforcement bars were uniformly distributed around the core perimeter giving a reinforcement ratio (2.56 %) of concrete

section. The core diameter, D_c was measured in relation to outside diameter of the transversal steel and was kept as constant as possible with 180 mm diameter for columns, yielding a core area equal to (72.2%) of the gross area of the columns. Steel forms were used in casting the test column specimens. To avoid premature failure, the formworks of columns were hunched at the ends.

Concrete was cast vertically in the forms, and was mechanically compacted using external vibrator to ensure full compaction of concrete inside the forms. Table 2 and Fig. 1 show all details of properties of tested columns specimens and all information concerning cube compressive strength; f_{cu} , at the time of testing.

Table 2. Details of Properties of Tested Column Specimens

Specimens	CR	C1sf	C2sf	C3sf	C4sf	C5sf
Fibres Content (Vf)%	0.0	.25 %	0.5 %	1.0 %	.25 %	0.5 %
Compressive Strength MPa	67.6	66.1	72.9	67.7	50.2	81.9
Variables	Reference	Fibres Content			Compressive strength	
Reinforcement	Longitudinal	4 Φ 16				
	Transverse	6mm@40 mm spiral				



all dimensions in mm.

Fig. 1. Reinforcement Details of the Tested Columns Specimens

TEST SETUP AND INSTRUMENTATION

The columns were tested by using 5000-kN AMSELLER Hydraulic Compression Machine. The setup for each test consisted of installing the tested column specimen in a vertical position between the machine heads. The machine heads insured that the load eccentricity was maintained at all stages of loading, also head bearing plates were adjusted to prevent any eccentricity from incorrect position or column head leveling. Fig. 2. shows a general view of test setup. The tested columns were loaded to failure. For each tested column, the data recorded were ultimate load capacity, concrete strains and steel reinforcement strains.

Strains were measured in the test zone of concrete for all tested columns specimens. The vertical strain in concrete of tested column specimens was measured using Linear Variable Displacement Transducers (LVDTs). The data from (LVDTs) were connected to Data Acquisition System. The position of (LVDTs) is shown in Fig.3 ..

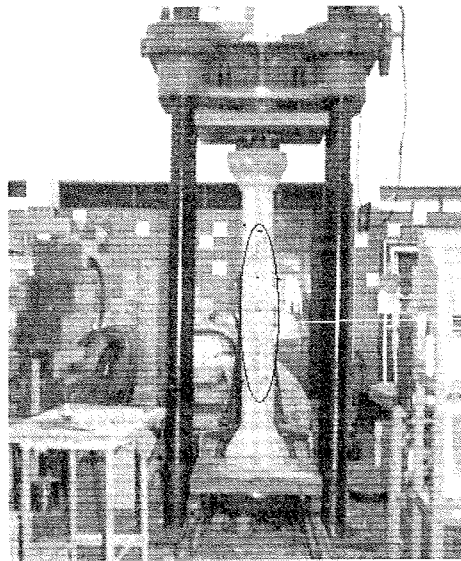


Fig. 2. Test set up of Tested Columns

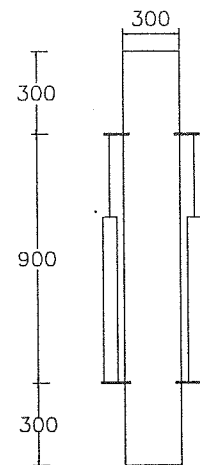
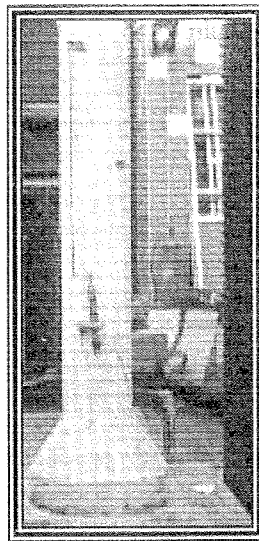


Fig. 3. The Position of LVDTs

Longitudinal and transverse steel strains were measured by electrical-resistance strain gages. Each column had two gages; one was placed in the mid height of longitudinal bar and the other on the top of stirrup. All strain gages were placed before casting columns. Strain gages with 10mm length, and 120 ohms, gage factor (2.04) were fixed by using epoxy. A wax film was layered on top of strain gage to protect it. All strain gages were placed facing the outside of the column. The steel strain gages were connected to strain indicator device to obtain the steel strains directly. The position of strain gauges on stirrups and longitudinal steel is shown in Fig.4.

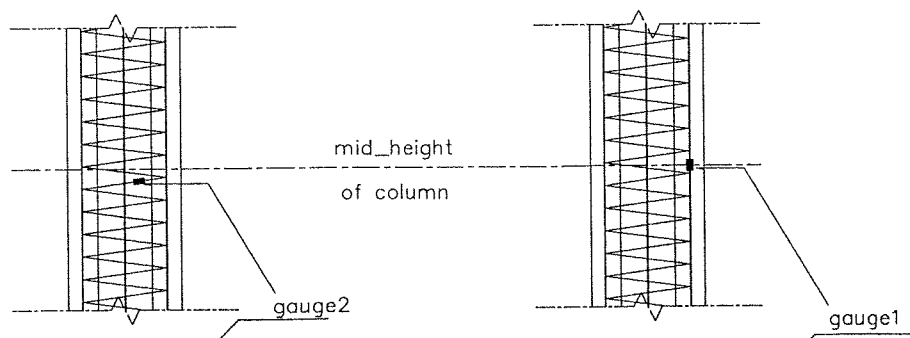


Fig. 4. Strain Gauges on Stirrups and Longitudinal Steel

The specimens were placed between the machine heads and centered with its axis. Throughout the test setup, care was taken to ensure that the applied load was as concentrically as possible. The strain gages wires were then connected to the data measuring devices. Although a rigorous procedure was followed for aligning the specimens, some eccentricities were unavoidable. Before loading, zero readings of steel strains and vertical concrete displacement were recorded. The pressure pump was activated and the load was applied gradually with load increment of 100 kN up to failure load. At each load value, total applied load, concrete vertical displacement and steel strains were recorded. Due to the nature of the loading system, it was difficult to obtain the complete unloading part of the load-deformation curves. However, an attempt was made to manually control the machine in order to trace the unloading part of the curves to some extent.

STRENGTH AND DUCTILITY MEASUREMENTS

Axial Strength

Two methods were used to evaluate the column strength. The first method is defined as the ratio between the confined core strength f_{cc} and the unconfined concrete strength f_{co} , based on the concrete cube strength f_{cu} . It is called the effective confinement.

$$k_c = f_{cc} / f_{co}$$

The second method is defined as the difference between the confined core strength, f_{cc} , and the unconfined concrete strength, f_{co} . It is called the gain of the confined core strength:

$$\Delta f_c = f_{cc} - f_{co}$$

Column Ductility

Ductility is defined as the ratio of the axial strain of the confined core at a certain level of loading in the descending part to the axial strain of the confined core at the ultimate strength, it is called axial strain ductility ratio. Ductility measures based on the confined core stress-strain curves have been used in this study. The strain ductility ratios were:

$$\begin{aligned} \mu_{0.85P_u} &= \xi_{0.85P_u} / \xi_{cc}; \\ \mu_{0.50P_u} &= \xi_{0.50P_u} / \xi_{cc}; \\ \mu_{0.85f} &= \xi_{0.85f} / \xi_{cc}; \text{ and} \\ \mu_{0.50f} &= \xi_{0.50f} / \xi_{cc} \end{aligned}$$

Where:

- $\mu_{0.85P_u}$ = Axial strains ductility ratio corresponding to $\xi_{0.85P_u}$;
- $\mu_{0.50P_u}$ = Axial strains ductility ratio corresponding to $\xi_{0.50P_u}$;
- $\mu_{0.85f}$ = Axial strains ductility ratio corresponding to $\xi_{0.85f}$; and
- $\mu_{0.50f}$ = Axial strains ductility ratio corresponding to $\xi_{0.50f}$

Fig. 5. shows ductility measurements for concentrically – loaded column.

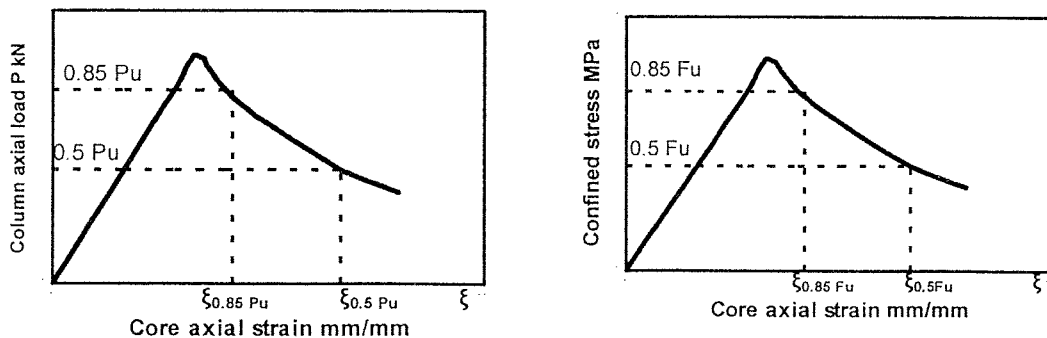


Fig. 5. Ductility Measurements for Concentrically – Loaded Column

COLUMNS TEST RESULTS

(Stress-Strain) Relations for Confined Core

Test results were recorded to plot stress-strain curves to establish the actual behavior of confined concrete core for circular columns. Fig. 6. shows the relations between confined core stress and core strain.

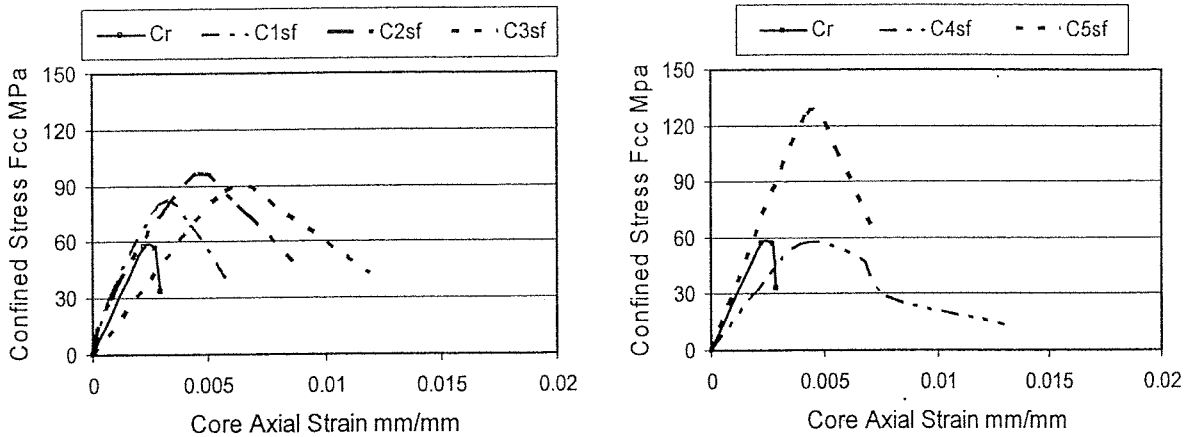


Fig. 6. Typical Stress-Strain for Tested Columns

Table 3. summarizes the significant results obtained from stress– strain curves of the confined concrete core for all tested columns. These results include the unconfined concrete stress f_{co} , which was considered to be 67% of the standard cube strength f_{cu} . The confined core axial strain ξ_{cc} at a confined core strength at 85% and 50% of the confined core stress of the descending part, $\xi_{0.85}$ and $\xi_{0.50}$, respectively. These values were obtained from table 3. and used to calculate the specimen ductility. The numerical results contained in same table indicate that the core axial strains are more sensitive to the degree of confinement and the concrete compressive strength than the core strength.

Table 3. Summary of Results for Tested Columns

Specimens		C R	C1sf	C2sf	C3sf	C4sf	C5sf
f_{cu} (MPa) Actual		67.6	66.1	72.9	67.7	50.2	81.9
Unconfined Concrete Strength $f_{co}=0.67 f_{cu}$ MPa		45.3	44.3	48.8	45.4	33.6	54.9
Confined Concrete Strength f_{cc} MPa		72.9	77.2	86.0	79.9	53.2	113.5
Confined Core Axial Strain mm/MM ξ	ξ_{cc}	0.00224	0.00211	0.00379	0.00421	0.00411	0.0029
	$\xi_{0.85Pu}$	0.0027	0.00278	0.00511	0.00577	0.006	0.00386
	$\xi_{0.50Pu}$	0.0029	0.00296	0.00621	0.00711	0.00686	0.00438
	$\xi_{0.85f}$	0.00271	0.00272	0.00504	0.0058	0.00592	0.0038
	$\xi_{0.50f}$	0.0029	0.00295	0.00587	0.007	0.00661	0.00444
Δ Gain of Core Strength $f_c = f_{cc} - f_{co}$ MPa		27.6	32.9	37.2	34.5	19.6	58.6

Effective Confinement $K_c = f_{cc}/f_{co}$		1.61	1.74	1.76	1.76	1.58	2.07
Axial Strain Ductility Ratio	$\mu_{0.85P_u}$	1.21	1.32	1.35	1.37	1.46	1.33
	$\mu_{0.50P_u}$	1.29	1.40	1.64	1.69	1.67	1.51
μ	$\mu_{0.85f}$	1.21	1.29	1.33	1.38	1.44	1.31
	$\mu_{0.5f}$	1.29	1.40	1.55	1.66	1.61	1.53

Longitudinal and Transverse Reinforcement Strains

Data of longitudinal and transverse reinforcement strains were recorded by using electric strain gauges and data logger system. Fig. 7. shows the relations between load and longitudinal steel strain. Strains measurements recorded for longitudinal reinforcement indicated that the steel did not reach the yielding value at ultimate loads. Fig. 8. shows the relations between load and transverse steel strain.

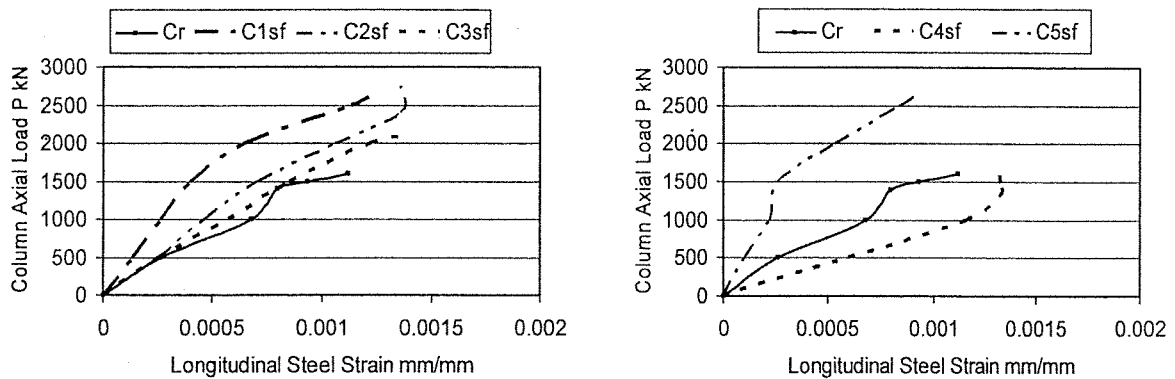


Fig. 7. Typical Load- Longitudinal Steel Strain for Tested Columns

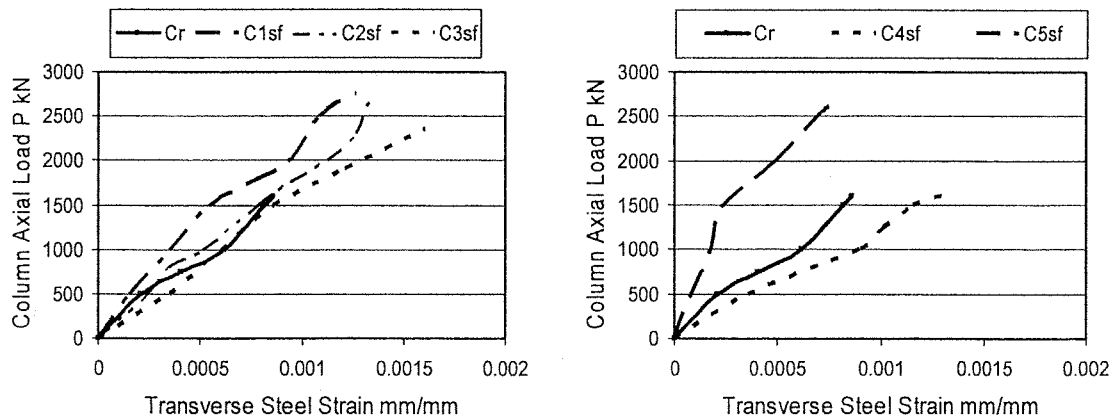


Fig. 8. Typical Load- Transverse Steel Strain for Tested Columns

Ultimate and cracking loads

Table 3. shows the ultimate and cracking load for all tested columns. The recorded ultimate and cracking loads for columns with concrete fibres are greater than that of the control column without fibres for both types of fibres. The results show that the crack load varied between 86 to 93% of ultimate load for columns with concrete steel fibers. However, for the control column, the crack load was 85% of the ultimate load.

Table 4. the ultimate and cracking load for tested columns

Specimen	CR	C1sf	C2sf	C3sf	C4sf	C5sf
f_{cu} (MPa) Actual	67.6	66.1	72.9	67.7	50.2	81.9
Ultimate Load (kN) P_u	2100	221	2480	2400	1640	3400
Cracking Load (kN) P_{cr}	1790	1990	2230	2060	1490	3160
P_{cr} / P_u	0.85	0.90	0.90	0.86	0.9	0.93

Cracking Behavior and Failure Mode

The first crack strength of (HSFRC) circular columns depends primarily on concrete characteristics rather than fibers parameters. After cracking, the effect of fibers initiate, they carry the entire load and tends to prevent continuity and propagation of cracks. The cover and core act as one part, therefore, they have the same stress behavior up to higher load levels than (HSRC) columns. The cover efficiency has a better effect after cracking, more deformations

followed by buckling of longitudinal bars, then failure occurs in a more ductile behavior than column without fibers. Columns with steel fibers have a better effect on the behavior of cracking and failure mode than column without fiber. Fig. 9. shows crack pattern at failure of tested columns..

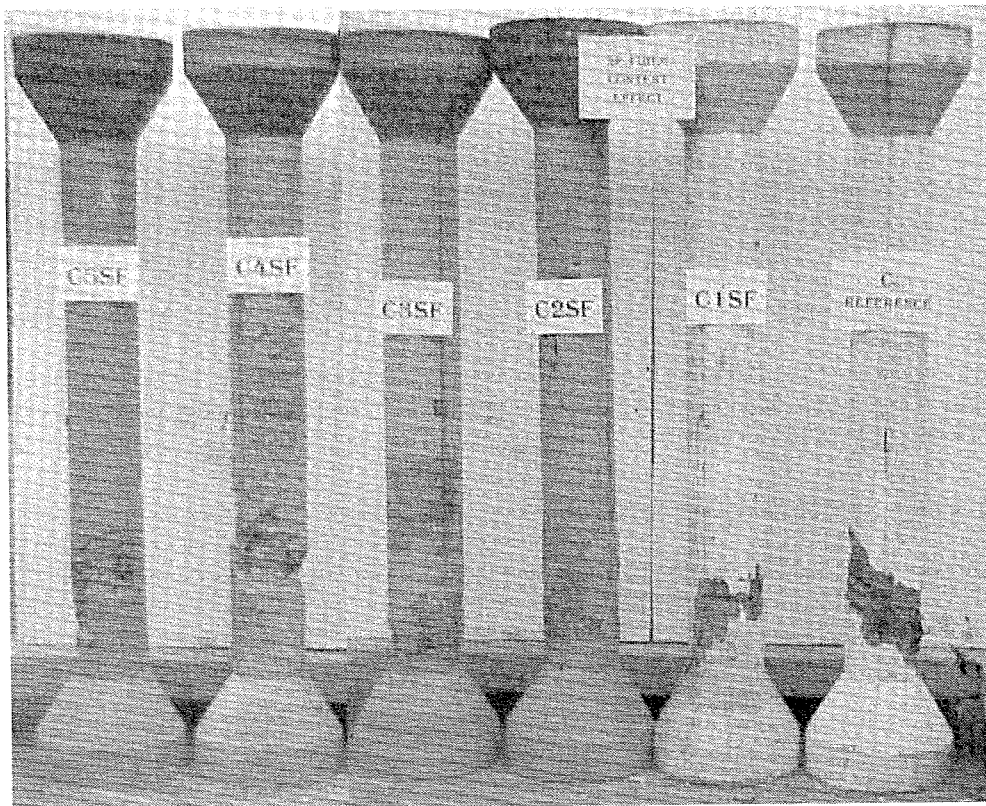


Fig. 9. crack pattern at failure of tested columns

EFFECT OF TEST VARIABLES ON BEHAVIOR OF CIRCULAR COLUMNS

The observed results of experimental tests aimed to investigate the effect of adding steel fibers on the behavior of (HSRC) columns. These show that the addition of any content of steel fibers

in concrete matrix leads to a noticeable change in load-strain response of concrete especially in the descending portion.

The ascending portion of load-strain curve changes slightly when compared with column without fibers but the descending portion of load-strain curve changes tremendously. The slope of the descending part decreases with increasing fibers content. With the addition of a reasonable amount of fibers to the concrete, higher strength and ductility can be achieved.

The ultimate load is slightly increased when compared with reference column without fibers, i.e. fibers had insignificant effect on ultimate load. Adding fibers increase the tensile stresses; but ultimate load didn't increase significantly as the failure was still mainly due to compression. Fibers act as a confinement factor beside stirrups leading to an increase of the lateral confinement.

Steel Fibers Content

For high-strength reinforced concrete columns with (SF), at first, the axial concrete strains changes slightly compared with reference column without fibers. After cracking at (85 – 88%) of ultimate load, the fibrous columns had higher deformations and there was an increase in axial strains. This may be attributed to the increase of ductility due to addition of fibers.

Table 3. shows an expected ductility due to effect of adding steel fibers where, as the content of steel fibers increases, the ductility of columns increases, then matrix were transformed from brittle to ductile material. By increasing fibers content from 0.0 to 1% , the increase in ductility ratios were ranged from 13.2% to 31%. Also table 3. shows that, as the (SF) content increases, strength increases up to fibers content (0.5%), then strength decreases for specimen with fibers content (1%). Increasing (SF) content from 0.0 to 0.5% caused an increase in gain of core strength by 34.78% and effective confinement factor k_c by 9.31%. This indicates that the (SF) gives an additional confinement to columns.

Also table 4. shows that increasing (SF) content from 0.0 to 0.5% increases the cracking load by (8.93%) while adding (1%SF), the cracking load was increased by (6.70%) only. The ultimate load was, also increased by (9.52%) and increased by (7.14%) only respectively. The relationship between stress-strain in vertical bars is shown in Fig. 7.. The Fig. indicates that there was an increase in strains due to the effect of increasing fibers content. Fig. 8. shows that the transverse reinforcement strains decrease as the (SF) increase due to the confinement mechanism of (SF).

(SF) help transverse reinforcement in carrying the lateral confinement forces, i.e. the force carried by the lateral confinement forces in (SF) concrete specimens was less for the specimens without fibers.

Effect of Concrete Compressive Strength

Fig. 7. shows the effect of concrete compressive strength on deformation of columns. Concrete compressive strength and deformability are inversely proportional. A lower strength concrete column has large deformation under concentric loads than higher strength concrete columns. The results indicate a consistent decrease in deformability with increasing the concrete compressive strength.

Table 3. shows the strain ductility ratios, it has highlighted the fact that column ductility is affected by concrete compressive strength. An increase in concrete compressive strength tends to result in lower ductility. It can be concluded that as the compressive strength increase, the ductility of column decrease.

Table 4. shows the effect of the concrete compressive strength on the ultimate load. Due to the increase of concrete compressive strength, there was an increase in column ultimate load. For steel fiber specimens, increasing compressive strength by 63.14% caused an increase in column ultimate load by 92.54% and the gain in core strength was 198.97%.

Figs 8. and 9. show the longitudinal and transverse steel strains. The Figs show that there was an increase in longitudinal and transversal steel strains for low strength concrete columns

compared with those of high-strength fibers concrete columns. This may be attributed to the less observed deformation in (HSRC) columns.

CONCLUSIONS

The following conclusions were drawn based on the experimental results.

1. Content of fibres has great effect on improving the behavior of (HSFRC) circular columns. Steel fibres optimum content that affects most of the characteristics of (HSFRC) circular columns is (0.5%). It produces a gain of core strength by (34.78%) and ductility ratio increased by (27.13%), also ultimate load increased by (9.52), but increasing (SF) content up to (1%), has a best effect on the ductility.
2. The addition of any content of (SF) developed more vertical deformations in (HSFRC) circular columns. So, concrete fibres leads to a noticeable change in load-strain response of circular columns especially in the descending portion compared with column without fibres, whereas the ascending portion modified slightly, but the descending portion modified significantly. High-strength steel fibres reinforced concrete circular columns had large vertical deformations and the basic characteristic of its load-strain curve modified tremendously due to its crimped shape especially in the descending portion.
3. For (SF) circular columns with concrete compressive strength 60 MPa exhibited an acceptable level of ductility. But, an increase in compressive strength by 41.52%, the ductility ratio decreased by 22.28%, while the gain of core strength was 315% .
4. Strain measurement recorded for steel indicated that, for (HSRC) circular columns, the strains in longitudinal bars and spiral stirrups were more than (HSFRC) columns, this could be attributed to the fact that fibres act as a lateral confinement. So, strains in both longitudinal bars and spiral stirrups did not reach the yielding value at ultimate loads.

REFERENCES

1. Wafa, F. F and Ashour, S. A.(1992), "Mechanical Properties of High-Strength Fiber Concrete" ACI Material Journal. Proceedings, Vol.89, No.5, September - October, pp. 445-449.
2. Hsu, L. S., and Thomas Hsu, C. T. (1994) "Stress-Strain Behavior of Steel-Fiber High-Strength Concrete Under Compression" ACI Structural Journal, Proceeding, Vol.91, No.4, July-August, pp 448-457.
3. Taerwe, L. R. (1992), "Influence of Steel Fiber on Strain-Softening of High-Strength Concrete" ACI Material Journal, Vol.88, No. 6, January-February, pp. 54-60.
4. Hassan, A. A. (1999) "Behaviour of high-Strength Fiber Reinforced Concrete Columns Subjected to Concentric and Eccentric Axial Loads" Msc., Thesis, Faculty of Engineering, Cairo University.

LATERAL STABILITY OF DEEP-THIN FLANGED I-SHAPED BEAMS WITH VERTICAL STIFFENERS

Sherif S. Safar

Lecturer, Faculty of Engineering, Cairo University, Cairo, Egypt

Email: sherifv99@yahoo.com

ABSTRACT

In this work, the effect of vertical stiffeners on the lateral stability of deep thin flanged I-shaped beams was investigated. A mathematical model was established to compute the magnification in the warping moment capacity when edge and intermediate vertical stiffeners were utilized. Hence the magnification in the beam moment capacity was determined as per the ratio of the stiffeners torsional stiffness to the compression flange flexural stiffness. A proposed design procedure for vertically stiffened deep-thin flanged I-beams was established by substituting the derived warping moment magnification factor in the nominal moment expression for buckling limit states of beams adopted in the ECP-LRFD. The proposed design procedure was verified by the finite element method using the general purpose finite element program, ANSYS. A wide variety of beams geometric dimensions was included in the analysis to cover both inelastic and elastic warping limit states. Four types of vertical stiffeners were studied including plate, opened angle, closed angle and box-shaped stiffeners. Material and geometric imperfections were incorporated in the finite element analysis. The effect of using vertical stiffeners on moment magnification of beams was assessed to encourage designers to account for their effect in the design of deep-thin flanged beams and to select the suitable stiffeners configuration.

Keywords: Lateral torsional buckling, inelastic buckling, elastic buckling, torsion, warping, stiffeners, imperfections, residual stresses, non-linear material behavior.

ELASTIC LATERAL TORSIONAL BUCKLING OF BEAMS

The elastic lateral torsional buckling moment of a perfect I-shaped beam with restrained ends and subjected to uniform moment loading was obtained [1], [2] and [3] as the resultant moment resistance of uniform torsion moment resistance M_t and warping moment resistance, M_w , as follows:

$$M_{cr} = \sqrt{M_t^2 + M_w^2} \quad (1)$$

The value of M_t was computed by the integration of uniform shear stresses developed in the beam section when subjected to twisting moment, whereas the value of M_w was determined from the flexural shear stresses developed when the beam ends were restrained against warping. The derived expressions for M_t and M_w were given as follows [2] and [3]:

$$M_t = \frac{\pi}{L_u} \sqrt{EI_y GJ} \quad (2)$$

$$M_w = \frac{\pi^2 E}{L_u^2} \sqrt{C_w I_y} \quad (3)$$

Where E is the young's modulus of elasticity, G is the shear modulus, L_u is the unbraced length of the compression flange, J is the I-section torsional constant, I_y is the moment of inertia about the beam weak axis of bending, Y axis (see Fig. 1) and C_w is the warping constant. For I-shaped sections composed of constant thickness plate elements such that the i^{th} plate with width b_i at least ten times its thickness, t_i , the value of J was determined as follows [1]:

$$J = \sum \frac{b_i t_i^3}{3} \tag{4}$$

For doubly symmetric I-shaped sections, the warping constant, C_w , is proportional to the square of the section depth, h and was determined as follows [3]:

$$C_w = \frac{I_f h^2}{2} \tag{5}$$

where I_f is the moment of inertia of the flange about the Y axis (see Fig. 1).

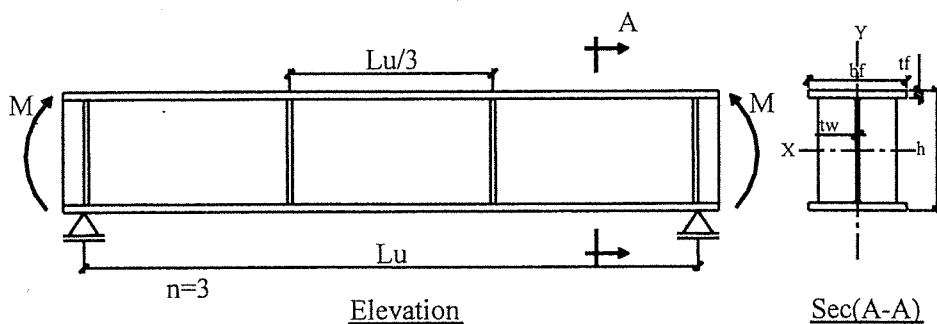


Fig. 1: Geometric Configuration of Vertically Stiffened Deep-Thin Flanged Beams

Neglecting the moment of inertia of the web about the Y axis, the expression of M_w presented in Equation (3) can be re-written as follows:

$$M_w = \left(\frac{\pi^2 I_f E}{L_u^2} \right) h \tag{6}$$

The warping moment resistance can be converted into a couple force equals to $P_{cr} = \pi^2 I_f E / L_u^2$ times the beam depth h . Consequently, it was concluded that the warping moment resistance, M_w , is controlled by the out-of-plane flexural buckling strength of the compression flange. The critical moment, M_{cr} , is governed by the larger of M_t and M_w (see Equation 1). Neglecting the contribution of the web in the moment of inertia of the beam about its minor axis of bending, the value of M_w exceeds M_t when the following relation is satisfied:

$$\left(\frac{h b_f}{L_u t_f} \right) > 0.80 \tag{7}$$

Therefore, for shallow-thick flanged sections the torsion resistance exceeds the warping resistance due to small values of h , and M_{cr} is mainly controlled by M_t . On the other hand, for deep-thin flanged sections the warping resistance controls due to a pronounced C_w that is proportional to the square of the section depth, h . Hence, the lateral stability behavior of such beams can be approximated by the out-of-plane buckling behavior of the compression flange acting as a hinged-hinged column.

MATHEMATICAL MODEL

Figure 2 illustrates the lateral torsional buckling mode shape for a vertically stiffened I-shaped beam. Since the rotation of the beam section takes place about a point other than the shear center, the out-of-plane deflection of the compression flange exceeds that of the tension flange at the same location along the beam span. Consequently, the slope of the compression flange elastic line at any section exceeds the slope of the tension flange at the same section and the vertical stiffener is subjected to twisting moment resulting from the lateral torsional buckling of the beam. Therefore, based on the above discussion, the lateral stability of deep-thin flanged beams can be represented by the flexural buckling problem of a hinged column with length L_y equals to the unbraced length of the beam and provided with rotational springs (see Fig. 3) at the location of vertical stiffeners. The moment of inertia of the column equals to the compression flange inertia about the beam weak axis of bending. Neglecting the web contribution to the stiffeners torsional stiffness, the rotational spring constant, R , was assumed to be equal to the stiffeners torsional stiffness.

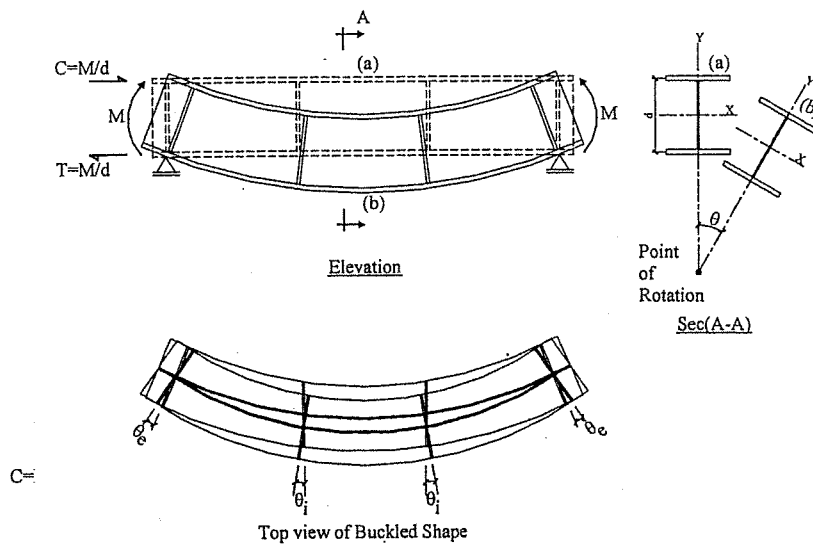


Fig. 2: Lateral Torsional Buckling of I-shaped Beam

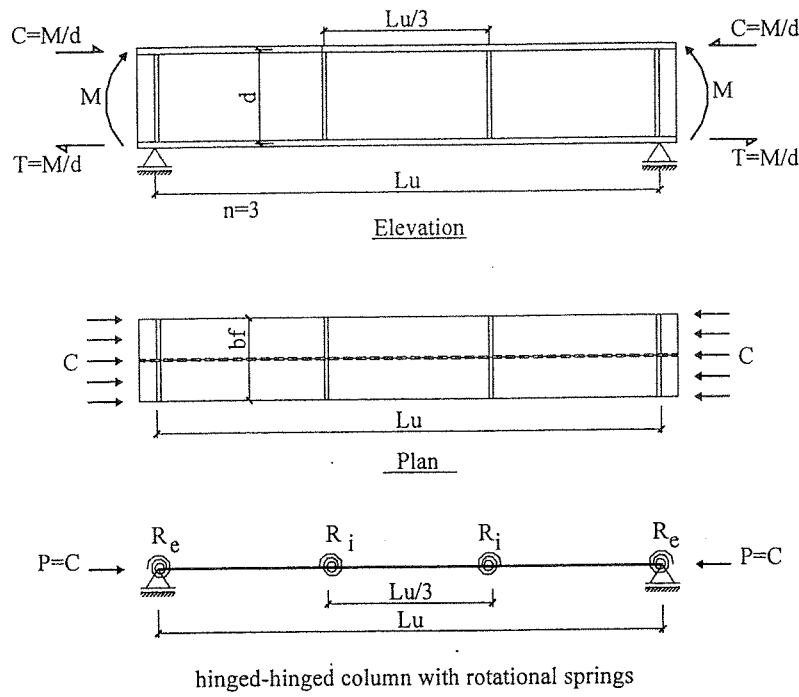


Fig. 3: Modeling of Compression Flange of Stiffened I-Beams

Beams with Edge Stiffeners:

The lateral stability of deep-thin flanged beams with edge stiffeners was studied by computing the elastic buckling load of a hinged-hinged column with rotational springs at both ends. Using the neutral equilibrium method, the elastic buckling load was determined by writing the equilibrium equation for the deformed configuration [3]. For a non-trivial solution, the elastic buckling load was determined by solving the characteristic equation:

$$\sin\left(\frac{KL_u}{2}\right) = \frac{KL_u}{\sqrt{(KL_u)^2 + (R_e L_u)^2}} \tag{8}$$

Where

$$K = \sqrt{\frac{P_{cr}}{EI_f}}$$

R_e = torsional stiffness of edge stiffeners.

The solution of Equation (8) can be obtained numerically by trial and error. However, an approximate expression for the critical load, P_{cr} can be determined as follows:

$$P_{cr} = \frac{S_f \pi^2 I_f E}{L_u^2} \tag{9}$$

Where

S_f = warping moment magnification factor.

$$= \left[1 + 3 \tanh \frac{\gamma_e}{8 + \sqrt{\gamma_e}} \right] \tag{10}$$

γ_e = stiffness ratio of edge stiffeners.

$$= \left(\frac{R_e L_u}{EI_f} \right) \tag{11}$$

Using Equation (6), the warping moment resistance of deep thin-flanged beams with vertical edge stiffeners can be determined as follows:

$$M_w = S_f \left(\frac{\pi^2 I_f E}{L_u^2} \right) h \tag{12}$$

It is to be noted that the warping moment magnification factor, S_f , computed by Eqs (10) equals to unity for $R_e = 0$ to represent the case of an un-stiffened beam. On the other hand, for large values of R_e the factor S_f reduces to 4 to mimic the case of beams with clamped ends against rotation about the Y axis.

Beams with Edge and Intermediate Stiffeners

The lateral stability of a deep-thin flanged beam with edge and intermediate vertical stiffeners is analogous to the flexural buckling of a column provided with rotational springs at both ends and at locations of intermediate stiffeners as depicted in Fig.3. It was assumed herein that all intermediate stiffeners were equally spaced and dividing the beam span into n intervals (see Fig. 3). The elastic buckling load of such column configuration was determined by writing the equilibrium equation for each interval and compatibility conditions at both ends of each interval. The critical load was determined by solving the characteristic equation obtained by equating the determinant of the matrix of coefficients to zero. Similar to the case of edge stiffened beams, an approximate mathematical expression for the numerical solution of the critical load was determined as the product of the hinged column buckling load and the warping moment magnification factor, S_f , given by the relation:

$$S_f = \left[1 + 3 \tanh \frac{\gamma_e}{8 + \sqrt{\gamma_e}} \right] \left[1 + \frac{\gamma_i}{10} \right]^{n-2} \tag{13}$$

Where $\gamma_i =$ ratio of torsional stiffness of intermediate stiffeners to the flexural stiffness of the compression flange about Y axis.

$$= \left(\frac{R_i L_u}{E I_f} \right) \tag{14}$$

$R_i =$ torsional stiffness of intermediate stiffeners.
 $n =$ number of equally spaced intervals (i.e. $n \geq 2$)

It can be concluded from Equation (13) that adding an intermediate stiffener at mid-span (i.e. $n = 2$) will have no effect on pronouncing the beam warping moment resistance since the slope of the flange elastic line at mid-span is zero, hence the stiffener is not twisted and will not provide any additional strength to the beam. The warping moment magnification factor, S_f , can be substituted in Equation (12) to determine the warping moment resistance of deep-thin flanged beams with edge and intermediate stiffeners.

Torsional Stiffness of Vertical Stiffeners:

The torsional stiffness, R , of stiffeners is defined as the twisting moment required for a unit twisting angle. Table 1 lists the value of R for each stiffener configuration as per elastic theory solution [4]. For each stiffener configuration, the ratio of the torsional stiffness, R , to stiffener volume, V_s , was also listed in Table 1.

It is evident from Table 1 that box and closed angle stiffeners are by far more efficient compared to plate and opened angle stiffeners respectively. On the other hand, the effect of adding plate or opened angle stiffener is almost identical as depicted by their R/V_s values listed in Table 1. The ratio R/V_s for box stiffeners is almost 70 times that of a plate stiffener whereas the R/V_s ratio of closed angle stiffener is almost 40 times that of an opened angle stiffener. This means that the use of box or closed angles stiffeners provides the most economic means to increase the moment capacity of beams using vertical stiffeners. Referring to Table 1, box stiffeners

provide more economic solution compared to closed angle stiffeners as long as $(1+f)h/fb_s \leq 2h/a$ otherwise closed angle stiffeners will be more economic.

PROPOSED DESIGN METHOD

The nominal flexural strength, M_n , of non-compact deep-thin flanged beams with vertical stiffeners can be computed as per the provisions of the Egyptian Code of Practice based on the load and resistance factor design [5], ECP-LRFD, with the application of the warping moment magnification factor, S_f , (Eqs.(10) and (13)). The value of M_n is computed according to the unbraced length as follows:

For yielding limit states ($L_u \leq L_p'$):

$$M_n = M_{p'} \tag{15}$$

$$M_{p'} = \left[M_p - (M_p - M_r) \left(\frac{\lambda - \lambda_p}{\lambda_r - \lambda_p} \right) \right] \tag{16}$$

$$L_{p'} = \left[L_p + (L_p - L_{rs}) \left(\frac{M_p - M_{p'}}{M_p - M_r} \right) \right] \tag{17}$$

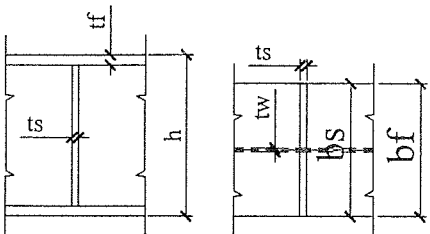
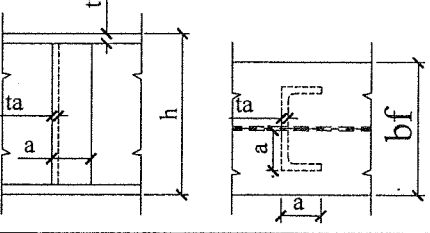
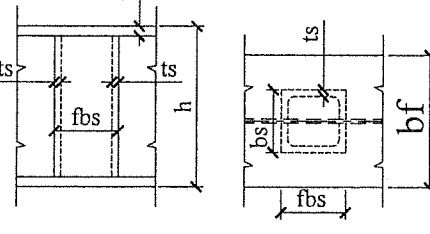
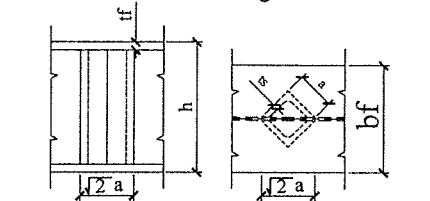
For inelastic lateral torsional buckling limit states ($L_p' < L_u \leq L_{rs}$):

$$M_n = C_b \left[M_p - (M_p - M_r) \left(\frac{L_u - L_p}{L_{rs} - L_p} \right) \right] \leq M_p \tag{18}$$

For elastic lateral torsional buckling limit states ($L_u > L_{rs}$):

$$M_n = C_b S_x \sqrt{\left(\frac{1380 A_f}{d L_u} \right)^2 + \left(\frac{20700 S_f}{\left(\frac{L_u}{r_T} \right)^2} \right)^2} \tag{19}$$

Table 1: Torsional Stiffness of Vertical Stiffeners

Type of Stiffener	Torsional Stiffness, R [4]	R/V_s
<p>Plate</p> 	$\frac{G b_s t_s^3}{3h}$	$\frac{G}{3 \left(\frac{h}{t_s} \right)^2}$
<p>Opened Angle</p> 	$\frac{4G a t_a^3}{3h}$	$\frac{G}{3 \left(\frac{h}{t_a} \right)^2}$
<p>Box</p> 	$\frac{2G f^2 b_s^3 t_s}{(1+f)h}$	$\frac{G}{\left(\frac{(1+f)h}{f b_s} \right)^2}$
<p>Closed Angle</p> 	$\frac{G a^3 t_a}{h}$	$\frac{G}{4 \left(\frac{h}{a} \right)^2}$

Where:

- M_p = plastic moment of the beam = $Z_x F_y \leq 1.5 M_y$.
- Z_x = plastic section modulus of the beam section.
- F_y = yield stress of steel used in beam section.
- M_y = yield moment of the beam = $S_x F_y$.
- S_x = elastic section modulus of the beam section.
- λ = governing slenderness parameter, flange or web width-to-thickness ratio.
- λ_p = limiting width-to-thickness ratio for compact flange or web [5].
- λ_r = limiting width-to-thickness ratio for non-compact flange or web [5].
- L_p = maximum un-braced length for yielding limit state = $80 r_y (F_y)^{1/2}$.
- L_p' = modified maximum un-braced length for yielding limit states.
- r_y = radius of gyration about weak axis of bending.
- L_{rs} = maximum un-braced length for inelastic lateral torsional buckling limit state.

$$= \left(\frac{1380 A_f}{d F_L} \right) \sqrt{0.50 \left(1 + \sqrt{1 + (2XS_f F_L)^2} \right)} \quad (20)$$

$$X = \left(\frac{0.104 r_T d}{A_f} \right)^2$$

$F_L =$ proportional limit stress
 $= F_y - 0.7 \text{ t/cm}^2$ (for rolled sections)
 $= F_y - 1.16 \text{ t/cm}^2$ (for welded built-up sections)
 $A_f =$ area of compression flange.
 $d =$ total depth of the beam
 $r_T =$ radius of gyration of compression flange and one-sixth the web about weak axis of bending.
 $C_b =$ bending coefficient to account for non-uniform moment diagrams [5].

Equations (15), (16) and (17) are used to determine the modified M_p and L_p to account for non-compact flange or web plates. If both the flange and web plates satisfy the compact limit, λ_p , Equation (16) reduces to M_p and Equation (17) reduces to L_p . On the other hand, if either the flange or the web satisfies the non-compact limit, λ_r , Equation (16) will reduce to M_r and Equation (17) will reduce to L_r . Equation (19) was essentially based on the elastic lateral torsional buckling moment (Equation (1)) with the application of the warping moment magnification factor, S_r and bending coefficient, C_b . The flexural design strength of beams shall be taken as the product of the bending strength reduction factor of 0.85 and the flexural nominal strength given by Eqs. (15), (18), and (19) and shall not be less than the applied ultimate moment load.

FINITE ELEMENT ANALYSIS

Verification of Warping Moment Magnification Factor:

In this section the warping magnification factor, S_r , was verified by comparing the magnification in elastic buckling moment obtained from the finite element solution to that obtained by the proposed mathematical model. A finite element model for each beam configuration was established using the general purpose finite element program, ANSYS [6]. All flange, web and stiffener plate elements were modeled by the isoparametric finite strain shell element, Shell181, built in ANSYS element library as depicted in Fig. 4. The beam was assumed to be simply supported in the plane of bending with the compression flange laterally braced in the out-of-plane at both ends. The beam was subjected to a uniform moment loading by applying a couple force at both ends as depicted in Fig. 3. The moment magnification factor was determined from the finite element solution as the ratio of the elastic buckling moment of the stiffened beam, M_{ns} , to that of an identical un-stiffened beam configuration, M_{nu} . Figure 5 depicts the lateral-torsional buckling mode obtained from ANSYS for an I-shaped beam provided with edge and intermediate stiffeners.

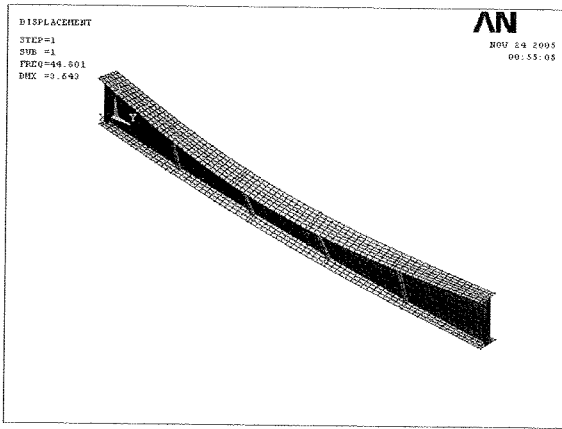


Fig. 5: Lateral-Torsional buckling mode for an I-shaped beam with vertical Stiffeners

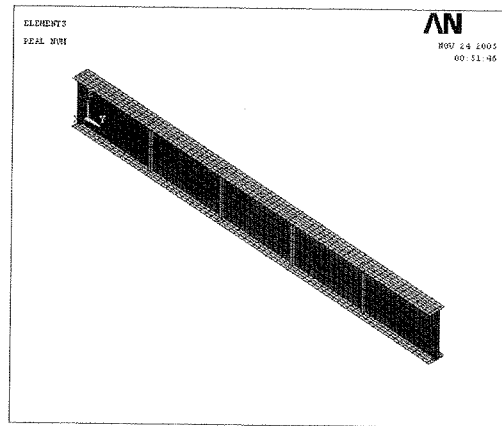


Fig. 4: Finite Element Model for an I-shaped beam with vertical Stiffeners

Elastic buckling analysis of beams with edge stiffeners

Based on the work presented above, the parameters that affect the elastic buckling moment of an edge stiffened beam include: beam slenderness parameter, L_u/r_T , ratio of warping moment resistance to torsional moment resistance represented by the ratio, $hb_f/L_u t_f$ and stiffness ratio of edge stiffeners, γ_e . In order to verify the moment magnification obtained using the factor S_f over a wide range of beam configurations, the value of each of the above parameters was varied independently within practical limits. The effect of stiffener shape was also investigated by considering the four stiffener shapes depicted in Table 1.

The moment magnification factor, M_{ns}/M_{nu} obtained from the finite element solution was compared to that computed using Equations (1), (2), (10) & (12) in Figs 6 to 9. Results indicate that the proposed mathematical model provides acceptable results compared to the finite element solution with maximum percentage difference of 3%. Figure 6 indicates that the stiffener shape is ineffective as long as the stiffness ratio, γ_e was kept unchanged. Both mathematical and numerical results indicated that the change in moment magnification was insignificant for large values of L_u/r_T when all other parameters were kept unchanged as depicted in Fig. 7. However, for L_u/r_T less than 90 the proposed mathematical method was conservative compared to finite element results. On the other hand, the moment magnification was pronounced with the increase in γ_e since the stiffeners provide more rotational restraint to the compression flange as depicted in Fig. 8. The moment magnification factor computed by the proposed mathematical model was in good agreement with finite elements results for $hb_f/L_u t_f \geq 1.5$, however, for shallow beams with smaller values of $hb_f/L_u t_f$ the proposed model was conservative compared to finite element results since the magnification in the torsional moment resistance is neglected (see Fig. 9).

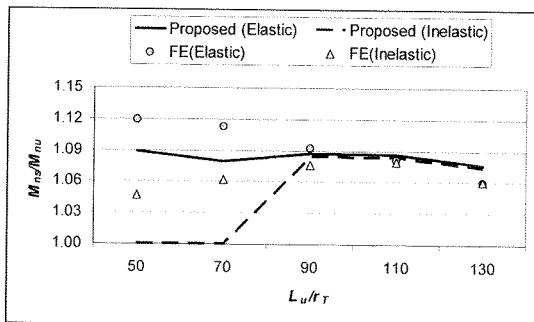


Fig. 7: Effect of L_u/r_T on M_{ns}/M_{nu}

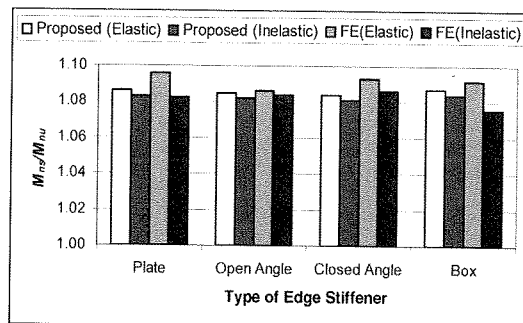


Fig. 6: Effect of stiffeners type on M_{ns}/M_{nu}

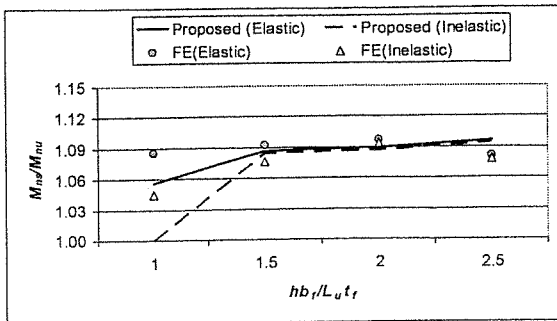


Fig. 9: Effect of $hb_f/L_u t_f$ on M_{ns}/M_n

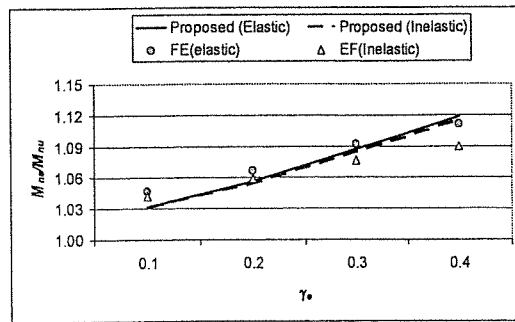


Fig. 8: Effect of γ_e on M_{ns}/M_{nu}

Elastic buckling analysis of beams with edge and intermediate stiffeners

The factor S_f determined by Equation (13) was verified by comparing the moment magnification factor, M_{ns}/M_{nu} computed using Eqs (1), (2), (12) and (13) to that obtained from the elastic buckling finite element analysis. The number of panels, n , based on number of intermediate stiffeners (see Fig.3) and stiffness ratio, γ_i , of intermediate stiffeners were added to the independent parameters describing the beam configuration. Each independent parameter was varied separately over a wide range of practical values and the value of M_{ns}/M_{nu} obtained from the finite element solution was compared to the respective value determined by the proposed mathematical model.

Comparison of results indicated good agreement between finite element and mathematical model results with maximum percentage difference of 4.4%. Similar to edge stiffened beams, the shape of intermediate stiffeners was insignificant for identical γ_i values (see Fig. 10). On the other hand, the moment magnification was proportional to the parameters n , γ_e and γ_i as depicted in Figs 11, 12 and 13 respectively since the warping moment resistance was increased by increasing the rotational restraint provided by vertical stiffeners. Similar to edge stiffened beams, the finite element results were in good agreement with the proposed mathematical model for $L_u/r_T \geq 90$ and $hb_f/L_u t_f \geq 1.5$ as depicted in Figs 14 and 15 respectively. However, for beams with smaller slenderness ratio L_u/r_T and/or shallow beams with smaller $hb_f/L_u t_f$ values the proposed mathematical model was generally conservative with maximum percentage difference of 4.4% compared to the finite element solution.

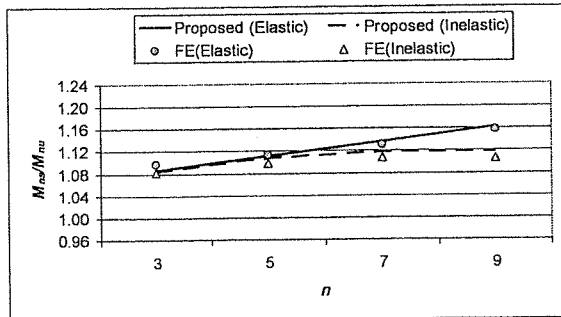


Fig. 11: Effect of n on M_{ns}/M_{nu}

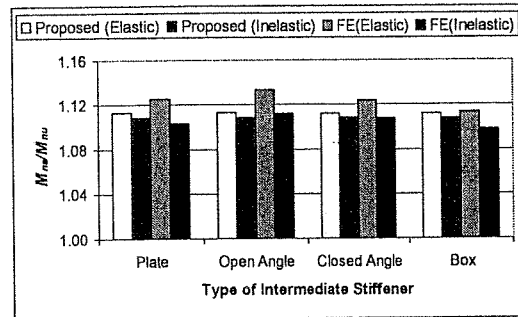


Fig. 10: Effect of type of intermediate stiffener on M_{ns}/M_{nu}

Verification of Proposed Design Method

The design method presented above was verified by comparing the magnification in nominal moment strength obtained by Eqs. (15) to (18) to the magnification in inelastic buckling moment M_n obtained by ANSYS incorporating material and geometric imperfections. The adopted geometric imperfection configuration was similar to the first Eigen mode of the perfect beam (Fig. 5) with an amplitude equals to 1/1000 of the beam unbraced length. A non-linear stress-strain relation [7] was adopted to account for residual stresses effect [3]. Loads were applied incrementally using the arc-length method [6] and the converged solution at each load

increment was obtained by iterations using the modified Newton-Raphson technique. The analysis was terminated when the maximum moment capacity was reached.

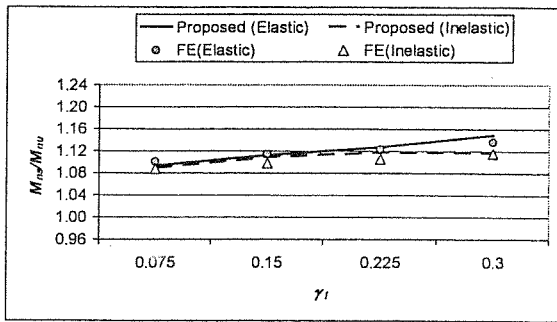


Fig. 13: Effect of γ_i on M_{ns}/M_{nu}

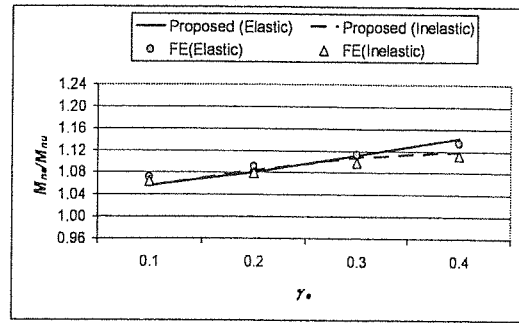


Fig. 12: Effect of γ_e on M_{ns}/M_{nu}

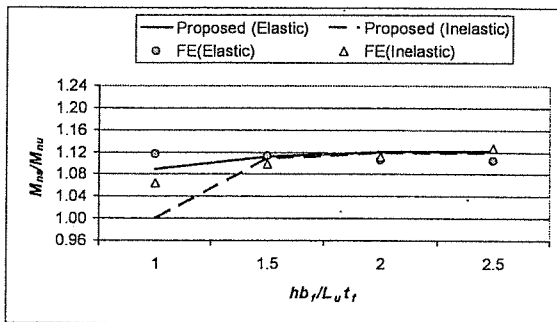


Fig. 15: Effect of $hb_f/L_u t_f$ on M_{ns}/M_{nu}

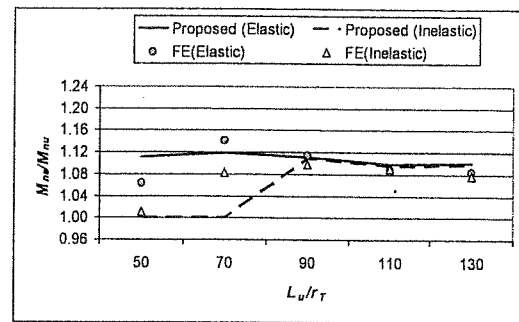


Fig. 14: Effect of L_u/r_T on M_{ns}/M_{nu}

Inelastic buckling analysis of beams with edge stiffeners

Figures 6 to 9 indicate that the finite element results agreed well with the proposed design method when material and geometric non-linearities effects were incorporated with maximum percentage difference of 6.2%. Similar to the elastic buckling analysis results, the effect of stiffeners shape on moment magnification, M_{ns}/M_{nu} , was insignificant as long as the stiffener stiffness ratio, γ_e was unchanged (see Fig.6). Figure 7 indicated that for large values of L_u/r_T the inelastic buckling analysis results were in good agreement with the proposed design method. However, when L_u/r_T was reduced, the proposed design method was conservative since the moment capacity was limited by yielding limit states as per ECP-LRFD design equations. The moment magnification computed by the proposed design method agreed with that obtained by finite element results and was proportional to γ_e as depicted in Fig. 8. For large values of $hb_f/L_u t_f$, the elastic and inelastic buckling results for M_{ns}/M_{nu} were almost identical since elastic buckling controls the behavior and were close to proposed design method results (see Fig. 9). However, when $hb_f/L_u t_f$ was reduced the proposed design method was conservative compared to finite element results as indicated above.

Inelastic buckling analysis of beams with edge and intermediate stiffeners

Similar to the elastic buckling results, Fig. 10 illustrates that the effect of stiffeners shape on M_{ns}/M_{nu} was insignificant when material and geometric non-linearities were introduced. Figures 11 to 13 also depict that the finite element results were in good agreement with the proposed design method. The moment magnification was proportional to n , γ_e and γ_i as depicted in Figs. 11, 12 and 13 respectively. However, the inelastic buckling analysis revealed that for large values of n , γ_e or γ_i the moment magnification was controlled by yielding and further increase in n , γ_e or γ_i turned to be impractical. Similar to edge stiffened beams, the moment magnification obtained by elastic and inelastic analysis was almost identical for large values of L_u/r_T and $hb_f/L_u t_f$ as depicted in Figs. 14 and 15 respectively. However, when the value of L_u/r_T and/or $hb_f/L_u t_f$ decreased the proposed design method was conservative as explained above.

ASSESSMENT OF VERTICAL STIFFENERS EFFECT ON MOMENT CAPACITY OF BEAMS

In this section, the effect of using vertical stiffeners was evaluated based on the moment magnification, M_{ns}/M_{nu} , computed by the proposed design method (Eqs. (15), (16) & (17)). Since the factor M_{ns}/M_{nu} is dependent on many parameters including: torsional stiffness and number of stiffeners, flexural stiffness of the beam compression flange, slenderness ratio for lateral torsional buckling, width-to-thickness ratio of web and flanges, and ratio of warping moment resistance to torsion moment resistance. Therefore, the effect of vertical stiffeners was evaluated qualitatively by graphical representation of M_{ns}/M_{nu} by assuming practical values of beam configurations.

Beams with Edge Stiffeners

Compact beams

Figure 16 depicts the variation of M_{ns}/M_{nu} with the un-braced length, L_u , normalized by the limiting buckling length of the unstiffened beam [5], L_{ru} (Equation 20 with $S_f = 1.0$), for different values of γ_e . The moment magnification, M_{ns}/M_{nu} , is proportional to γ_e for all values of L_u/L_{ru} , however, when $L_u \leq L_p$ the use of vertical stiffeners was ineffective since the moment capacity was governed by the plastic moment and M_{ns}/M_{nu} reduced to unity regardless to the value of γ_e . The moment magnification, M_{ns}/M_{nu} , increases when L_u increases from L_p to L_{ru} and reaches its maximum value at $L_u = L_{ru}$. However, when L_u exceeds L_{ru} the moment magnification is reduced, this is mainly attributed to the reduction in the ratio of the warping moment resistance to the torsion moment resistance with the increase in L_u and therefore the addition of vertical stiffeners is less effective. Consequently, the moment magnification, M_{ns}/M_{nu} , is proportional to the ratio $hb_f/L_u t_f$ (see Fig. 17) since the use of vertical stiffeners pronounces the warping moment resistance that governs the lateral stability of beams with larger $hb_f/L_u t_f$ value.

Non-Compact beams

When the width-to-thickness ratio of the beam flange and/or web exceeds the compact limit [5], the full plastic moment capacity reduces to M_p' (Equation 16) to account for local buckling of flange and/or web. On the other hand, the limiting unbraced length for yielding limit states increases to L_p' (Equation 17). Therefore, the use of vertical stiffeners is ineffective as long as $L_u \leq L_p'$ since the moment capacity is governed by flange and/or web local buckling in that range. Similar to compact beams, the moment magnification, M_{ns}/M_{nu} , increases when L_u increases from L_p' to L_{ru} and reaches its maximum value at $L_u = L_{ru}$ as depicted in Fig. 18. Similar to compact beams, the moment magnification is proportional to the ratio $hb_f/L_u t_f$.

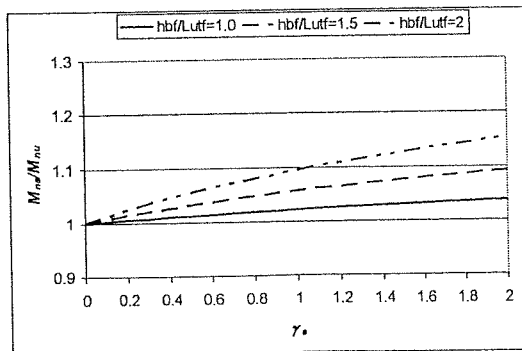


Fig. 17: Effect of $hb_f/L_u t_f$ and γ_e on M_{ns}/M_{nu}

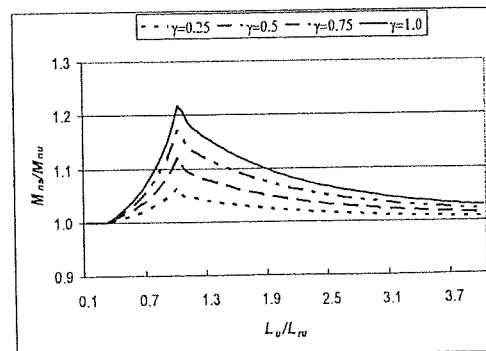


Fig. 16: Effect of γ_e and L_u on M_{ns}/M_{nu}

Figure 19 depicts the effect of the web slenderness parameter on M_{ns}/M_{nu} . It is shown that as the web slenderness increases the maximum moment capacity of the beam, M_p' is reduced and bounds the ratio M_{ns}/M_{nu} . Therefore, it is concluded that there is a limiting value of γ_e for each beam configuration beyond which the increase in γ_e is ineffective. Consequently, flange and/or web local buckling stipulates an upper bound on the moment magnification factor. However, for $M_{ns} < M_p'$, the effect of flange and or web slenderness parameter on moment magnification remains insignificant.

Beams with Edge and Intermediate Stiffeners

Compact beams

Since addition of intermediate stiffeners increases the warping moment resistance magnification factor, S_f , the moment magnification M_{ns}/M_{nu} is proportional to stiffness ratio of intermediate stiffeners γ_i and number of stiffeners as depicted in Figs. 20 and 21 respectively. Comparison of Figs. 20 and 21 indicates that the effect of increasing the number of stiffeners is more significant on moment capacity compared to increasing the stiffness ratio, γ_i with the number of stiffeners unchanged.

Non-compact beams

The behavior of non-compact beams with edge and intermediate stiffeners is similar to non-compact beams with edge stiffeners only. When the flange and/or web slenderness parameter exceeds the compact limit [5], the limiting unbraced length for yielding limit states, L_p' increases and the maximum moment capacity, M_p' decreases regardless to stiffeners configuration. The moment magnification M_{ns}/M_{nu} is proportional to n and γ_i , however, the former is more effective as illustrated by comparing Figs. 22 and 23. Since the flange and/or web local buckling bounds the moment capacity of stiffened beams, M_{ns} to M_p' , there will be a certain limiting configuration of intermediate stiffeners (i.e. γ_i and n) beyond which the increase of stiffeners stiffness ratio or number will be ineffective as depicted in Figs. 24 and 25. Such limiting configuration is dependent on the slenderness ratio, L_u/r_t , stiffness ratio of edge stiffeners, γ_e and the ratio $hb_f/L_u t_f$.

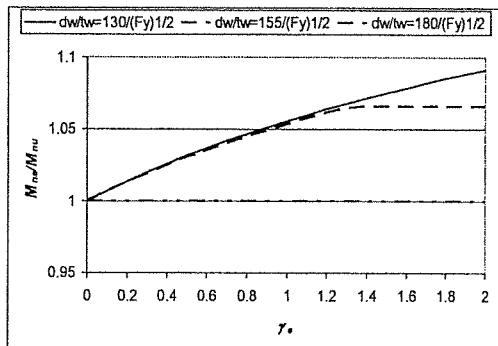


Fig. 19: Effect of d_w/t_w and γ_e on M_{ns}/M_{nu}

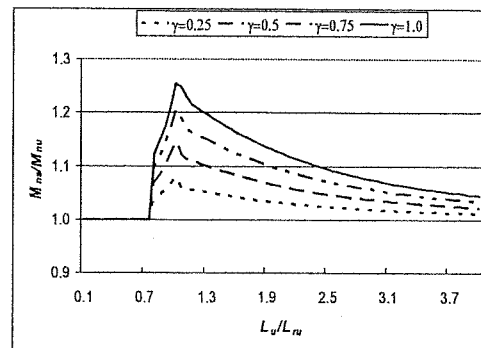


Fig. 18: Effect of γ_e and L_u on M_{ns}/M_{nu}

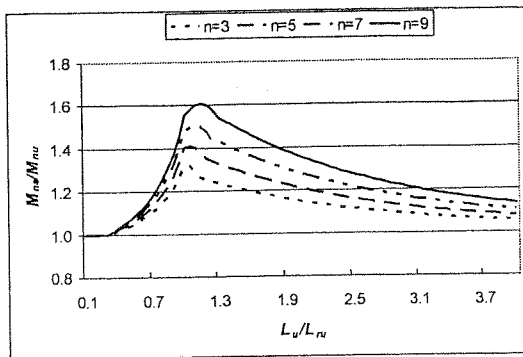


Fig. 21: Effect of n and L_u on M_{ns}/M_{nu}

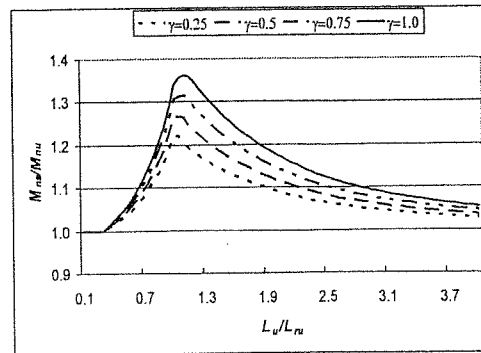


Fig. 20: Effect of γ_i and L_u on M_{ns}/M_{nu}

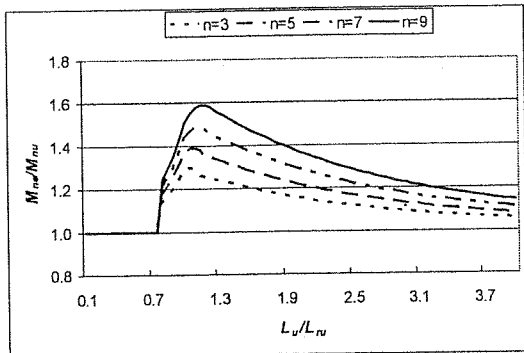


Fig. 23: Effect of n and L_u on M_{ns}/M_{nu}

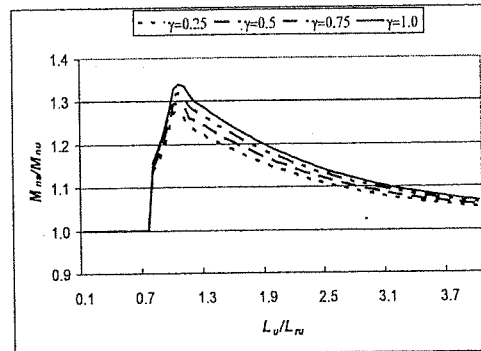


Fig. 22: Effect of γ_i and L_u on M_{ns}/M_{nu}

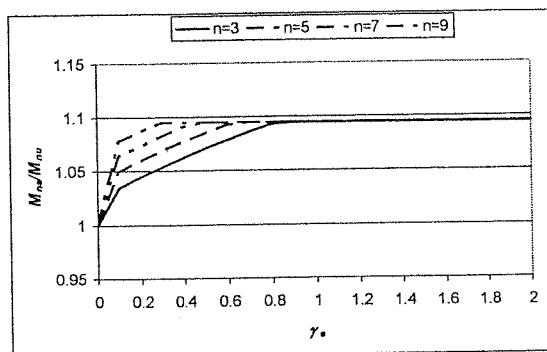


Fig. 25: Effect of n and γ_e on M_{ns}/M_{nu}

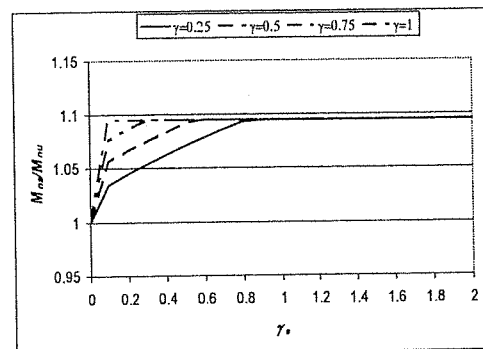


Fig. 24: Effect of γ_i and γ_e on M_{ns}/M_{nu}

SUMMARY AND CONCLUSIONS

In this work, the effect of vertical stiffeners on the lateral stability of deep-thin flanged beams was investigated analytically and numerically. An expression for the warping moment resistance magnification factor was obtained analytically by representing the stiffened beam compression flange by a hinged-hinged column provided with rotational springs at locations of vertical stiffeners. A proposed design method for stiffened beams was established by introducing the warping moment magnification factor into the nominal moment expressions for buckling limit states of beams adopted by the ECP-LRFD. The proposed design method was verified numerically by comparison with finite element results considering a wide variety of stiffened beams configurations that cover elastic and inelastic buckling limit states. Four types of stiffeners were incorporated in the analysis including: plate, opened angles, closed angles and box stiffeners. Based on the proposed design method, it was recommended to use box shaped or closed angles stiffeners since they possess the largest torsional stiffness with the least weight of added material. It was concluded that the moment magnification is mainly dependent on the

torsional stiffness and number of stiffeners used. On the other hand, the use of vertical stiffeners is ineffective as long as the unbraced length is less than the limiting unbraced length for yielding limit states. For compact and non-compact beams, the moment magnification due to the use of vertical stiffeners is peaked when the unbraced length is equal to the limiting unbraced length for inelastic buckling of the respective unstiffened beam configuration. For non-compact beams, there exists a limiting stiffeners configuration corresponding to each beam configuration beyond which the increase in stiffeners stiffness or number will be ineffective as the moment capacity is limited by yielding and local buckling limit states.

REFERENCES

1. Salmon, C.G. and Johnson, J.E.(1996), "Steel Structures Design and Behavior", 4th Edition, Printice Hall.
2. Machaly, E.S. (2002), "Behavior, Analysis and Design of Structural Steel Members", 2nd Edition.
3. Chen, W.F. (1983), "Structural Stability Theory", 2nd Edition, McGraw Hill.
4. Boresi, A.P. and Sidebottom, O.M. (1985), "Advanced Mechanics of Materials", 4th Edition, John Wiley and Sons.
5. Egyptian Code of practice for Steel Construction -Load and Resistance Factor Design- (2005), 1st Edition, Housing and Building Research Center.
6. Desalvo, G.J., and Gorman, R.W.(1989), "ANSYS User's Manual", Swanson Analysis Systems, Houston, PA.
7. Safar, S.S. and El-Shaer, M. (2002), "A Column Formula for Compact and Non-Compact Compression Members, Using LRFD Method", ENGG.RES.Jour, Helwan University, Faculty of Engineering, Mattaria, Cairo, pp. 39-56.

FATIGUE STRENGTH OF CORRUGATED STEEL BOLTED LAP JOINTS UNDER FLEXURE

Hesham El-Sayed Hamed Mohammed

Associate Professor, Structural Engineering Dept., Cairo University, Egypt

Email: heshamhamed01e@hotmail.com

ABSTRACT

Soil-steel structures have been used successfully in constructing underground conduits of medium and short spans. In the recent years, manufacturers of these structures in the United States and Canada ventured into using this economic type of construction to replace the old and deteriorated short-span concrete bridges. Under the conditions of long span and shallow cover conditions, the surrounding soil may not be able to provide the required support for the structure. As a result, the conduit tends to deform more freely, given rise to a considerable increase in the bending moment under both the construction load and the live loads. As a result, several cases of distress are observed in these structures. In this work, the fatigue behavior of lap joints used in constructing the structure is studied. The effect of bolt arrangement, steel sheet thickness and initial misalignments on the plastic moment capacity and in the moment rotation is investigated. The study recommended a group of (S-N) curves, derived from the least squares method of analysis, recommended for the design of the lap joints under cyclic loading.

Keywords: Short Span Bridges; Fatigue strength, Fatigue tests, Lap Joints, Finite Element Analysis, Corrugate Steel Sheets; Bolted Joints.

INTRODUCTION

A soil-steel structure derives its load carrying capacity from the interaction of highly flexible steel structure with the surrounding engineering soil. Over the last five decades, soil-steel structures have been used successfully in constructing underground conduits of medium and short spans. These structures are built with different shapes (circular pipes, ellipses, pipe arches, arches, and reentrant arches and under different ranges of soil cover (shallow and deep). These structures are constructed from corrugated steel sheets lapped together using bolted joints to form the required shape. In the recent years, manufacturers of these structures in United States and Canada ventured into using this economic type of construction to replace old and deteriorated short-span concrete bridges. The economic viability in using them for relatively long spans is mainly dependant on the required minimum depth of soil cover, since any increase in the soil cover will directly effect the construction cost associated with the amount of backfill and the need for longer ramps. For this reason, attempts are made to build these structures under the shallowest possible depth of cover to increase the structure economy. An example of such conditions exists at the Cheese Factory Bridge, Located in Wellington County Ontario, Canada which built in 1984, with depth of soil cover of 2 m [1]. Under the conditions of long span and shallow cover conditions, the surrounding soil may not be able to provide the required support for the structure. As the result, the conduit tends to deform more freely, given rise to a considerable increase in the bending moment under both the construction load and the live loads. Traditionally, the design of soil steel structures is based on compression theory, in which it is hypothesised that the corrugated steel sheets are subjected only to compression. This

assumption is considered to be accurate for structures under high depth of cover to radius ratio having circular cross-section and backfilled carefully with well compacted engineering soil. To account for the bending moment due to the conditions mentioned above, The Federal Highway Administration in USA developed the computer package Culvert Analysis and Design CANDE [2]. This package is using the finite element method in calculating the bending moment in the corrugated steel and thus it can be used in the design. Also, in designing the corrugated steel sheet no account is made for the effect of the lap joint in reducing the fatigue strength of the connection. As a result several cases of distress are observed in these structures [3-5]. The effect of the bolt arrangement on the lap joint moment capacity is studied experimentally and correct and incorrect lap joint is identified [6, 7]. The correct lap joints are identified as those where the bolts in the row closer to the visible edge of the corrugated sheet should be placed in the valleys, and those in the other row on the ridges. Fig. 1 show the distress in the structure due to the bending moment in both the correct and incorrect lap joints.

In this work, the fatigue resistance of the lap joint of the corrugated steel sheet is evaluated experimentally as well as using finite element analysis. Different cases of sheet thicknesses, bolt configuration and initial misalignments are investigated.

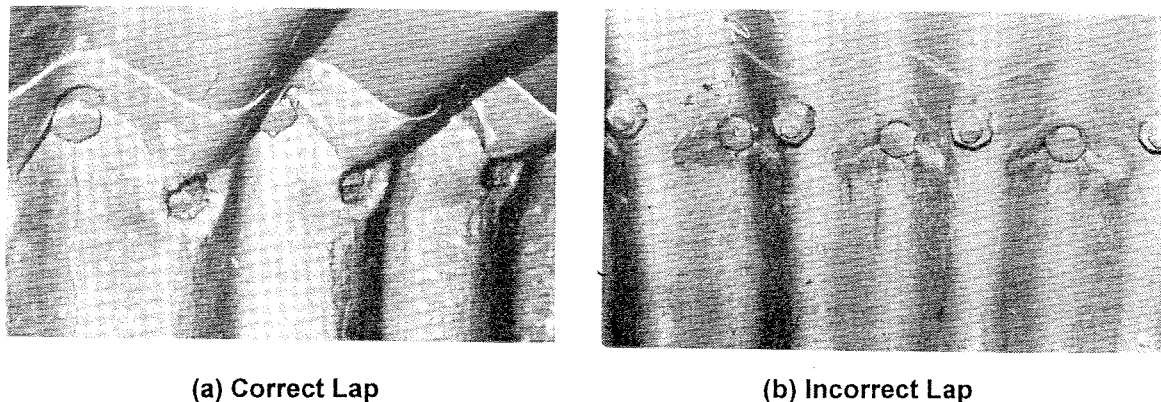


Fig. 1. Observed Joint Cracks in the Corrugated Steel Structures

FATIGUE TEST SETUP

The corrugated steel lap joints are tested using INSTRON Machine in the University of Windsor using the test setup shown in Fig. 2. The INSTRON machine consists of two major parts. The first part is the loading frame with the actuator and the second part is the computer system controlling load and displacement applied to the specimen. An additional steel frame is built and is connected to the loading frame to allow for fixing the specimen. The specimen is connected to the loading frame using bolted joints on either sides of the specimen. The specimen is loaded using two line loads connected to the loading device. To prevent any load concentration on the specimen surface, the surface of the line loads is having the same shape of the corrugation of the steel sheet surface and rubber interface element is used between the line load and the specimen. Fig. 3 shows the steel frame used for fixing the specimen, the side end connections of the specimen and the two line loads.

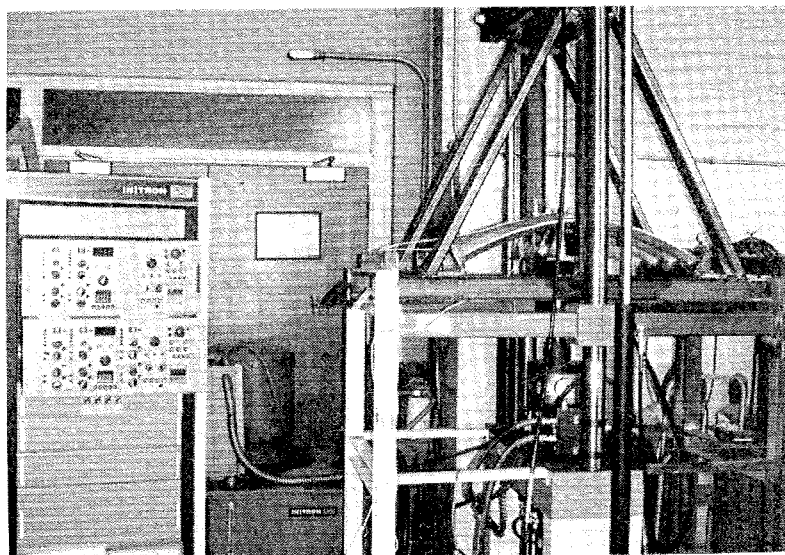


Fig. 2. Test Setup



Fig. 3. Tested Lap Joint and Loading Device

The setup described before is used to test a total of nine full scale correct lap joints. The tested joints are having 3, 4 and 5 mm thickness. The specimen is curved having 750 mm radius and 995 mm overall length. The specimen width is 457.2 mm (three complete corrugations). The joint is assembled using 18 bolts Φ 19 mm diameter, 6 bolts are used for the lap joint and the remaining 12 bolts are used for connecting the specimen to the loading frame. The bolts are having an edge distance of 35 mm and 86 mm for the bolt on the crown and on the valley respectively. These edge distances are the industrial edge distance standard for the corrugated lap joints. Torque wrench is used to tighten the bolts to 250 N.m (as recommended by Ontario Highway Bridge Design Code). Fig. 4 shows the typical lap joint tested specimen. The typical observed cracks at the bolt holes are shown in Fig. 5. The test result of the nine tested lap joints is summarized in table 1.

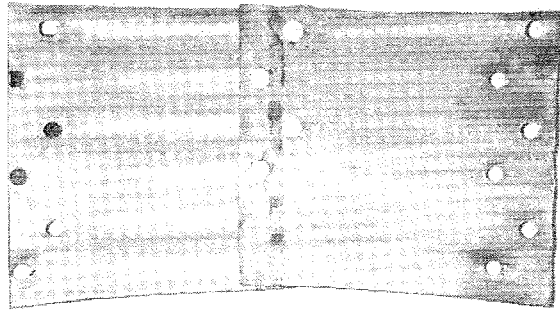


Fig. 4. Top View of Tested Joint (Correct Lap)

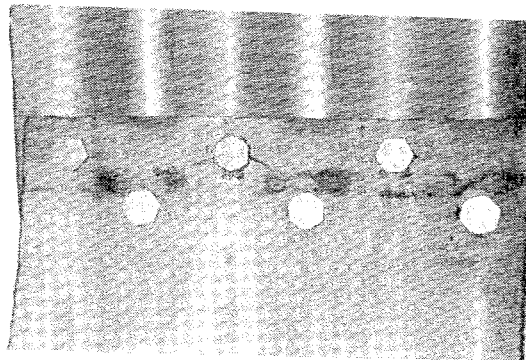


Fig. 5. Typical Observed Crack in the Tested Joints (Correct Lap)

Table 1. Fatigue Data of Corrugated Steel Lap Joint (correct lap)

Specimen	Lap Connection Type	Plate Thickness	Sr	N
		(mm)	(Mpa)	(Cycle)
CORR-31	Correct	3	110	2320000
CORR-32	Correct	3	135	500000
CORR-33	Correct	3	151	920000
CORR-41	Correct	4	112	1240000
CORR-42	Correct	4	146	470000
CORR-43	Correct	4	162	165000
CORR-51	Correct	5	136	530000
CORR-52	Correct	5	147	330000
CORR-53	Correct	5	170	100000
UNCORR-31	Incorrect	3	43	335619
UNCORR-32	Incorrect	3	73	27485
UNCORR-33	Incorrect	3	92	11545
UNCORR-41	Incorrect	4	35	1300000
UNCORR-42	Incorrect	4	55.5	120000
UNCORR-43	Incorrect	4	75	31875
UNCORR-51	Incorrect	5	37	977677
UNCORR-52	Incorrect	5	50	165400
UNCORR-53	Incorrect	5	91	12200

FINITE ELEMENT MODEL

The multi-purpose finite element package ANSYS is used to analyze the corrugated steel lap joints. The analyzed lap joints are having the same dimensions as the tested specimens. In the analysis, the 4-Node shell elements are used to model the steel corrugated sheet. The bolts are modeled using three dimensional beam element. The bolt shank is modeled using 8 link members connecting 8 nodes on the periphery of the bolt holes on one sheet to the respective nodes on the other sheet. The total cross-sectional areas of the 8 links are equivalent to the cross-section area of the bolt shank. Both the bolt head and nut are modeled using beam elements connecting the nodes on the bolt holes periphery. Initial pre-tension is applied on the link members representing the bolt tightening. The overlap surface between the two corrugated steel sheets is covered with interface elements which would allow the separation between the two surfaces, if they are subjected to tension. The lap joints are loaded using two line loads at 298 mm distance. The load is applied using displacement control technique to allow for more stable analysis during the post peak loading. Fig. 6 shows the lap joint statical system and dimensions.

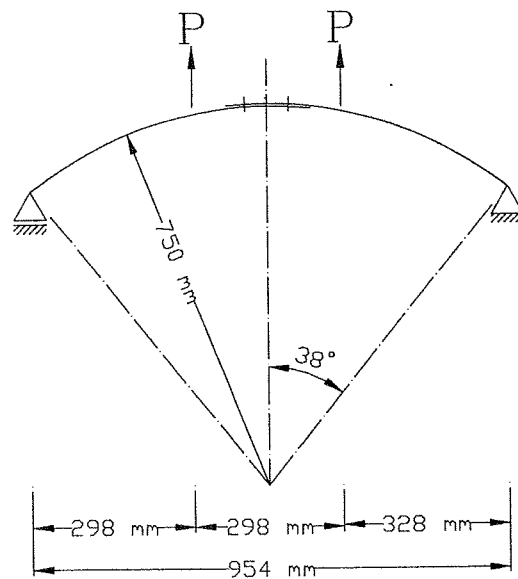


Fig. 6. Model Dimensions and Statical System

The corrugated steel is made from St 36 with Elastic Modulus of 200,000 MPa, Poisson's ratio of 0.3 and Yield stress of 230 MPa. In the analysis, the steel is modeled as elastic perfectly plastic material using von Mises failure criterion. The lap joint is considered to be simply supported. To achieve that, hinges are installed on one side of the specimen at the mid-height of the corrugation and rollers are installed on the other side. At the two sides of the lap joints, the rotation and lateral displacement were restrained to represent the continuity of the corrugated steel sheet. The finite element mesh is created and is refined at the location of the bolt holes to allow capturing the high stress variation at this area. Fig. 7 shows the typical finite element mesh used in the analysis. The model is loaded incrementally with maximum increment 0.05 of the full load and the results of all load steps are stored for future use. The analysis is conducted until the displacement at the load location reaches 60 mm (large displacement span/16).

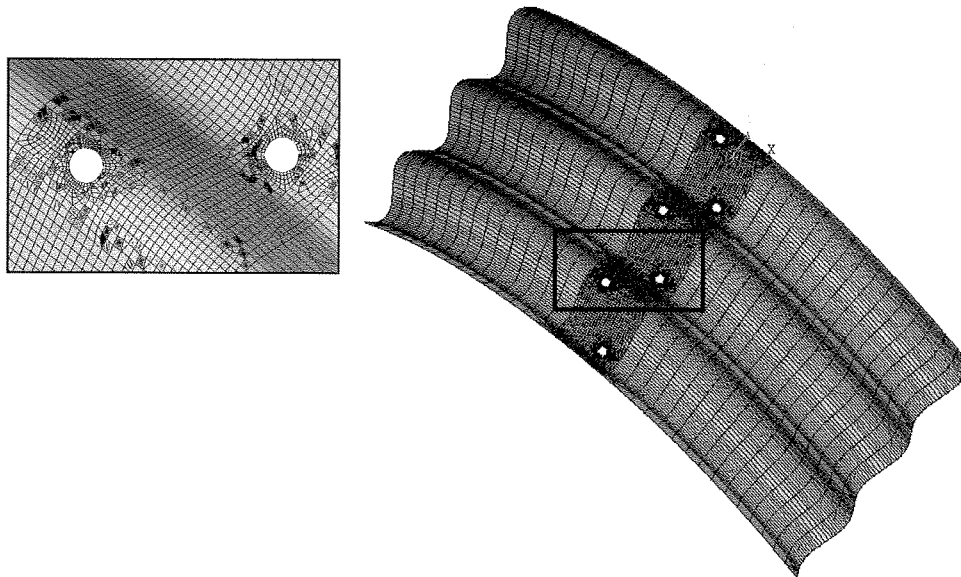
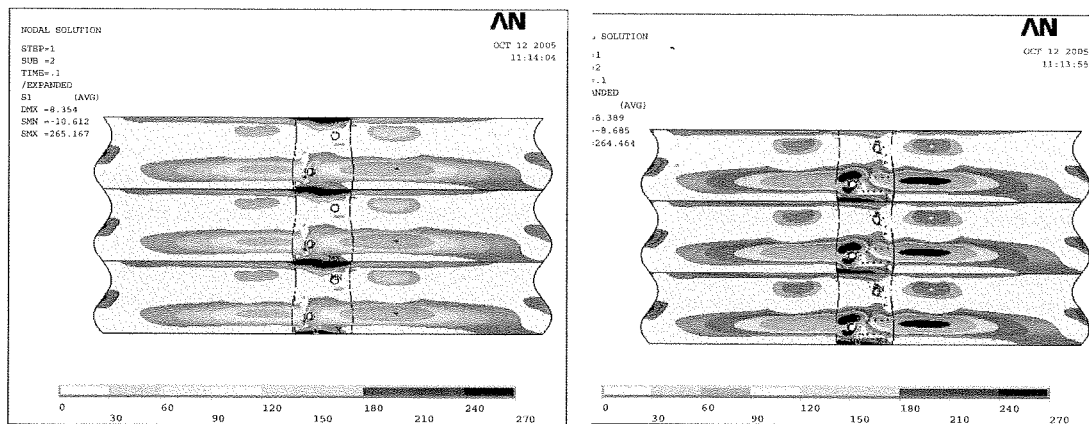


Fig. 7. Finite Element Mesh Used in the Analysis

The finite element model described above was used to analyze a total of 30 joints. Different corrugated sheet thicknesses of 3, 4, 5, 6 and 7mm were analyzed for the case of joints with correct lap and the case of joints with incorrect lap conditions. Also, for the cases mentioned above, three conditions were considered. First the condition of perfect alignment, second the condition of having 2 mm misalignment and finally the third condition of 4 mm misalignment. For all cases, the applied load, the resulting displacements, the stresses and strains were calculated at each load increment of maximum 0.05 the full load step to evaluate the joint behavior under all load levels until complete plasticity of the joint occurs. The finite element model analysis is used in evaluating the stress concentration about the bolt holes for the lap joints. Fig. 8 shows the maximum tensile stress in the corrugated steel sheets for both the correct and incorrect lap joints. From the figure, it is clear that the incorrect lap joint experiences larger zone of high tensile



stresses than the correct lap

(a) Correct Lap

(b) Incorrect lap

Fig. 8. Stress Distribution in the Lap Joint

Similar results, not shown here, are obtained for the maximum plastic strains which have an important effect on the fatigue life of the joint. It is to be noted that some high tensile stresses area is shown in the figure for both the correct and incorrect lap on the edges of the specimens which is attributed to the boundary condition effect. The finite element analysis results are used in evaluating the maximum stress and the maximum plastic strain around the bolt holes at every load step. These results are used in predicting the fatigue life of the specimen under different load levels. The low cycle fatigue concept is used in estimating the fatigue life crack. The fatigue resistance of a smooth specimen subjected to completely reversed cyclic loading can be characterized by Eqs. (1) and (2) and four material parameters which relate the stress amplitude ($Ds/2$) and to the fatigue life ($2N_f$) [8],

$$\frac{\Delta\sigma}{2} = \sigma_f' (2N_f)^b \tag{1}$$

and
$$\frac{\Delta\varepsilon}{2} = \frac{\sigma_f'}{E} (2N_f)^b + \varepsilon_f' (2N_f)^c \tag{2}$$

- Where:
- E = the elastic modulus
 - σ_f' and b = the fatigue strength coefficient and exponent
 - ε_f' and c = the fatigue ductility coefficient and exponent
 - $2N_f$ = the fatigue life of the smooth specimen

For steel ASTM A-36 mild steel the values of the parameters are , $\sigma_f' = 1,016$ MPa; $b = -0.132$; $\varepsilon_f' = 0.27$ and $c = -0.451$ [9,10]. In the presence of a mean stress (σ_o), Eq. (1) and (2) can be modified by introducing a mean stress term to account for the mean stress effect on the stress/strain-life relationships [11];

$$\frac{\Delta\sigma}{2} = (\sigma_f' - \sigma_o) (2N_f)^b \tag{3}$$

and
$$\frac{\Delta\varepsilon}{2} = \frac{(\sigma_f' - \sigma_o)}{E} (2N_f)^b + \varepsilon_f' (2N_f)^c \tag{4}$$

DISCUSSION OF RESULTS

The Experimental results are used to construct the S-N curve and to verify the finite element results for the case of correct and incorrect lap joints under no misalignment conditions. The verified finite element model is then used in constructing the curves for the other cases, correct and incorrect lap joints under 4 mm misalignment.

Definition of Design S-N curve

The definition of the design S-N curves given in the department of Energy Guidelines was adopted in the analysis. The department of Energy Guidelines defines the design S-N curve as the mean minus 2 standard deviation curve of the relevant experimental data [12]. For the normally distributed population of given mean m and a standard deviation s, the $m \pm 2s$ contains about 95% of the population [13]. The design S-N curves were determined for the case when log N is the dependant variable for the liner model.

$$\log N = A + B \text{Log } S \tag{5}$$

The design S-N curve is given by the equation

$$\log N = A + B \text{Log } S - 2 \sigma_{\log N} \tag{6}$$

Analysis of Fatigue Data

The analysis of the fatigue test data, for the correct and incorrect lap joints with no misalignments, is carried out using the least-squares method of analysis. The analysis is conducted by assuming that log N is the dependant variable, such that the linear mode, log N = A + B. Log S is determined. Thus both the parameters A and B of the S-N curve are estimated. Figures 9 and 10 show the S-N curves for the cases of correct and in correct lap joints. On the same curves, the design S-N curve is also plotted. On the same curve, the results obtained from the finite element analysis are also plotted. From the curves, it is clear that the results from the finite element analysis correlate well with the mean S-N curve obtained using the experimental results. This observation is valid for both the correct and incorrect lap joints. The finite element method is used to analyze the correct and incorrect lap joints with 4 mm misalignments. The finite element model results are used to construct the S-N curves for those cases since no experimental results were available. Figures 11 and 12 show the S-N curves for these cases. On the same curves, the design S-N curve is also plotted.

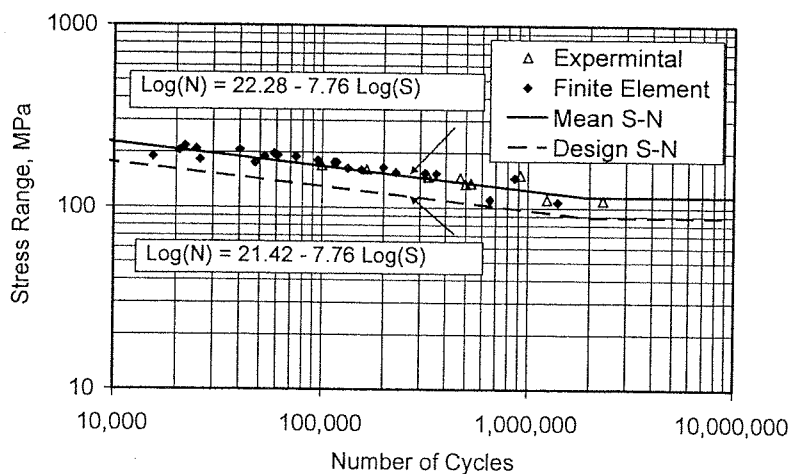


Fig. 9. S-N Curve for Correct Lap Joint (No Misalignment)

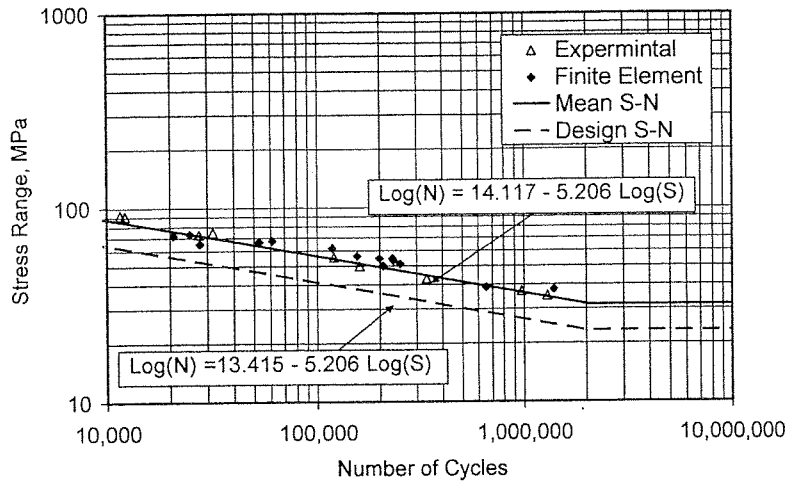


Fig. 10. S-N Curve for Incorrect Lap Joint (No Misalignment)

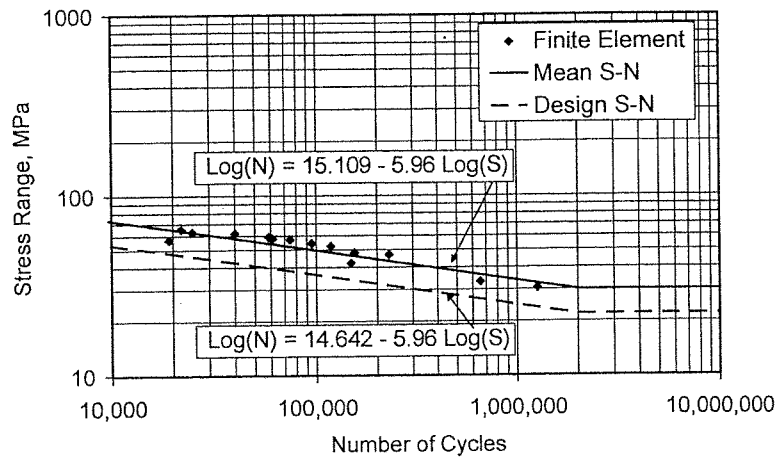


Fig. 11. S-N Curve for Correct Lap Joint (4 mm Misalignment)

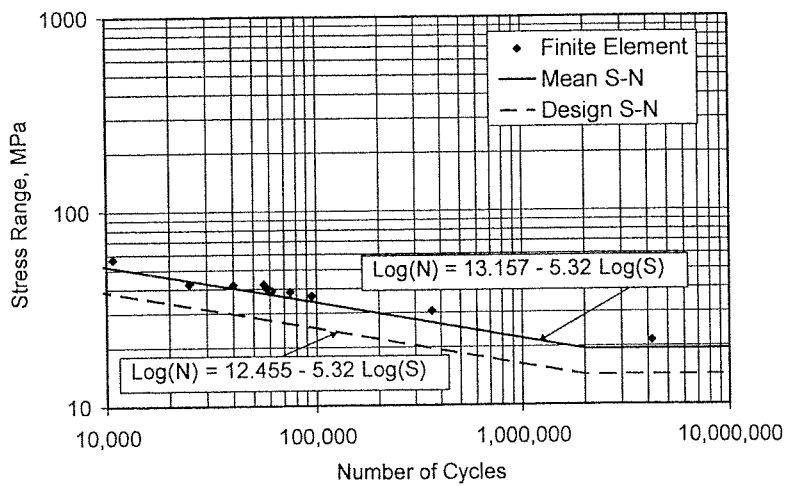


Fig. 12. S-N Curve for Incorrect Lap Joint (4 mm Misalignment)

To conduct a comparison between the behaviors of different lap joints, the design S-N curves for all the four cases are plotted in Fig. 13. From the figure, it can be observed that the correct

lap joint with no misalignment show a superior fatigue strength over the other three other connections. From the curve, it can be observed also that useing of incorrec lap, even with no misalignment, causes a tremendous reduction in the joint fatigue strength. The effect of misalignment in reducing the fatigue strength of the lap joint is also shown in the curve. This is in the contrary to the reported lap joint behavior under static loading in which the results of static loading on lap joints show that the joint misalignment and the use of incorrect lap has no effect on the ultimate moment capacity of the joint [6].

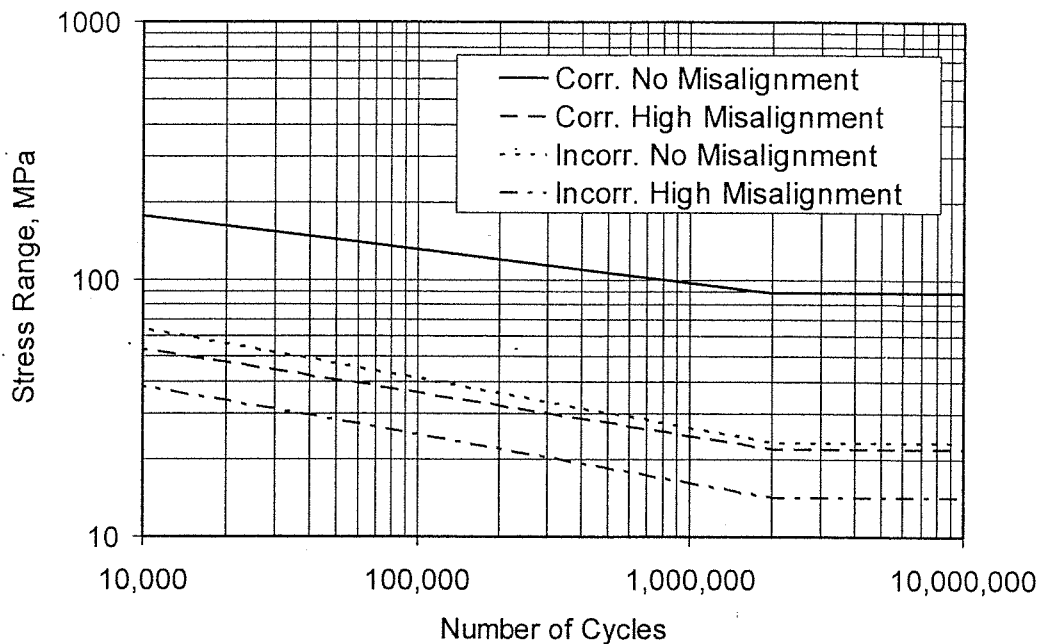


Fig. 13. Comparison between S-N Curves for Different Lap Joints Configurations

SUMMARY AND CONCLUSIONS

Fatigue tests on full scale corrugated steel lap joints are conducted on 18 lap joints. Of these 18 lap joints, 9 were of correct lap and 9 of incorrect lap. All the tested joints were having no misalignments. Also, stress analysis of corrugated steel sheet lap joint is conducted on 35 joints. Different lap joint configuration, plate thickness and misalignment level are considered. The joints are analyzed using the multi purpose finite element package ANSYS. The material plastic behavior is considered in the analysis using Von Mises yield criteria and interface element is used to allow the separation between the two metal sheet due to the tension caused by the applied bending moment. The results of finite element model are used to evaluate theatrically the fatigue life of the joints. The laboratory fatigue tests are used to verify and substantiate the finite element model results. Both the finite element model results and the laboratory test results are used to construct the design S-N curves for different lap joint conditions. Specifically, the above study shows that:

1. The correct lap joint with no misalignment has a superior fatigue strength in comparison with the incorrect lap one.
2. The lap joint misalignment causes a reduction in the fatigue strength of the joint.
3. The fatigue strength of the lap joint need to be considered in the design soil metal structure under shallow cover condition and in soil steel structure with variable curvature like pipe arches and reentrant arches.

REFERENCES

1. Mohammed, H., Kennedy, J.B., and Smith, P. (2002), "Improving the Response of Soil-Metal Structures during Construction" ASCE Journal of Bridge Engineering Div., pp. 6-13.
2. Musser, S.C.G (1989). "CANDE-89 culvert analysis and design computer program user manual" Rep. No. FHWA-RD-89-169, Federal Highway Administration, Washington, D.C.
3. Engineering News Record. (1983), "Culvert Failure kills Five" January 27, pp. 12
4. Moore, R.G. (1986), "Observed Signs of Distress in Soil Steel Structures."Proceeding of the Second International Conference on Short and Medium Span Bridges, Ottawa, Ont., Vol. 1, pp. 343-457.
5. Bakht, B., and Agarwal, A. (1987), "On Distress in Pipe Arches". Ministry of Transportation, Ontario, Downsview, Ont.
6. Lee, R.W.S, and Kennedy, D.J. (1988), "Behavior of Bolted Joints of Corrugated Steel Plates". Structural Engineering Report 155, Department of Civil Engineering, University of Alberta, Edmonton
7. ABDEL-Sayed, G., Bahkt, B. and Jagar, L. (1994), "Soil-Steel Bridge". McGraw Hill, Inc.
8. Morrow, JoDean, 1965, "Cyclic Plastic Strain Energy and Fatigue of Material", ASTM STP 378, American Society for Testing and Materials.
9. Rolfe, S. T. and Barsom, J. M., (1977), "Fatigue Control in Structures – Applications of Fracture Mechanics", Prentice Hall, Inc., Englewood Cliffs, New Jersey.
10. Mattos, R. J. and Lawrence, F. V., Jr. (1975), "Estimation of the Fatigue Crack Initiation Life in Welds using Low Cycle Fatigue Concepts", FCP Report No. 19, College of Engineering, University of Illinois, Urbana, IL.
11. Morrow, JoDean, (1968), "Fatigue Properties of Material", SAE Fatigue Design Handbook.
12. Department of Energy, (1990), "Offshore Installation: Guidance on Design, Construction and Certification", 4th Ed. HMSO, London, UK.
13. Little, R.E., and Jebe, E. H. (1975) "Statistical design of Fatigue Experiments", Applied Science, Essex, U.K.

THE INFLUENCE OF PRINCIPAL AXES ON DYNAMIC BEHAVIOUR OF IRREGULAR STRUCTURES

Khaled Zaky Soliman

*Assistant Professor, Department of Reinforced Concrete,
Housing and Building National Research Center, Giza, EGYPT.*

ABSTRACT:

The current seismic codes suggest that dynamic analysis should be performed in the principal directions for irregular structures. However, they didn't give any guidance for their determination. This can lead to relatively weak structural design in one direction. Therefore, the paper discusses the effect of geometric aspect ratios on the principal axes of L-Shapes irregular structures. Three basic models, having regular geometric plan, are chosen to conduct this study. They are five, ten, and fifteen stories. For each model, the first change is only in the structure plan-configuration to form 15 cases of L-shape building. Then the later variation takes place in the vertical configuration to form another 15 cases of L-setback buildings for each assumed setback height of 0.2, 0.4, 0.6 and 0.8 of the original height. The total number of studying cases is 225. Nonlinear Structural Analysis software and Statistical Software were used during this research. Four numerical equations were developed to determine the fundamental time period, and the principal axes for both L-Shapes and L-setback irregular structures. These suggested equations have accuracy not less than 80%. It is observed that, there is a significant effect on base shear value and consequently the straining action of the structure members, when performing the dynamic analysis in the principal directions of the building. Therefore, it is recommended to use these developed equations for helping the structural engineer in performing accurate dynamic analysis.

Keywords: Irregular structure, Principal axes, principal directions, Seismic analysis, Dynamic analysis, Nonlinear Analysis, L-Shapes buildings, L-setback buildings.

INTRODUCTION:

The design of buildings for earthquake loading requires an early and close collaboration between the architect and engineer to arrive at the optimum structural design. One of the greatest causes of damage to buildings has been the use of improper architectural-structural configurations. Building configuration is an important characteristic that affects building response. In a more complex T or L shaped buildings, forces concentrate at the inside corners created by those shapes. The earthquakes can severely damage those irregular buildings, when transmitted through them, because the seismic forces often exceed the forces that the structure can sustain. Therefore, the structural codes, Ref.(1,2,3,4,5,6&7), stated that, the building configuration is a main issue in defining or selecting the method of structural analysis.

Irregular structures are defined as those having significant physical discontinuities in configuration or in their lateral-force resisting systems. Irregular structures generally require to be designed by the dynamic lateral force procedures where a computer program is used to mathematically model the building so the response of the structure can be studied at each moment in time.

In all current codes, IBC-UBC- EUC- ECPLC Ref. (1,2,3&4), there is a lack of principal axes identification for irregular buildings. They only mention the importance of principal axes on the

structures behavior without any guidance on their determination. The scaled spectra approach will produce a different input motion in each building direction, i.e., a different design base shear. Therefore, the current codes dynamic analysis approach can result in a structural design which is relatively weak in one direction.

If the structural engineer is allowed to select an arbitrary reference system, the dynamic base shear will not be real, and each reference system will result in a different design. One solution to this problem, that will result in a realistic design base shear, Ref. (8), is to tune the structure plan. It is possible to convert the geometrically irregular structure to a dynamically regular structure. Consequently, the structure will achieve adequate lateral- force resistance in all directions.

The paper aimed at developing equations for principal axes of structures to help the structural engineer in calculating the principal directions of irregular structures having L-shape or L-setback geometric configuration. As a result the structural engineer could achieve the maximum stresses & forces that would be applied on the structure elements, when applying the earthquake loading excitations in the principal directions. Equations for fundamental time period of these structures will be developed, as well.

THEORY OF STRUCTURAL PRINCIPAL AXES

Due to the lack of principal axes identification for irregular buildings, this research tries to create phenomena to determine the principal axes of structures. It is based on the structure three dimensional mode shapes, because they present the relation between masses distribution and the lateral resisting stiffness systems. Therefore, the essential step of the proposed method is the calculation of the three dimensional mode shapes. Each mode shape can be considered to be a deflection due to a set of static loads. Six base reaction forces can be calculated (F_x , F_y , F_z , M_x , M_y , M_z). However, three base reactions are associated with each mode shape.

The current Egyptian code, Ref. 1., defines an "irregular structure" as one which has an irregular geometrical shape or in which stiffness and/or mass discontinuities exists. As mentioned in Ref. (8&9), the mode shapes of symmetrical structure are uncoupled and have displacement in one direction. Therefore, a more rational definition is that a regular structure is one in which there is a minimum coupling between the lateral displacements and the torsion rotations for the mode shapes associated with the lower frequencies of the system. Therefore, if the model is modified by studying the three dimensional mode shapes during the preliminary design phase, it may be possible to convert a geometrically irregular structure to dynamically regular structure.

It's noted that some three dimensional mode shapes tend to have directions that are 90° apart, while, the others have different directions and large torsion component, i.e., torsion modes. However, the directions associated with the pairs of the three dimensional mode shapes are not mathematically unique.

It was suggested to use the direction of the base shear associated with the fundamental mode of vibration as the major principal direction for the structure. However, the minor principal direction will be 90° from the major axis, as shown in Fig. (1).

IRREGULAR STRUCTURES COMPUTER MODELS:

The study targets to obtain reasonable formulae governing the values of the fundamental natural time period, as well as, the identification of the principal directions to L-shape, and L-Setback geometric structural shapes.

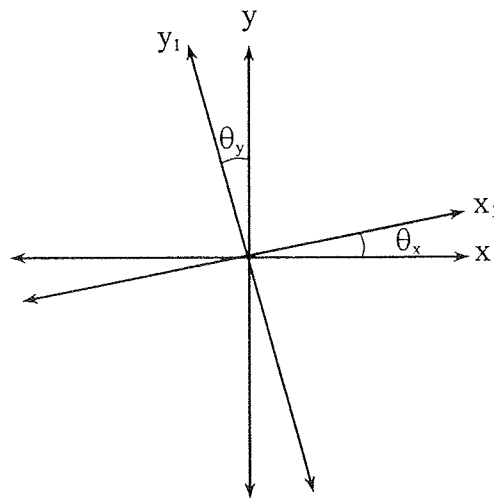


Fig. 1. Orientation of Principal Axes

Therefore, the paper discusses the effect of geometric aspect ratios on the principal axes of L-Shapes irregular structures. Three basic models, having regular geometric plan, are chosen to conduct this study. They are five, ten, and fifteen stories, with a plan consisting of four bays in each X and Y direction. For each model, the height is assumed to be constant, while the change will first vary in the structure plan-configuration, taking L-shape configurations to form 15 cases, as shown in Fig. 2.. Then, the later variation takes place in the vertical configuration to form L-setback buildings with different height, H_s , of 0.2, 0.4, 0.6 and 0.8 of the original height, as shown in Fig. 3.. The total number of studying cases is 225

The P-delta effects were included in all structural models. The effect of including the P-delta displacements in a dynamic analysis results in a small increase in the period of all modes in addition to being more accurate. The masses of the structures of the control buildings are estimated with a high degree of accuracy using the nonlinear structural analysis programs PC-ANSR and SAP2000, Ref. 10&11.

Statistical analysis for Models data:

The SPSS Computer program, Ref (12), was used to perform multi-variable regression analysis to get the correlation between the relative geometrical dimensions of the irregular structures and their both natural time period, T, and the angle of principal axes, θ_x . Further, a step wise curve estimation regression analysis was also conducted to get the relation between the independent parameters, the relative geometrical dimensions, and the dependent parameters T and θ_x .

The values of the regression correlation coefficient (R^2) of the estimated equations for the parameters, T and θ_x , were found equal 99.9 and 79% respectively for L-shape structures. In case of L-setback structures, the values equal to 99.4 and 81.7% respectively. Further, the SPSS program was used in developing equations for both T and θ_x as function of the geometric aspect ratios of the irregular structures are as follows:

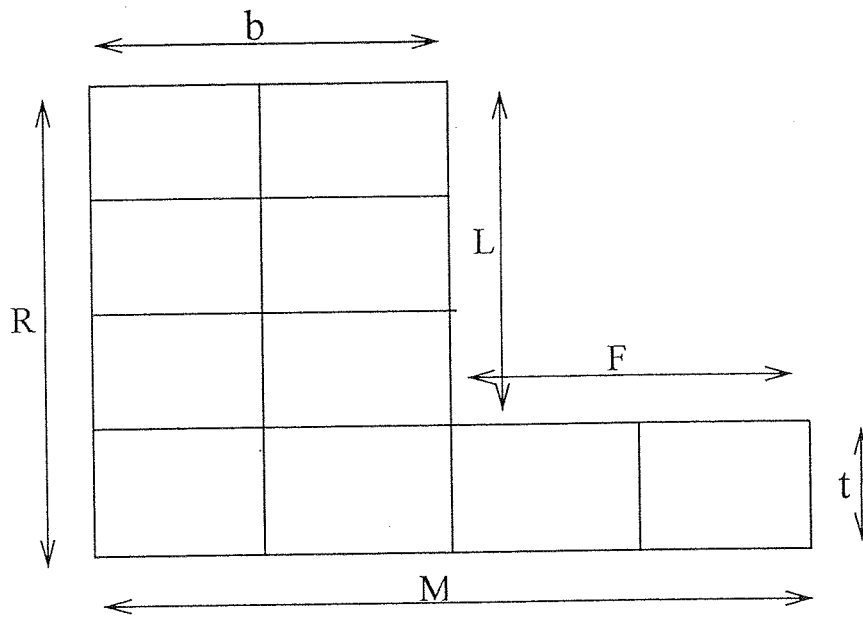


Fig. 2. General Plan for L-Shape Buildings

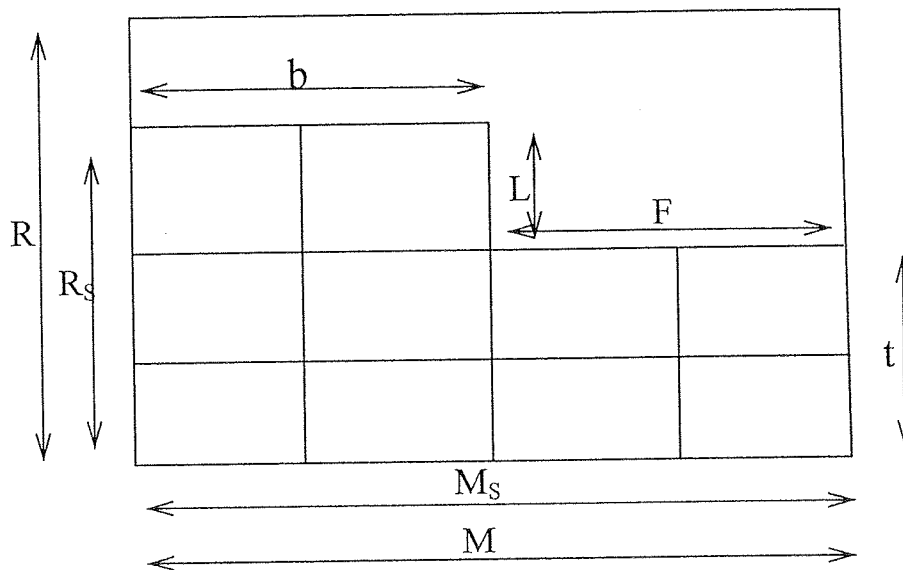


Fig. 3.: General Plan for L-Setback Buildings

For L-shape structures:

a- Time Period, T :

It was found that, there is a Linear correlation between the natural time period (T) of the L-shape structure and the presented relative geometric dimensions, aspect ratios, presented in the equation.

$$T = 0.0013 \times T_{estimated} \quad (1)$$

Where:

$$\begin{aligned} T_{estimated} = & 0.528 \times \ln(b) + 28.9 \times H \\ & + 3 \times \left(\frac{b}{H}\right) - 2.04 \times \left(\frac{b}{H}\right)^2 + 0.336 \times \left(\frac{b}{H}\right)^3 \\ & + 7.9 \times \left(\frac{F}{M}\right) - 17.5 \times \left(\frac{F}{M}\right)^2 + 11.68 \times \left(\frac{F}{M}\right)^3 \\ & + 2.8 \times \left(\frac{L}{H}\right) - 1.84 \times \left(\frac{L}{H}\right)^2 + 0.3 \times \left(\frac{L}{H}\right)^3 \\ & + 9 \times \left(\frac{L}{R}\right) - 21.02 \times \left(\frac{L}{R}\right)^2 + 14.55 \times \left(\frac{L}{R}\right)^3 \\ & + 2.522 \times \left(\frac{t}{F}\right) - 1.64 \times \left(\frac{t}{F}\right)^2 + 0.311 \times \left(\frac{t}{F}\right)^3 \\ & + 4.24 \times \left(\frac{t}{L}\right) - 4.16 \times \left(\frac{t}{L}\right)^2 + 0.96 \times \left(\frac{t}{L}\right)^3 \\ & + 0.473 \times t - 0.066 \times t^2 + 0.003 \times t^3 \\ & + 0.274 \times \left(\frac{M}{t}\right) \end{aligned} \quad (2)$$

b. Principal Axis Identification:

It was found that there is a Linear correlation between the measured angle θ_x and the relative geometric aspect ratios presented in Eq. 3..

$$\left(\frac{\theta_x}{H}\right) = 0.259 \times \left(\frac{\theta_x}{H}\right)_{estimated} \quad (3)$$

Where:

$$\begin{aligned} \left(\frac{\theta_x}{H}\right)_{estimated} = & \frac{0.66}{b} - 0.053 \times \ln\left(\frac{b}{F}\right) + 0.022 \times \left(\frac{H}{b}\right) \\ & + 0.069 \times \left(\frac{L}{b}\right) - 0.15 \times \ln\left(\frac{b}{M}\right) \end{aligned} \quad (4)$$

L- Setback Structures:

a- Time Period, T

It was found that there is a Linear correlation between the natural time period, T and the presented relative geometric dimensions, relative geometric aspect ratios, Eq. 5..

$$T = 0.0012 \times T_{estimated} \tag{5}$$

Where:

$$\begin{aligned} T_{estimated} = & 0.528 \times \ln(b) + 28.9 \times H + 0.1 \times H_s - 0.002 \times H_s^2 \\ & + 3 \times \left(\frac{b}{H_s}\right) - 2.0 \times \left(\frac{b}{H_s}\right)^2 + 0.336 \times \left(\frac{b}{H_s}\right)^3 \\ & + 7.9 \times \left(\frac{F}{M}\right) - 17.5 \times \left(\frac{F}{M}\right)^2 + 11.68 \times \left(\frac{F}{M}\right)^3 \\ & + 2.8 \times \left(\frac{L}{H_s}\right) - 1.8 \times \left(\frac{L}{H_s}\right)^2 + 0.3 \times \left(\frac{L}{H_s}\right)^3 \\ & + 9 \times \left(\frac{L}{R}\right) - 21.02 \times \left(\frac{L}{R}\right)^2 + 14.55 \times \left(\frac{L}{R}\right)^3 \\ & + 2.522 \times \left(\frac{t}{F}\right) - 1.64 \times \left(\frac{t}{F}\right)^2 + 0.311 \times \left(\frac{t}{F}\right)^3 \\ & + 4.24 \times \left(\frac{t}{L}\right) - 4.16 \times \left(\frac{t}{L}\right)^2 + 0.96 \times \left(\frac{t}{L}\right)^3 \\ & + 8.12 \times \left(\frac{H_s}{H}\right) - 18.17 \times \left(\frac{H_s}{H}\right)^2 + 12.13 \times \left(\frac{H_s}{H}\right)^3 \\ & + 0.473 \times t - 0.066 \times t^2 + 0.003 \times t^3 + 0.274 \times \left(\frac{t}{H_s}\right) \end{aligned} \tag{6}$$

b- Principal axis identification :

It was found that there is a quadratic correlation between the measure of the angle θ_x and the relative geometric dimensions in Eq. (7).

$$\left(\frac{\theta_x}{H}\right) = -0.0251 \times \left(\frac{\theta_x}{H}\right) + 0.1223 \times \left(\frac{\theta_x}{H}\right)^2 \tag{7}$$

Where:

$$\begin{aligned} \left(\frac{\theta_x}{H}\right)_{estimated} = & e^{-0.48 \times \left(\frac{H_s}{f}\right)} + e^{-0.735 \times \left(\frac{H_s}{L}\right)} + e^{-0.089 \times H_s} \\ & + e^{-0.89 \times \left(\frac{b}{f}\right)} + e^{-1.28 \times \left(\frac{t}{L}\right)} \end{aligned} \tag{8}$$

APPLICATION

Two L-shape and two L-Setback buildings were used to check the accuracy of the developed equations. The first building is a six- stories L-shape building with a total height, H, equals 18m with equal bays of span 3.0m each. The second is a twelve stories L-shape building of height

equals 36 m with equal bays of span 5m each. The third example is the same as the first building, but with a setback height, H_s , of 3m. The fourth example is the same as the second building, but with a setback height, H_s , of 6m.

Three dimensional computer models were created for each building in which all structural elements are modeled, considering the P-delta effect. The directional and torsional properties of the mode shapes were used to improve the design. As mentioned before, the structure should have a minimum amount of torsion in the mode shapes associated with the lower frequencies of the structure, Ref. (8 ,9 &13).

L-shape Buildings:

Table 1. shows a comparison among the values obtained from the developed equations for the natural time periods concerning the L-Shape buildings, and those obtained from the computer model and the values of the time period recommended by the UBC 1997 & ECPLC, Ref. (1&3). In addition, table 2. shows the actual values of the angles of orientation of the principal axis with respect to the original X and Y axes.

L-Setback Buildings:

Table 3. shows a comparison among the values obtained from the developed equations for the natural time periods concerning the L-Setback buildings, and those obtained from the computer model and the values of the time period recommended by the U.B.C 1997 & ECPLC, Ref. (1&3). In addition, table 4. shows the actual values of the angles of orientation of the principal axis with respect to the original X and Y axes.

Table 1. Estimated Fundamental Time Period for L-Shapes

CASE	Time Period (T) (sec.)		
	Computer Analysis	Developed Equations	code
6-Stories bldg	0.635	0.63	0.63
12-Stories bldg	1.29	1.26	1.1

Table2. Estimated Principal Axes for L-Shapes

Case	θ_x (Degrees)		
	Computer Analysis	Developed Equations	Code
6-Stories bldg	1.34	1.2	Undefined
12-Stories bldg	2.33	2.77	Undefined

Table 3. Estimated Fundamental Time Period for L-Setback

CASE	Time Period, T, (sec.)		
	Computer Analysis	Developed Equations	Code Recommendations
6-Stories bldg	0.56	0.63	0.637
12-Stories bldg	1.206	1.26	1.15

Table4. Estimated Principal Axes for L- Setback

Case	θ_x , (in degree)		
	Computer Analysis	Developed Equations	Code
6-Stories bldg	9.4	10.6	Undefined
12-Stories bldg	17.68	18	Undefined

From studying Tables (1,2,3,4), It is obvious that the developed formulae obtain accurate values, as if a three dimensional dynamic analysis has been applied for the structure. It should be noted that, the values presented by the developed equations depend on the relative geometric aspect ratios of irregular structures. In other meaning, the equations clarify how far the relative geometric aspect ratios of the structure could affect its dynamic behavior.

The Effect of Principal Axes on Structures Dynamic Responses:

The four buildings, mentioned above, were undergoing a dynamic excitation in both original axes and the obtained principal axes. Considering the 6 and 12 -stories L-shape buildings, the recommended angle of orientation to be taken as an excitation angle for each structure was taken equal to obtained θ_x . In other meaning, the principal axes were observed by the computer dynamic analysis to be at 1.34 and 2.33 degrees respectively. For 6 and 12 stories L-setback buildings, the principal axes were also observed to be at 9.4 and 17.68 degrees respectively.

The response spectrum analysis was first performed in X and Y axes, i.e., the excitation angle equals zero. Then, it is re-performed in the directions of calculated principal axes. The presented charts, Figs (4&5) explain the great influence of tuning the structure in its principal directions and the significant effect of entering the angle of excitation in the dynamic analysis procedure on the values of base shear forces that affect the structure.

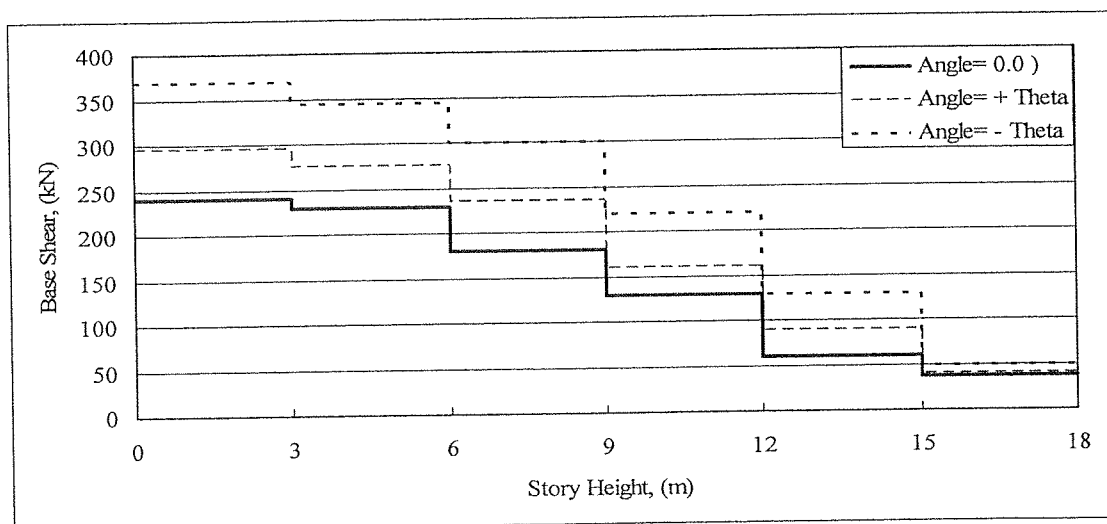


Fig. 4. Base Shear (U1 – Excitation) for 6 -Stories L-Setback Bldg.

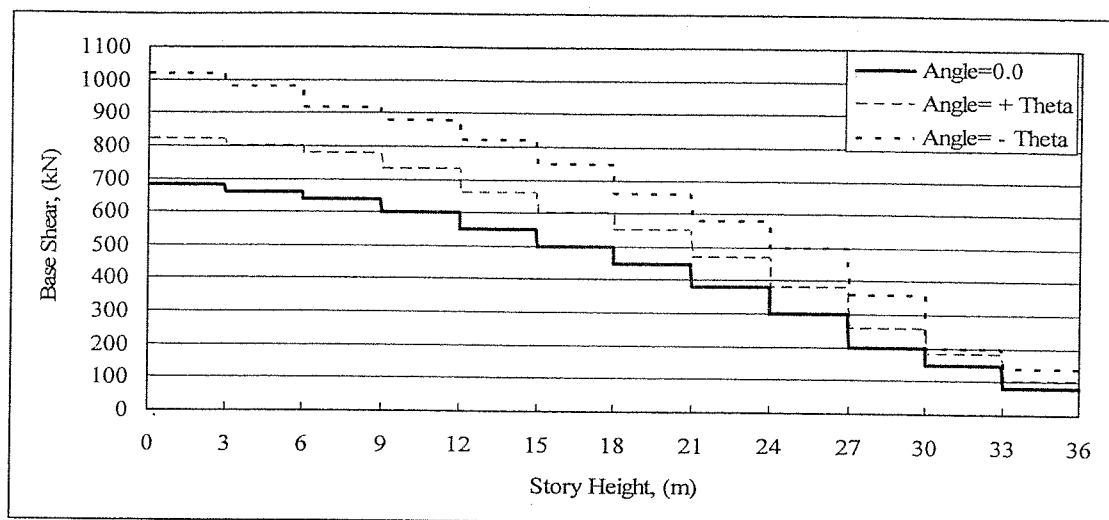


Fig. 5. Base Shear (U1 – Excitation) for 12 -Stories L-Setback Bldg.

CONCLUSION

The current seismic codes recommend that dynamic analysis should be performed in the principal directions for irregular structures to avoid the relatively weak structural design in one direction. After discussing the effect of geometric aspect ratios on the principal axes of L-Shapes irregular structures, the following items could be concluded:

1. The developed formulae obtain accurate values, as if a three dimensional dynamic analysis has been applied for the structure, in addition, they clarify how far the relative geometric aspect ratios of the structure could affect its dynamic behavior.
2. Determination the natural time period of the structure in the preliminary design case, by substituting in the developed equation with geometric aspect ratios of the structure.
3. Identification of the principal axis using the proposed equations in the study allows the structural engineer finding the angle of excitation to be taken into consideration while performing the dynamic analysis process.
4. There is a significant effect of entering the angle of excitation in the dynamic analysis procedure on the values of base shear forces that affect on the structure

REFERENCES

1. Egyptian Code of Practice for Load Calculations, ECPLC, (2004), by Ministry of Housing and Development, Housing and Building Research Centre, , Cairo, EGYPT.
2. European Standard, Eurocode 8, (2003). "Design of Structures for earthquake resistance", by European Committee for Standardization.
3. Uniform Building Code, UBC, (1997). Volume 2, "{Structural Engineering Design Provision}", by International Conference of Building officials , Whittier, California.
4. International Building Code, (2000), by IBC Structural Committee, Whittier, California.
5. Applied Technology Council, ATC, (1997). "NEHRP Guidelines for the seismic Rehabilitation of Buildings", published by the Federal Emergency Management Agency, FEMA 273 Report, Washington, DC.
6. Structural Engineers Association Of California, SEAOC, (1996). "Recommended Lateral Force Requirements and Commentary", Sixth. Edition, Seismology Committed.
7. Ministry of Public Works and Settlement, MPWS, (1997). "Specifications for structures to be built in disaster areas, PART III- Earthquake disaster prevention", Government of Republic of Turkey.

8. Wilson, (1997). "Seismic Analysis Modeling to Satisfy Building Codes", University of California, Berkeley, CA, Press Web Site at <http://www.csiberkeley.com/>.
9. C. Menun and A. Der Kiureghian, (1998). "A Replacement for the 30% Rule for Multi component Excitation", Earthquake Spectra, Vol. 13, Number 1, February.
10. Maison, B. F., (1992). "PC-ANSR: A Computer Program for Nonlinear Structural Analysis", National Information Service for Earthquake Engineering, University of California, Berkeley, CA.
11. "SAP2000-Ver. 9: A Computer Program for Linear and Nonlinear Structural Analysis", National Information Service for Earthquake Engineering, University of California, Berkeley, CA, 2004.
12. SPSS Program, (1997), by SPSS Inc. Headquarters, 233 S. Wacker Drive, 11th floor Chicago, Illinois 60606.
13. Clough, R. W., and Penzien, J., (1993). "Dynamics of Structures", Published by McGraw-Hill Co., Singapore.
14. Mahmoud Khalifa, Safinaz, (2005), "The Effect of Aspect Ratio on the Behavior of Irregular Structures During Earthquakes", M. Sc. Thesis, Ain Shams University, under supervision of Prof. A. Aly & Assistant Prof. Khaled. Z. Soliman.

EFFECT OF CLAY SOIL DEPOSITS ON GROUND MOTION CHARACTERISTICS AND ON STRUCTURE BEHAVIOR

Khaled Zaky Soliman

Dept. of Reinforced Concrete, Housing & Building National Research Center

Ahmed Thabet M. Farid

Dept. of Soil Mech. & Found. Eng, Housing & Building National Research Center

ABSTRACT:

Previous researches mentioned that many buildings, which were designed according to international building codes, were severed or totally collapsed during earthquakes. They pointed to the totally distinguish results in the behaviors and surviving of the same type of buildings that located at different sites equally distanced from the epicenter. This research was conducted to study the effect of clay soil of different consistency, and different height strata on the earthquake properties, i.e., ground acceleration, time history, and spectra acceleration values. The SHAKE 91 and SEISMOSIGNAL computer programs were used during this study. Moderate and strong earthquake records, with PGA ranges from 0.20 g to 0.35 g, were used in the analysis. SDOF systems of different time periods were used to study the effect of soil-structure interaction on the behavior of superstructure. It is concluded that the clay consistency and the height of the clayey soil strata above the rock base layer have a significant effect on the earthquake properties. It is also found that, the spectral displacement and base shear forces for SDOF systems were varied, according to the fundamental time periods, by 50% to 230% compared to rock stratum. Finally, the soil deposit under structures was found having great effect on the earthquake properties as well as the behavior of superstructure. It is recommended to consider a site specific influence in design procedures in building codes.

INTRODUCTION

Amplification of seismic motions under different soil deposit can be significant, especially at sites with clay soil conditions. As an example, the local site amplification effect were observed during earthquakes^{1&2}, the subsequent analysis of measured ground motions during these earthquakes indicated that the spectral acceleration were amplified many times over adjacent rock sites. For the approximately equally distanced sites from the epicenter, the same type of buildings had distinguish results in both behavior and in surviving. The present paper attempts to study clay soil conditions impact to the characteristics of the earthquake motions. The assumed near surface geologic profile consists of clay deposits extending to about 150 meter depth. Evaluation of both sites spectra and amplification influence for suggested different soil consistency, and comparison with the base rock stratum is studied in this research. The effect of clay soil on the characteristics of selected earthquake motions was carried out assuming horizontally stratified soil deposits and vertically propagating seismic waves³. The soil properties are varying with depth but remain constant in horizontal direction. Generation of acceleration time histories, frequency content, Spectral accelerations, and amplification factor related to bed rock were performed at different heights above bedrock, using SEISMOSIGNAL and SHAKE91 programs^{3,4&5}. The structural response amplification of SDOF systems situated on clay soil foundation was also investigated. The displacement time responses and base shear forces of the SDOF systems were discussed under the selected earthquake motions. The control motions have been specified at the bedrock as datum for the analysis. The zero period ground acceleration for these earthquakes is assumed as 0.10g during this study.

The recording data at soil surface normally reflect the seismic characteristics of the soil layers at that site, therefore to obtain the response of any soil deposit the following items should be studied:

1. Determination of the soil surface topography⁶.
2. Determination of the underlying rock configuration⁷.
3. Dynamic module and damping ratio properties of soil layers^{8,9,10 &11}.
4. The characteristics of earthquake motions.

GROUND MOTION RECORDED

Table (1) shows the selected ground motions used in this study. The earthquakes had peak acceleration ranging from 0.20g to 0.35g. The two earthquakes records are normalized to 0.10g. They are used to plot the spectral displacement curves for 5% damping.

Table 1. Characteristics of Earthquake Ground Motions

EARTHQUAKE RECORD	DATE OF EARTHQUAKE	PEAK ACCELERATION (% OF G)	GROUND VELOCITY (MM/SEC.)	GROUND DISPLACEMENT (MM)	DURATION TIME (SEC.)
EL-CENTRO ELC-S60E	05/8/40	0.348	334	124	55.76
TAF TAF-S86W	7/21/52	0.179	177	105	52.10

Soil Surface Topography

To conduct this study, two types of clay soil with different consistency and height strata were used. The first one is a soft clay of plasticity index ranged from 40% to 80% with a bulk density ranged from 17 kN/m³ at top soil surface to about 18 kN/m³ above bedrock layer. The shear wave velocities range from 90 to 180 m/sec. The latter one is a stiff clay of plasticity index ranged from 10% to 20% with a bulk density ranged from 18 kN/m³ at top soil surface to about 20 kN/m³ above bedrock layer. The shear wave velocities range from 210 to 330m/sec. The depth of each type of investigated soil is 150m above the bedrock formation. The geotechnical data regards to dynamic module and damping ratio properties were chosen from previous researches 8,9,10,11 &12.

Dynamic Module and Damping Ratio

The geotechnical data of soft and stiff clay deposit with regard to dynamic module and damping ratio properties dependences upon the strain level are shown in Figures 1 and 2.

ANALYSIS METHODS

The effect of site conditions on seismic ground motions are usually interpreted to mean how the waves from the underlying rock are affected by the geometrical and geological structures of the softer surface deposits during wave's transmission to the surface. Seismic loads on structure situated on a soil deposit may be greater than those on the same structure standing on rock. The effect of soil deposit on the earthquake time history acceleration, frequency content, spectrum acceleration curves, amplification factor between bed rock and the top soil surface, and Fourier amplitude will be discussed in the following:

Earthquake Time History

The selected earthquake motions are used as input motions at the bed-rock formation. The acceleration time histories are then computed at the tops of all layers. Figures 3 and 4 show the varying time history acceleration of earthquake wave propagation through soil layers from the underlying bed-rock layer till top surface for soft and stiff clay deposits, respectively. From these Figures, it is obvious that, the acceleration time histories had been filtered during passing the soil deposit, i.e., they have larger zero peak ground acceleration (ZPGA) and long time periods at top soil surface.

Earthquake Response Spectrum

The response spectrums are plotted in Figures 5 and 6 for different soil layers. They give a good indication of the potential effects of the ground motions on different structures. From studying these Figures, the acceleration at zero time period was amplified by 40 to 50% for soft clay and by 10 to 30% for stiff clay compared to the control motion at the bedrock. The spectral accelerations ratios (amplification factors) between top surface and bed-rock are found increasing till 4.0 times that for clay deposit in both ELC and TAF cases, as shown in Figure 7.

Earthquake Fourier Spectrum

As shown in Figures 8, the Fourier spectrum is a plot of amplitude versus frequency for soft clay, stiff clay and bedrock. The Fourier amplitude spectrum illustrates the frequency content of the motion. It appears that, there is a big difference in the amplitude for lower frequencies for both soil types.

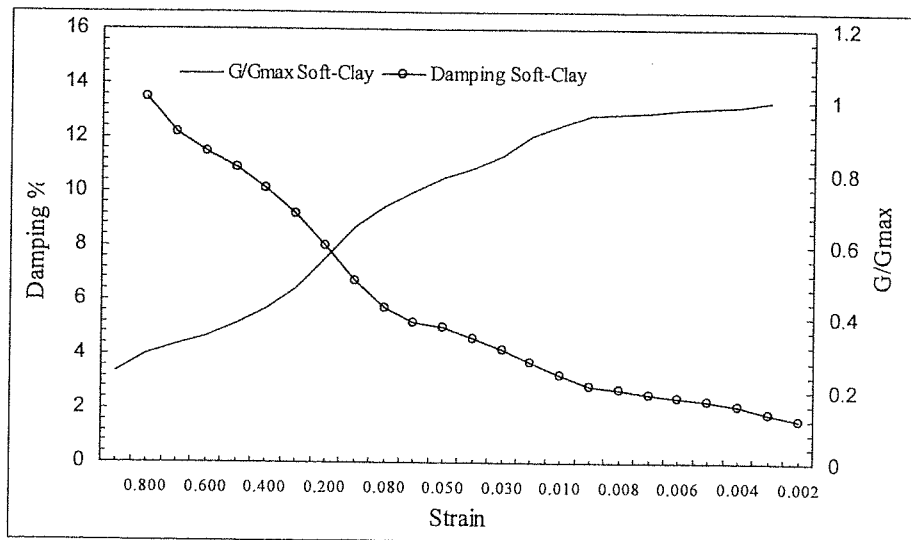


Fig. 1. Shear Modulus and Damping for Soft Clay

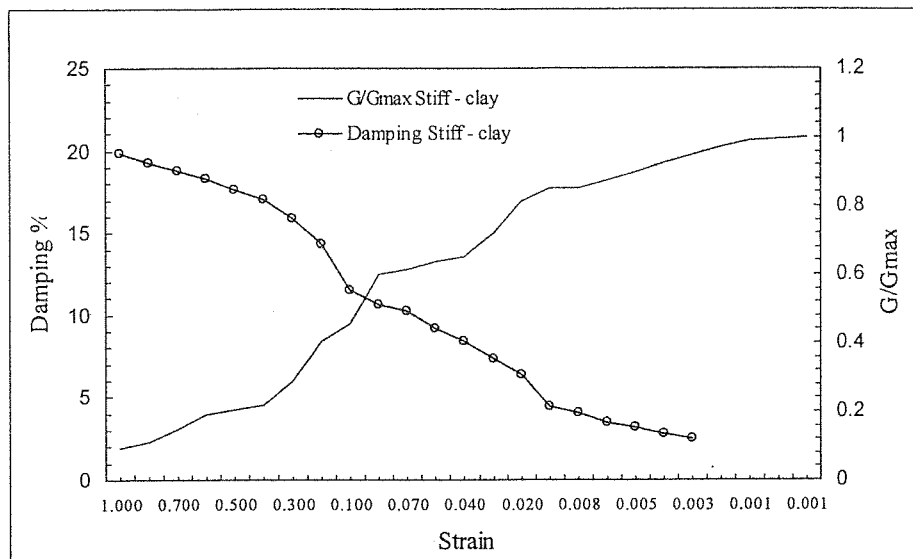


Fig. 2. Shear Modulus and Damping for Stiff Clay

STRUCTURAL RESPONSE

In order to examine the structural response due to clay deposits, SDOF systems with fundamental time periods equal to 0.5, 1.0 and 3.0 seconds were analyzed. The used earthquakes are the original records, Rock accelerogram, and the free field records generated by SHAKE91 at 150m for soft and stiff clay deposits. The response time history of SDOF systems were obtained by exciting their bases with the selected earthquakes. The displacement time history for SDOF structure with 0.5 second fundamental time period and damping ratio equal to 0.05 is shown in Figure 9. Tables 2 and 3 show the spectral displacement and the base shear forces due to earthquake excitations. From these Tables, it is illustrated that, The displacement time histories of SDOF systems were amplified by factors ranged between 50% to 230% comparing to bedrock foundation. As well as, the base shear forces have the same behavior. Added to that, as the fundamental time periods increases, the spectral displacement for SDOF systems are increasing while the base shear forces are decreasing.

CONCLUSIONS

The amplification of seismic motion under different clay soil deposits was found significant. The effect of clay soil deposit of different consistency and different height strata on earthquake properties was studied. The response of SDOF systems situated on clay soil foundation amplified with increasing the thickness of clay soil deposits. The following issues could be concluded as follows:

1. The amplification Spectrum between soil deposits on surface and bedrock reaches 4.50 to 5.00 times for soft and stiff clay, consequently.
2. The amplification value of control motion (ZPGA) at the bedrock is varying from 40% to 50% for soft clay and from 10% to 30% for stiff clay.
3. The amplitude of the selected earthquakes increased for both soft and stiff clay deposit compared to the bedrock case.
4. The higher amplitude values occurred for higher fundamental time periods in case of soft and stiff clay deposits.
5. For both selected earthquakes, the acceleration time histories had long periods and larger (ZPGA) at top soil surface.

6. The displacement time histories of SDOF systems were amplified by factors ranged between 50% to 230% comparing to bedrock foundation. As well, the base shear forces have the same behavior.
7. As the fundamental time periods increase, the spectral displacement for SDOF systems increases while the base shear forces decrease.

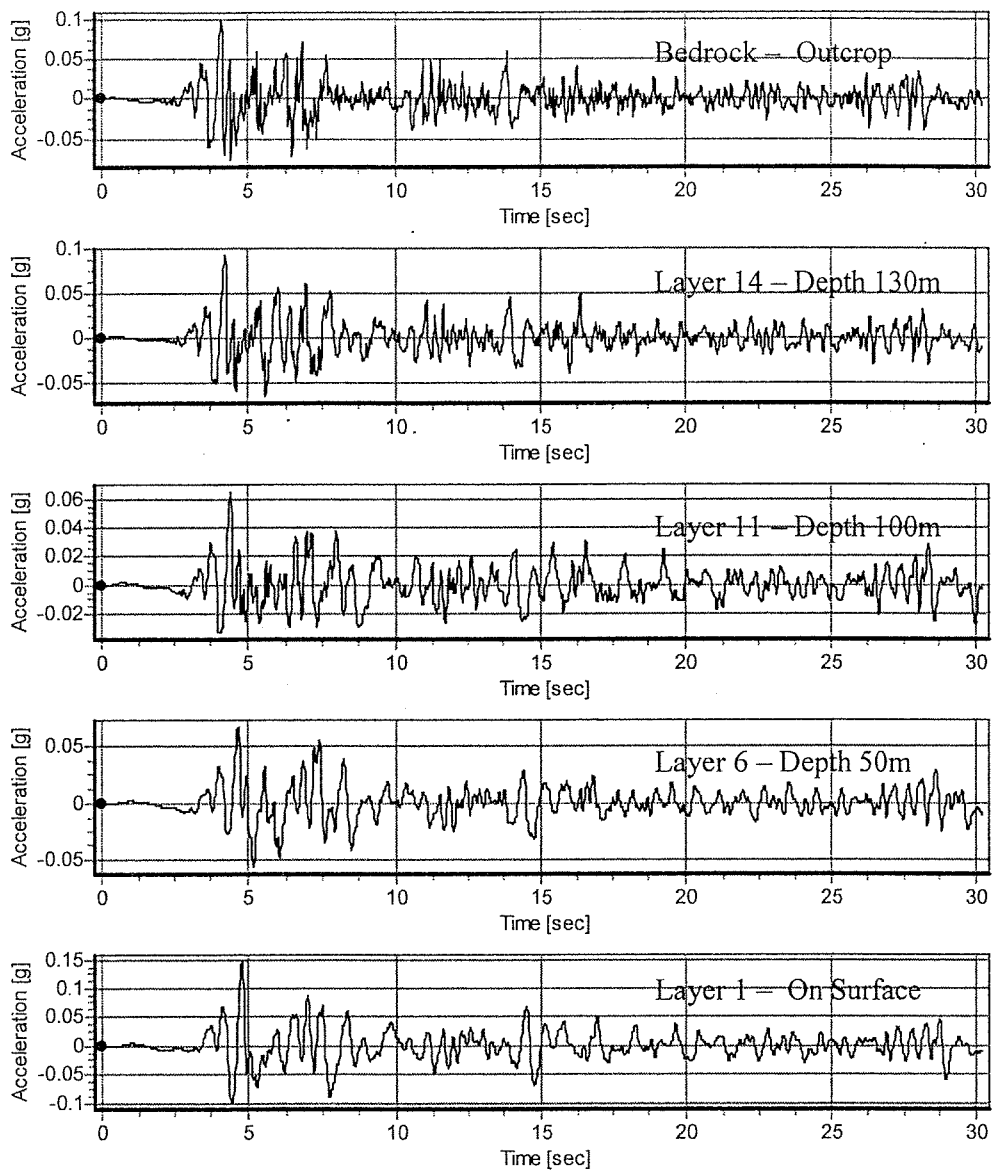


Fig. 3. Calculated Acceleration on Time Histories, Soft Clay Deposit (The Top Chart is the Original EI-Centro Earthquake Readings)

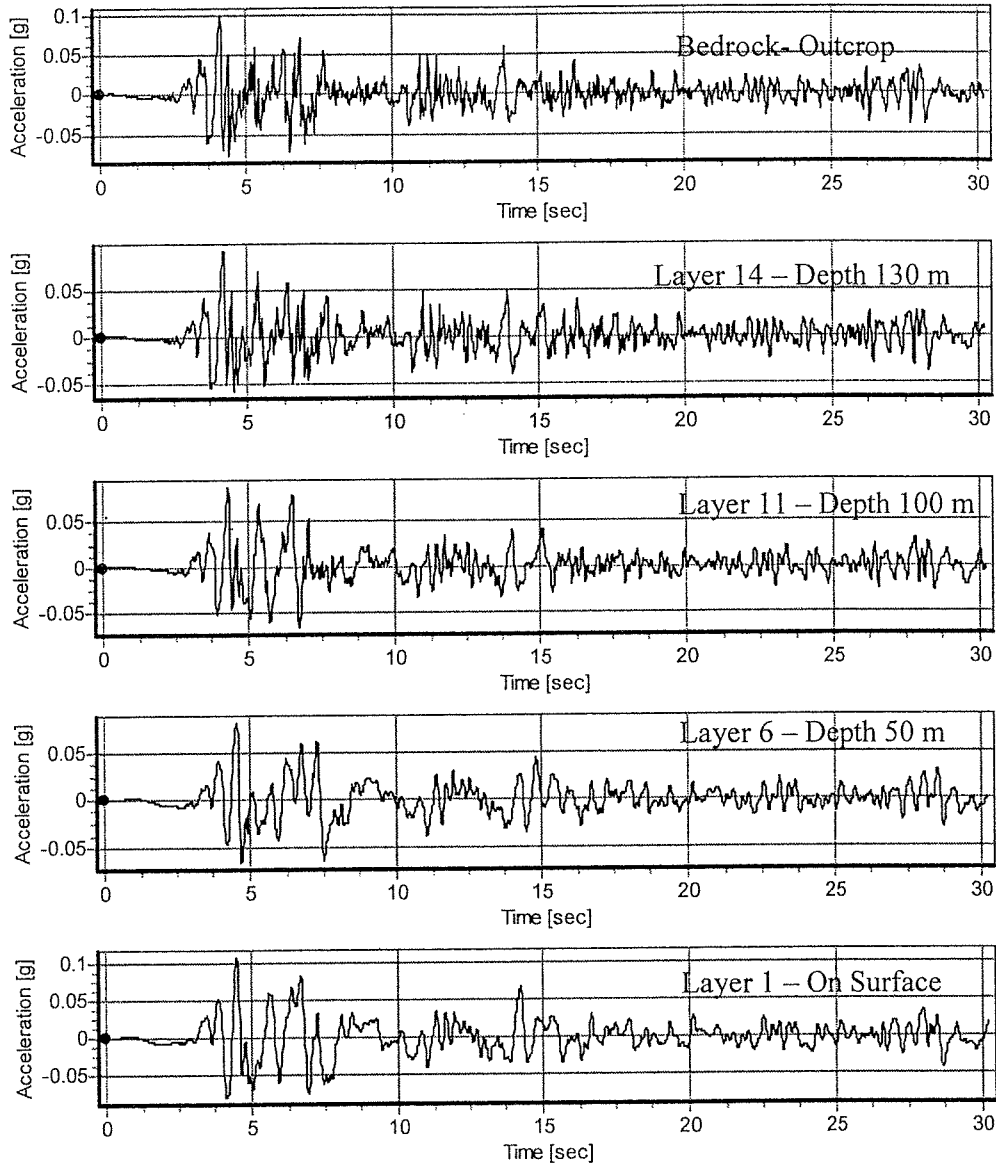


Fig. 4. Calculated Acceleration on Time Histories, Stiff Clay Deposit (The Top Chart is the Original El-Centro Earthquake Readings)

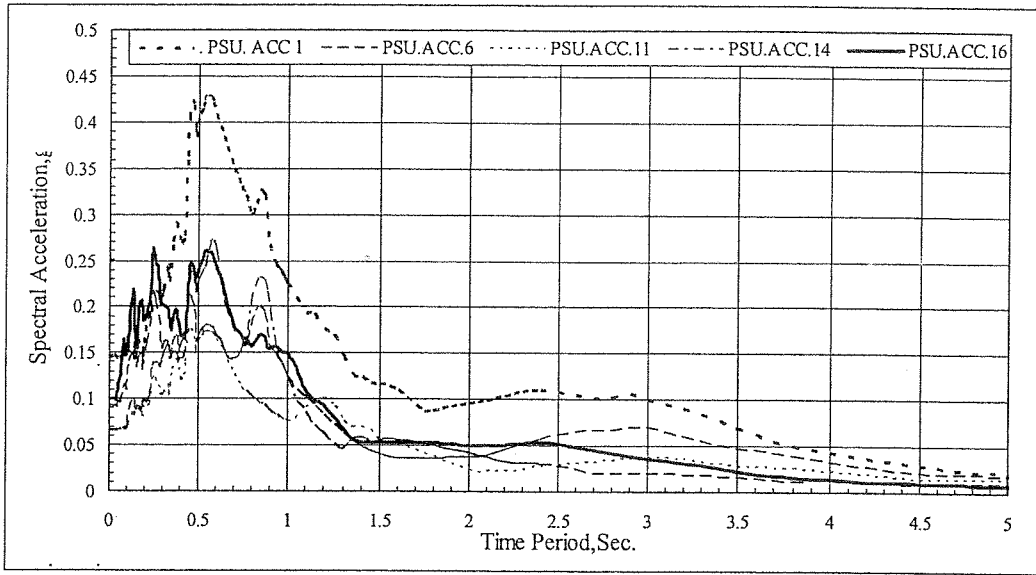


Fig. 5. Computed El-Centro Acceleration Response Spectrums of the Soft Soil Layers

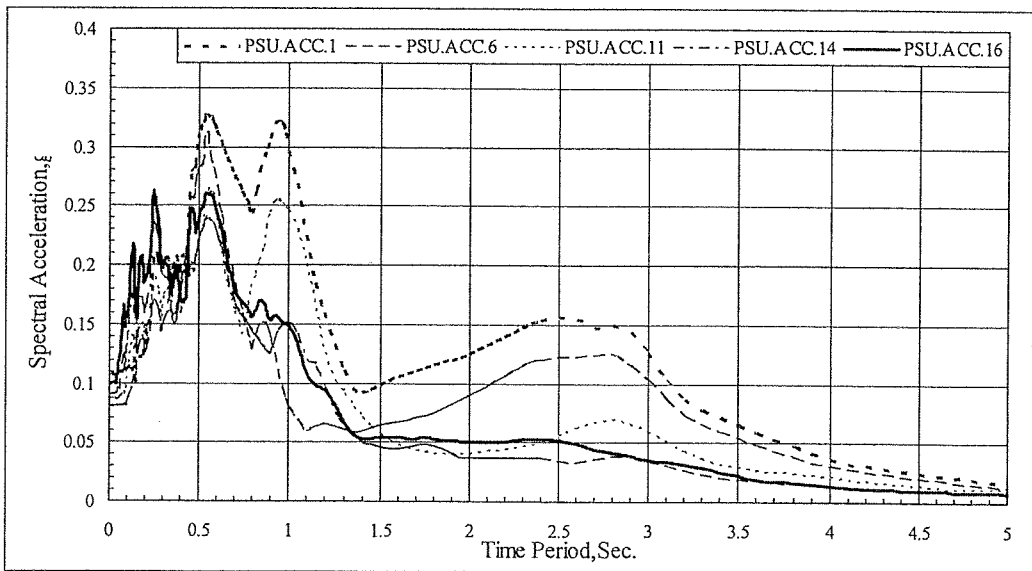


Fig. 6. Computed El-Centro Acceleration Response Spectrums of the Stiff Soil Layers

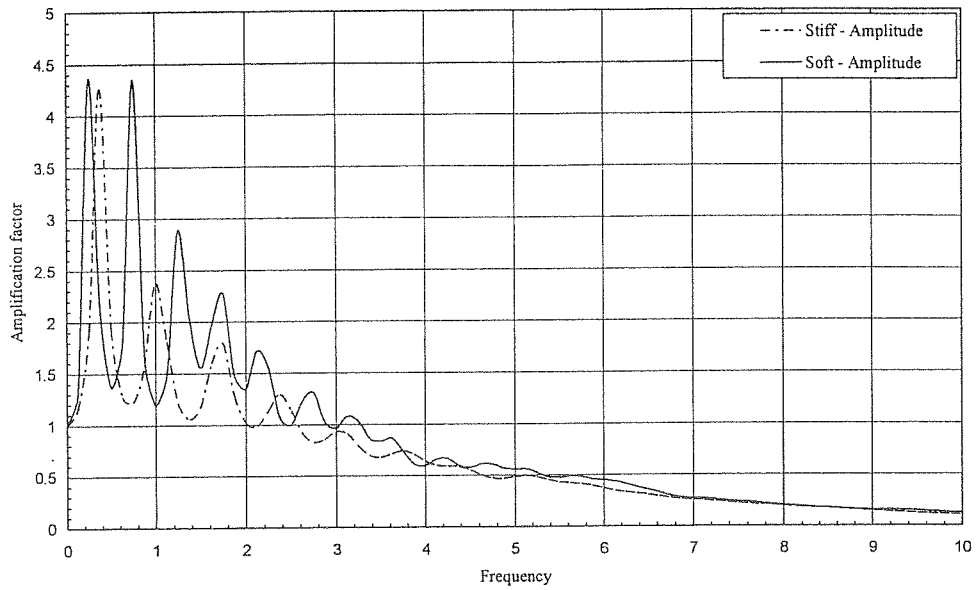


Fig. 7. Amplification Spectrum between Bedrock and different Soil Deposit on Surface, for El-Centro Earthquake.

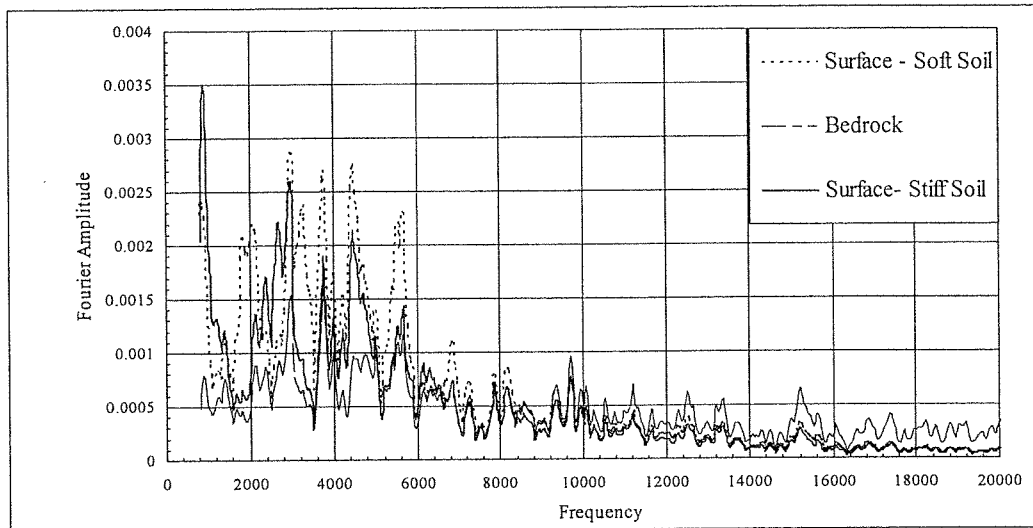


Fig. 8. Fourier Spectrum between Bedrock and different Surface clay Soil, for El-Centro Earthquake.

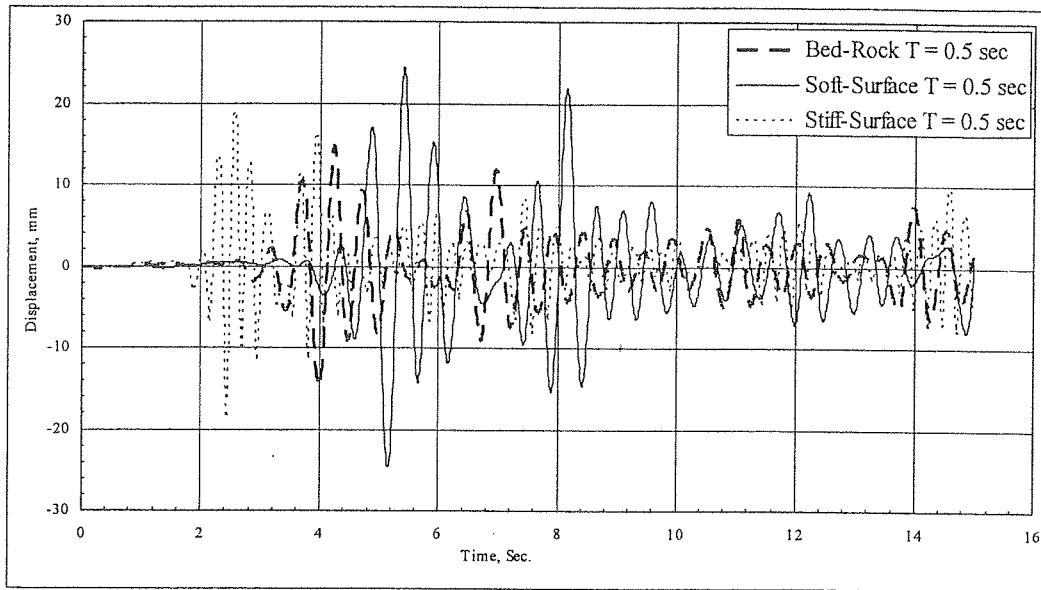


Fig. 9. Displacement Time History for SDOF system, Damping 5%, El-Centro Earthquake.

Table 1: Spectral Displacement, mm, for SDOF systems, Damping 5%, El-Centro and Taft Earthquakes

Period \ Soil type	T = 0.50 (sec.)		T = 1.00 (sec.)		T = 3.00 (sec.)	
	Elc.	Taft	Elc.	Taft	Elc.	Taft
Bedrock	14.48	11.82	36.92	21.81	79.12	59.95
Stiff clay-Surface	19.05	19.24	74.00	55.78	281.0	181.9
Soft clay-Surface	24.8	17.93	56.00	40.79	223.7	199.4

Table 2: Base Shear, tons, for SDOF systems, Damping 5%, El-Centro and Taft Earthquakes

Period \ Soil type	T = 0.50 (Ton)		T = 1.00 (Ton)		T = 3.00 (Ton)	
	Elc.	Taft	Elc.	Taft	Elc.	Taft
Bedrock	2.358	1.892	1.466	0.868	0.350	0.265
Stiff clay-Surface	3.022	3.050	2.937	2.212	1.240	0.800
Soft clay-Surface	3.915	2.846	2.220	1.620	0.987	0.878

REFERENCES

1. Zadoyan, P. (2000), "Site Amplification Effect at the Giumri Industrial Site," Nuclear and Radiation Safety Centre, civil Engineering, Ph.D. Dissertation, Press Web Site at <http://www.aaspe.am/>.
2. Charles, K. and Pong, L.J. (2005), "Structural Response Amplification due to Soft Soil Effect and the Effectiveness of the NBCC 2005 in Accounting for these Effects," Department of civil Engineering, University of Toronto.
3. Schnabel, P.B. and et al. (1972), "SHAKE: A Computer Program for Earthquake Response Analysis of Horizontally Layered Sites," University of California, EERC, Berkeley, California.
4. Idriss, I.M., and Sun, G.I.(1992), "SHAKE91: A Computer Program for Conducting Equivalent Linear Seismic Response Analyses of Horizontally Layered Soil Deposit ," University of California, Davis, California, 13pp.
5. Nawy, E. G. (2005), "SEISMOSIGNAL: A Computer Program for Earthquake Characteristics," Version 3.1.0 , Press Web Site at <http://www.seismosoft.com/>.
6. Macky, T.A.(1992), "Earthquake Effect on Response of Soil Deposit," Housing and Building Research Center, Egyptian Society for Soil Mechanics and Foundation Engineering., Vol.7.
7. School of Civil & Environmental Engineering.(2005), "Ground Motion Amplification of Soils in the Upper Mississippi Embayment," Georgia Institute of Technology, Press Web Site at <http://www.ce.gatech.edu/>.
8. Seed, H.B. and Idriss, I.M.(1970), "Soil Moduli and Damping Factors for Dynamic Response Analysis," University of California, EERC 70-10, Berkeley, California.
9. Sun, J.I., Golesorchi, R., and Seed, B.H., "Dynamic Moduli and Damping Ratios for Cohesive Soils," University of California Berkeley, EERC-88/15.
10. Dobry, R., and Vucetic, M., "Dynamic properties and Seismic Response of soft clay Deposits," proceeding, International Symposium on Geotechnical Engineering of Soft Soils, Mexico City, Vol.2, pp.51-87.
11. Saxena, S.K., Avramidis, A.S., and Reddy, K.R.(1988), "Dynamic Moduli and Damping Ratios for Cemented Sands at Low Strains," Canadian Geotechnical Journal, Vol.25.
12. ProShake User Manual (1996), " PROSHAKE: Ground Response Analysis Program Version 1.1," EduPro Civil Systems, Inc., Redmond, Washington.
13. Sandford, T.C. et al.(2004), "Soil – Structure Interaction of Buried Structures," University of Maine, A2K04: Committee on Subsurface Soil Structure Interaction.

MANUFACTURING HIGH QUALITY ROTATING BIOLOGICAL CONTACTOR'S FOR THE UK WATER INDUSTRY

D. Mba¹, R.H. Bannister¹ and G.E. Findlay²

1School of Engineering, Cranfield University, Cranfield, Beds. MK43 0AL, UK.

2 Copa Ltd, Unit 11 Credenda Road, West Bromwich B70 7JE, UK.

ABSTRACT

The principle of the Rotating Biological Contactor (RBC) was originated in the early part of the century and today there are many thousands of units operating world wide. However, the RBC has been plagued with mechanical deficiencies since its conception. This paper presents a brief insight into some of the major mechanical defects associated with RBC's. These findings have been documented as part of the largest mechanical survey of operational RBC units ever undertaken. Having the benefit of a thorough understanding of the mechanisms and reasons for mechanical failure, a new approach to designing RBC's is discussed. This has resulted in Water companies and independent operators seeking a new generation of RBC with a guaranteed operational life of twenty years. Furthermore, it displays the benefits of Academia working in partnership with Industry to produce low cost, high quality equipment.

The manufacture of the 'Cranfield' designed RBC unit is undertaken by Copa Ltd. The design offers a twenty year warranty and is currently supplied to a few of the major Water companies in the United Kingdom. This warranty is unique within the United Kingdom Water Industry where guarantees of 3 to 6 years have previously been provided by manufacturers of water industry plant.

INTRODUCTION

The principal of the Rotating Biological Contactor (RBC) was first developed in the late 1920's (Doman, 1929), however, it was not until the 1960's that the first commercial system was installed in West Germany (Tchobanoglous, 1990; Gray, 1989). Thereafter, the popularity of RBC's grew and they are currently operated worldwide. The RBC is primarily used for sewage treatment in small communities, though it is now being used for larger treatment operations (Findlay et al., 1998). They consist of discs attached together to form a media pack as illustrated in figure 1. The polymer discs, also referred to as media panels, are held within an enclosed basin, submerged by approximately 40% of the surface area. Wastewater passes through the basin as the disks slowly rotate, at approximately 1 rev/min, exposing the biological growth (biomass) alternately to the wastewater, and to the surrounding air. The RBC operates continuously throughout its life, any break in operation will necessitate attention by the operator to maintain imposed consent standards. Typically, a media pack consisting of a collection of media panels, represents one stage of the treatment process. The RBC can consist of up to four or even five separate media packs depending upon the population served.

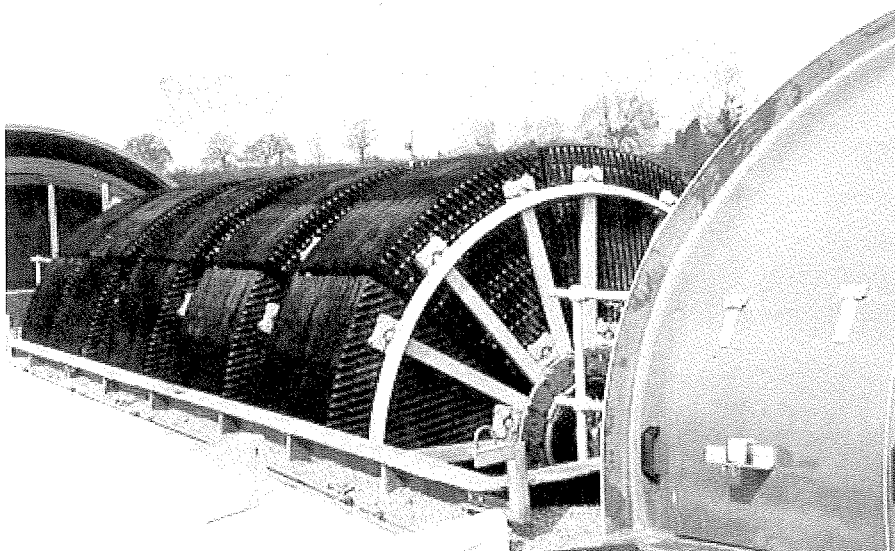


Figure 1 Typical Rotating Biological Contactor

Whilst it is recognised that the RBC is effective for sewage treatment, several Water Companies in the U.K and abroad, have experienced mechanical failures well before their expiry dates. This results in the user adopting an alternative treatment method and /or redirecting the sewage liquor whilst the plant is out of operation, at an additional operating cost. An in-depth investigation by the U.S Environmental Protection Agency (Brenner) into the design, operation and maintenance of RBC's, concluded that whilst improvements in the design of RBC's can result in more robust units, the loss of mechanical integrity of these units is common and unpredictable. In a separate report Weston stated: "It is recommended that design engineers should seek an RBC equipment warranty of sufficient duration and scope to protect the owner from failure. It is the opinion of the authors that equipment manufacturers would eventually solve the equipment problems."

These findings were reiterated in the largest survey on the mechanical integrity of operational RBC units ever undertaken (Mba et al.). Typical failures reported by Brenner and Mba included shaft breakage, stub shaft damage, media degradation and damage, media support structure fracture and degradation, and bearing failure. Any one, or combination, of these faults will require prompt replacement of the failed component.

Brief description of mechanical deficiencies associated with the RBC.

A mechanical survey of over two hundred and fifty operational RBC's highlighted several common mechanical deficiencies, which are detailed as:

I. Shaft failure

Shaft fracture has been experienced on several RBC's, resulting in complete collapse of the unit. This mode of failure is considered to be the most severe form of mechanical breakdown, due to total replacement costs.

II. Media Support Structure failure

The RBC media support structure generally consists of between four to twelve equal segments which are contained within a common frame, dependent on the size of the RBC. Each individual segment is usually supported by three through rods attached at their ends to a supporting structure. Fatigue failure of this structure has been experienced, particularly on the larger RBC's, see figure 2

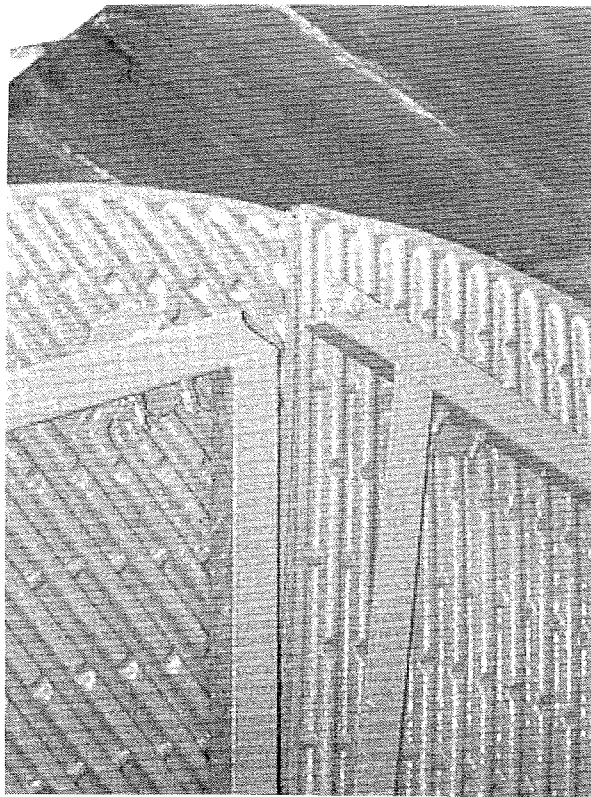


Figure 2 Damaged media support structure

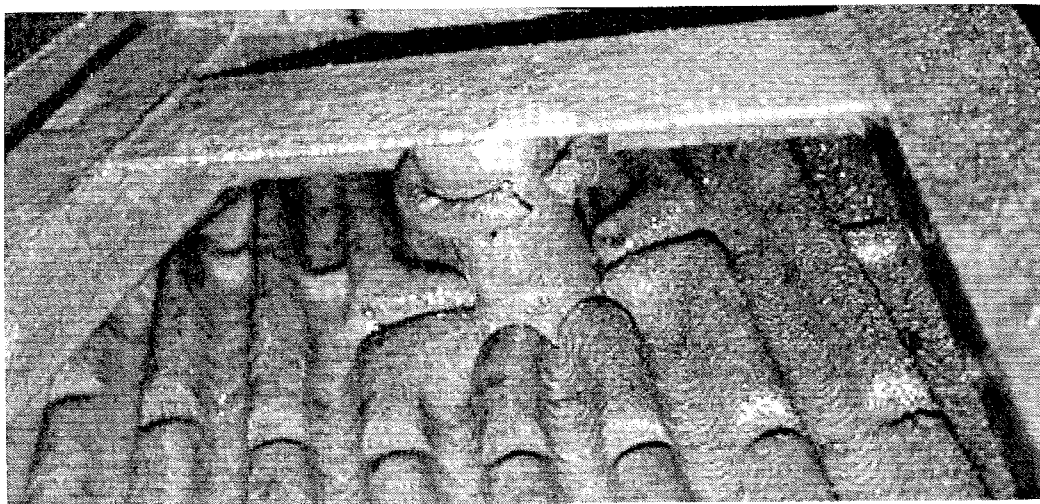


Figure 3 Fractured 'U' strap

In addition, clamps securing the through rods to the supporting frame have in many instances lost their clamping efficiency, as a result of inadequate design. In several instances this has resulted in the through rod becoming loose and moving axially along the length of the rotor, eventually catching the concrete or GRP basin/tank, resulting in major damage, see figure 4.

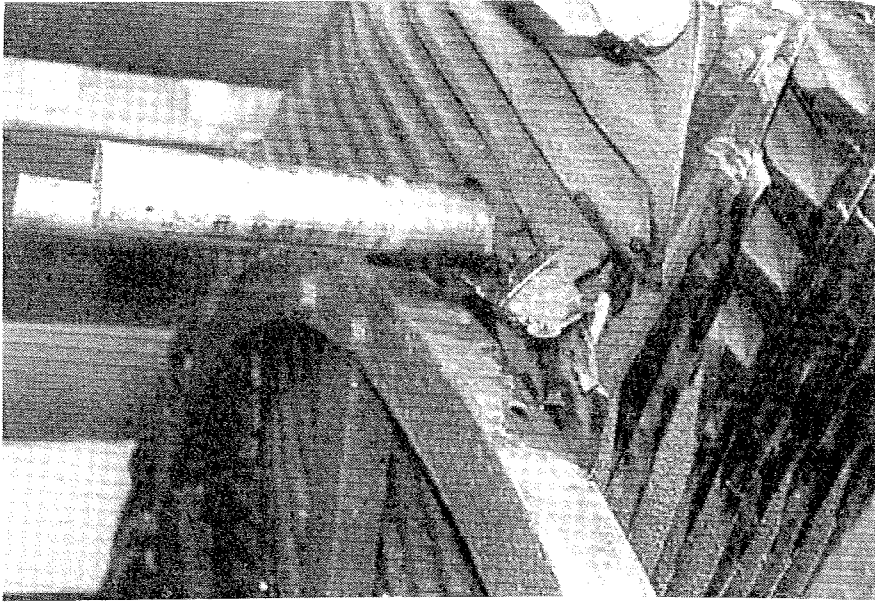


Figure 4 Loss of clamping efficiency resulting from a fractured 'U' strap

III. High density polypropylene media panels

Tearing, loss of rigidity and crumbling of these media panels are common and highlighted in figures 5 and 6, depicting mechanical inadequacies in designs of media panels. Tearing generally occurs in the region through which the support/through rods pass and is attributed to Hertzian stress concentrations in the vicinity of the through rod hole. In addition, poor quality of finish during manufacture results in the creation of jagged edges giving rise to stress concentrations, which eventually lead to crack growth and tearing in this vicinity, see figure 7.

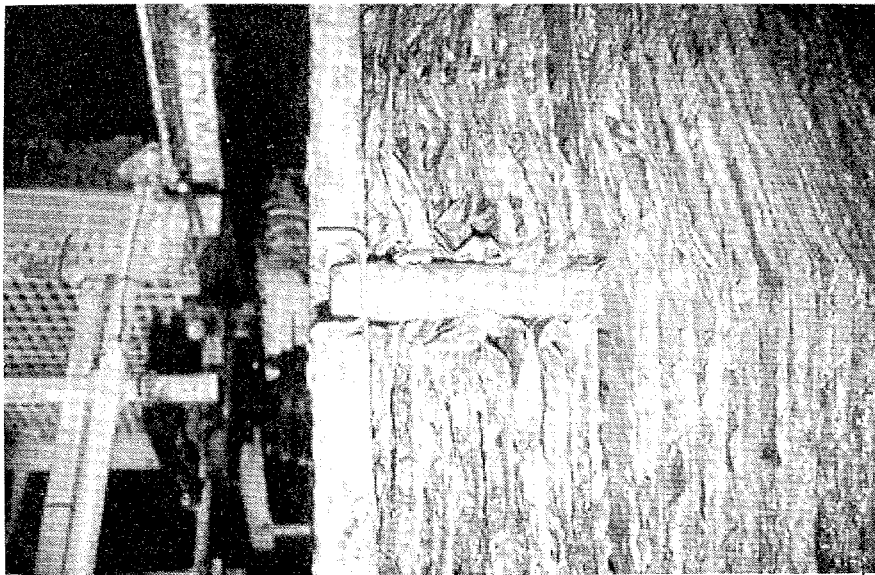


Figure 5 Tearing of high-density polypropylene media panels

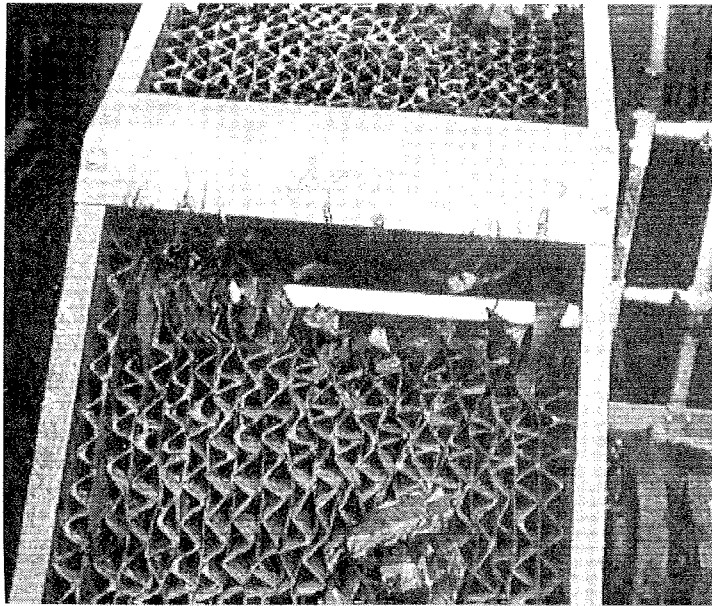


Figure 6 Loss of media pack due to tearing of HD polypropylene media panels

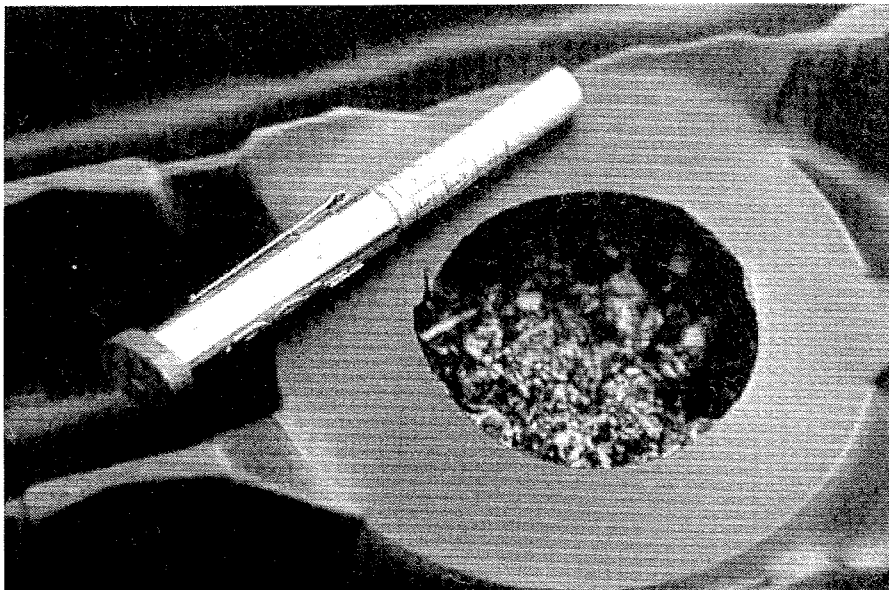


Figure 7 Stress concentrations on the media panel

IV. Inadequate locking of nuts and bolts

Looseness of nuts and bolts is very common on RBC's. A common form of locking is the application of a nylon-locking nut; however, these have also been known to become loose. In addition, where differing materials have been employed on the media support structure and retaining bolts, plastic washers have been used to separate these materials in an attempt to avoid galvanic corrosion. However, with time the plastic washers creep, leading to loss of tightening torque, see figure 8.

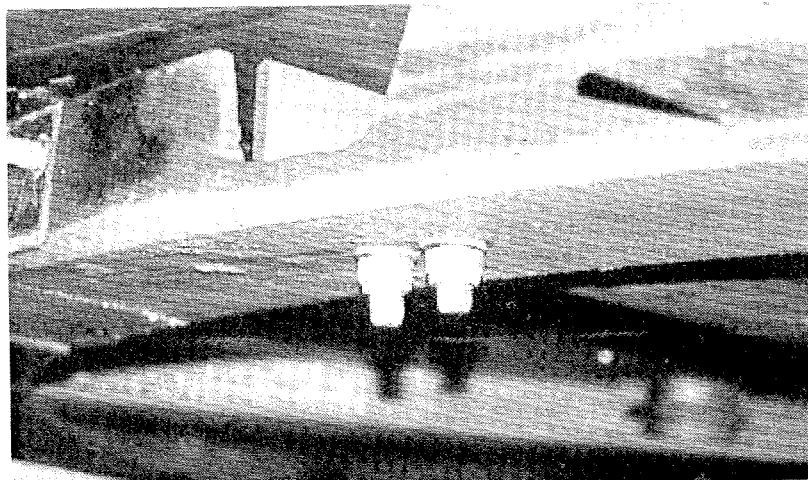


Figure 8 Loose clamping bolts

V. Others

Bearing failure are very common on RBC's and can result in loss of operation for up to two weeks, depending on severity.

The most influential factor affecting the life of RBC units, particularly the shaft and media support structure, is low frequency corrosion fatigue. Further details of the reasons of such defects have been detailed by Mba et. al.

THE NEW DESIGN

It is shown that the evolution of mechanical design of RBC's has largely been directed by economies of manufacture and operational requirements. However, the advances in the mechanical design of the RBC supporting structure is largely influenced by overcoming known mechanical deficiencies as well as increasing operational life. This section depicts the current technology and practice of UK based manufacturers.

Before attempting to design any machine component, it is most important to understand the mechanism by which the component is subject to force loading, and whether the loading is static or cyclic. For example, on most medium size RBC's the media segment is supported by three through rods, whereby each rod is reacted back onto the media support frame and held in position by some form of end clamp. When establishing the magnitude of loading applied to each of through rods per media segment, it is a common misconception to assume that each through rods supports the same load and that the loading is constant. Unquestionably by making such an erroneous assumption can result in premature failure of the through rod and rod end clamp.

The actual load value is dependent on the type, size and orientation of the media corrugations, moreover, the loading is "dynamic" resulting from rotation. For example, as the media emerges from the liquor, draining off water has to be considered in addition to the biomass loading. Furthermore, as the media segment re-enters the liquor the loading has now changed both in magnitude and direction, thereby causing reversed cycle loading, which is an important factor when selecting the size of through rod and rod end clamp design. By undertaking a finite element analysis, it has been shown that as a consequence of the corrugations, one of the three through rods will be subjected to a much higher load value, compared to the other two rods supporting the same media segment. This is probably why tearing of the media in the vicinity of the through rod hole always occurs at the one hole before progressing onto the next. Identifying which of the through rods is subjected to the highest dynamic loading, and by taking cognizance of the design employed for the media pack support frame, the size of rod can be established.

However, it is important to acknowledge that for each rotation of the shaft, the through rod end

clamp has to sustain both direct loading combined with bending couples, moreover, the direction of the load experiences a 270 degree change in direction. This change in direction also causes the through rod to rotate if the ends are not rigidly clamped. This phenomenon of rod rotation has been observed on many RBC's. Therefore, the most efficient method of securing the through rods to the media pack support frame is to offer clamping rigidity for the 270-degree change in load direction.

Different manufacturers approach this problem in a number of ways. The approach embraced by Cranfield University, is to provide a four point, line contact, method of support by employing a double "vee block" design illustrated in figure 9. Furthermore, the wall thickness of the through rod has to be sufficiently rigid so as not to allow crushing of the tube wall, therefore the tightening torque of the clamping bolts is also part of the design specification, together with the axial length of the vee block. Best practice relating to the design of through rod end clamps is governed by the design of the media pack support frame, moreover, most manufacturers acknowledge the loading pattern described above will give rise to bolt loosening. Therefore, positive mechanical bolt locking is highly recommended.

Surface protection of the through rod is also an important consideration when studying the fatigue life. For example, galvanising can reduce the expected service life. This is because zinc has a lower fatigue strength than that of hot rolled steel tubing and micro cracks in the zinc can propagate into the steel substrate thereby reducing the expected services life.

Over the period of investigation experience has shown that all RBC components have experienced fatigue failure, thereby suggesting that the designers have used inappropriate fatigue data. To achieve a twenty-year operational life, with a biomass loading equivalent to 5mm thickness on the inlet media pack, the following design criteria have been proposed (Mba et. al)

- a. Stainless Steel should not be used on future RBC's.
- b. Polymers must not be subject to compression or tension strengths above 4MPa.
- c. Stresses within the frame and shaft must be subject to a limiting bending stress of 20 MPa.

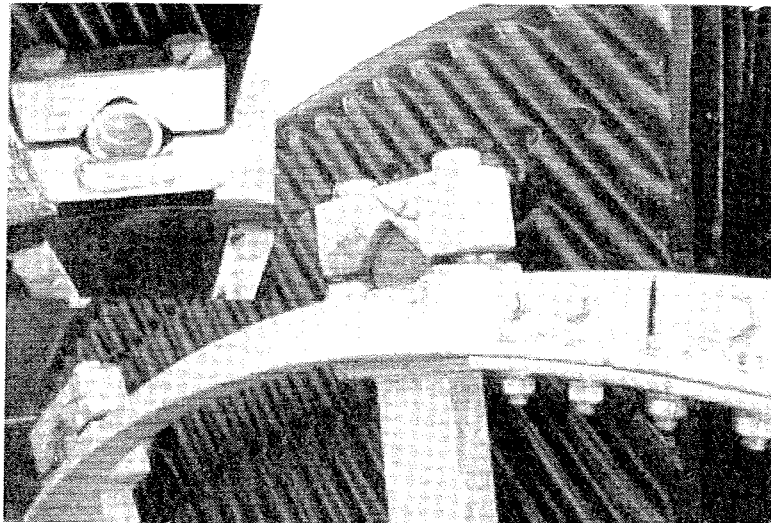


Figure 9 Four point line contact 'vee' block

Furthermore, to combat loss of bolt tightening torque use is made of positive locking for both nuts and bolts, see figure 10. Initial difficulties of properly aligning tab washers has been overcome by preforming the washer on a jig there by ensuring the "upturned" section always aligns with the flat of the nut or bolt.

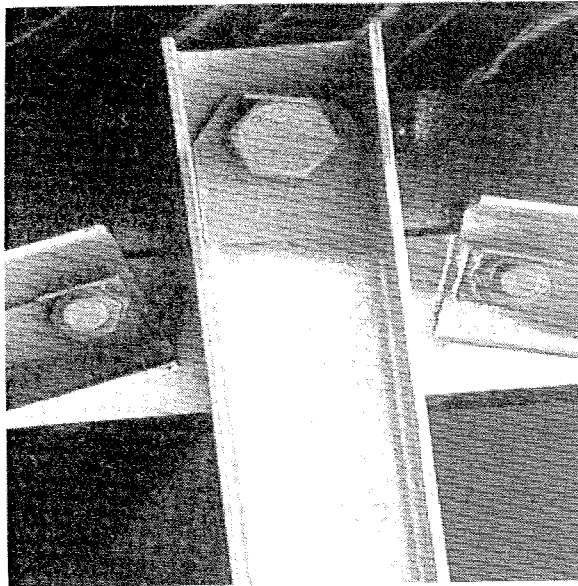


Figure 10 Useo Use of positive locking plates on nuts and bolts

To overcome this problem, the particular region has been strengthened and more stringent finishing requirements are requested, sees figure 11. Furthermore, it was noted that the thickness of high-density polypropylene employed (0.5mm) was insufficient to avoid tearing and retain rigidity. An increased thickness of 0.9mm is currently successfully employed.

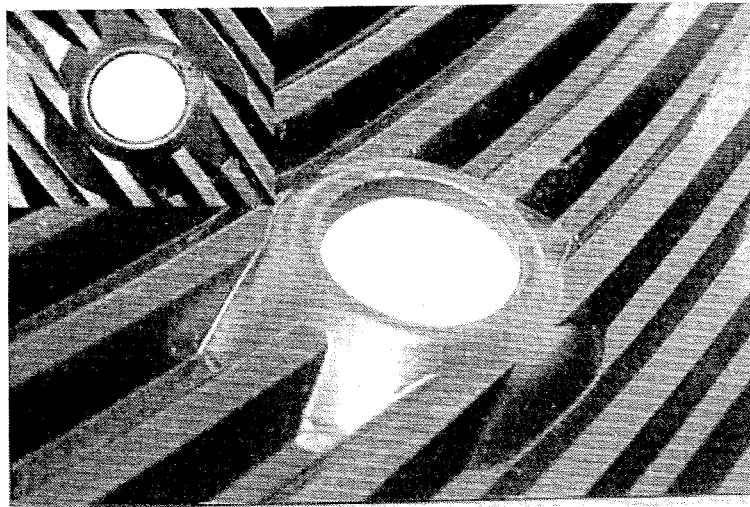


Figure 11 Strengthened ring on media panel

In addition to the normal design specifications it is strongly advised care must be exercised to ensure that stresses are not induced during manufacture or at installation due to misalignment. Any misalignment would result in raised stresses beyond the permissible fatigue stress limit. It should be noted that clamping the through rods to the frames avoids stresses been raised to manufacture

CONCLUSION

The mechanical design of an RBC is not simply concerned with the corrosion and fatigue behaviour of the various materials chosen at low speeds of loading, but also understanding the dynamic loading on the structure and bolts. Failure to understand these requirements is probably why so many failures have been experienced after the unit has been in operation only a few months or years of service. As a direct result of the research discussed in this paper, a mechanical specification for all RBC manufacturers has been established

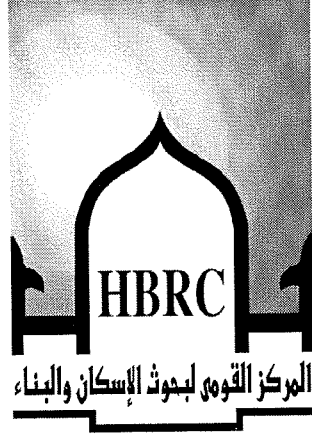
As a result of the Cranfield initiative, not only is the failure mode of RBC's fully understood but it is now possible to purchase an RBC warranted for 20 years, meeting the 'Weston' criteria. These design improvements are incorporated in the RBC's manufactured by Copa Ltd.

ACKNOWLEDGEMENTS

Mr. G. E. Findlay would like to thank Mr Michael Froud, Managing Director, Copa Ltd, for his support and commitment.

REFERENCES

1. Brenner, R.C. and Opaken, E.J. (1984) Design information on Rotating Biological Contactors Design, Technical report no. EPA-600/2-84-106, NN15 PB84 -199561. Municipal environmental research laboratory, Cincinnati, Ohio, USA.
2. Doman, J. (1929) Results of operation of experimental contact filter process with partially submerged rotating plates, Sewage works journal, 1, 555-560pp.
3. Findlay, G. E. Bannister R, (1998) The Severn Trent RBC and reed bed process, Proc of the Water Institute of Southern Africa Biennial Conference, Cape Town, Community Water Supplies and sanitation
4. Gray, N. F. (1989) Biology of Wastewater Treatment, Oxford science publications. ISBN0-19-859014-8
5. Mba, D., Bannister, R. H., Findlay, G. E. (1999) Mechanical redesign of the rotating biological contactor, Water Research, 33 (18), 3679-3688pp.
6. Tchobanoglous, G. and Burton, F.L. (1990) Wastewater Engineering Treatment, Disposal and Reuse, publisher Metcalf & Eddy Inc., 3rd edition. Copyright McGraw-Hill, USA. ISBN 0-07-041690-7.
7. Weston, R.F (1985) (US National Technical Information Service). Report PB85 - 80545."Review of Current RBC Performance and Design Procedures"



HBRC

News



International Workshop on
**Innovations in Materials and Design
of Civil Infrastructure**

28-29 December 2005 Cairo, Egypt

**WORKSHOP RECOMMENDATIONS
AND FUTURE COOPERATIONS BETWEEN EGYPT AND USA**

1. Encourage the collaboration between Egyptian and American institutes and professors in all aspects of civil engineering and infrastructure management research including:
 - Innovative techniques for infrastructure health monitoring and rehabilitation in Egypt
 - Innovative techniques for buildings health monitoring and restoration in Egypt
 - Innovative techniques for measuring dynamic response of different types of structures and infrastructures
 - Innovative buildings for dry arid zones
 - Smart buildings and nanotechnology research and applications
 - Innovations in materials for producing Low cost structures and affordable housing
 - Innovations in materials such as the high-strength, high corrosion-resistant steel
 - Innovations for the strengthening, retrofitting and rehabilitation of different types of structures
 - Innovations in construction and design techniques
 2. Encourage exchange of visits and research ideas between Egyptian and American professors and researchers
 3. Encourage Egyptian students to study in the USA and encourage the American to study in Egypt
 4. Encourage the exchange of facilities between Egyptian and American institutes such as libraries and Laboratories
 5. Encourage and educate engineers and researchers to practice design for life and utilizing lean and sustainable construction practices
 6. Encourage the Egyptian and American Scientists to apply for Joint-Research Funds that usually available online starting from July every year
 7. Encourage the collaboration between the Egyptian and American Institutes for the use of joint research program using the Virtual Labs and super computers using the facilities of Internet-2
 8. Recommend the holding of similar workshops yearly to discuss the innovations in the field of civil engineering and infrastructure management for this purpose. The University of Alabama was suggested for this purpose
 9. Encourage the research efforts towards the extraction of certain substances from some vegetation that can be used in manufacturing some construction materials.
- To ensure the follow-up the application of the above recommendations it is proposed to make a joint permanent committee between the Egyptian and American Professors and Researchers



Ministry of Housing, Utilities & Urban Development
Housing & Building National Research Center

International Conference on
**Bridge Management Systems - Monitoring ,
Assessment and Rehabilitation**

21-23 March 2006, Cairo, Egypt

Under The auspices of
Eng. Ahmed El-Maghraby
Minister of Housing, Utilities and Urban Development

Conference Chairman
Prof. Dr. Ali Sherif Abdel-Faiad
Chairman of the Housing & Building National Research Center

Second Call For Papers

OBJECTIVES

The conference offers an opportunity to exchange experiences and practices among the interested parties in the field of bridge management systems. The main objective of this conference and the accompanying workshops is providing the state-of-the-art knowledge about bridge management and other related issues such as monitoring, assessment and rehabilitation techniques. These activities are expected to benefit engineers , scholars and construction companies.

ORGANIZER

Founded in 1954, the Housing & Building National Research Center is an independent governmental research establishment subordinate to the Ministry of Housing, Utilities & Urban Development. HBRC consists of eleven scientific institutes and performs a leading role in enhancing the performance of the building sector through scientific researches and development of building codes and technical specifications. HBRC also provides engineering consultations, field inspection, quality control and experimental testing services.

CO-ORGANIZERS

- Western Michigan University , USA
- Kansas State University , USA
- Construction technology Laboratories (CTL Group) , USA

CONFERENCE THEMES

1. Bridge Management
2. Assessment and Condition Evaluation
3. Non Destructive Techniques for Bridge Evaluation
4. Bridge Maintenance Techniques
5. Lifecycle Cost Analysis
6. Decision Support Systems
7. Superstructure Rehabilitation
8. Substructure Rehabilitation
9. New Construction Materials for Bridges
10. New Construction Methods
11. Design Theories and Practice
12. Case Studies



Housing & Building National Research Center (HBRC)

HBRC Journal

Conference & Workshop

(International Conference on Bridge Management Systems -Monitoring , Assessment and Rehabilitation)

21-23 March 2006 Cairo, Egypt

WORKSHOPS

1. Bridge Design and Practice in USA & Egypt
2. Assessment and Condition Evaluation of Bridges

CALL FOR PARTICIPATION

Researchers and interested parties are invited to participate in the conference.

Online Registration is available on www.hbrc.edu.eg

IMPORTANT DATES

February 15, 2006 - Receipt of full papers

February 21, 2006 - Receipt of revised papers

February 28, 2006 - Notification of final acceptance

WHO SHOULD ATTEND

Structural engineers, bridge designers, bridge construction and maintenance companies , project managers, bridge owners, transportation policy makers, and other bridge engineering professionals

LANGUAGE

The conference will be conducted in English. All abstracts, papers, presentations and posters shall be in English.

CONFERENCE PROCEEDINGS

The conference proceedings will be available on CD's upon registration. Selected papers will be published in a special issue of the HBRC Scientific Journal.

CONFERENCE VENUE

The venue for the conference is the Housing & Building National Research Center (HBRC),

87 El-Tahrir Street, Dokki, Cairo, Egypt

Tel. : (+202) 3351564, 7617057

Fax : (+202) 3351564, 3367179

All presentations, lunch and coffee breaks will be at that location. For information on how to get to the venue, Please visit: www.hbrc.edu.eg.

More information about Egypt can be found on www.sis.gov.eg

FURTHER INFORMATION

All Conference details and the full program will be available on www.hbrc.edu.eg

SOCIAL / CULTURAL PROGRAM

An interesting one day tour will be organized on

Friday March 24, 2006

CONTACT

For more information, please contact the conference coordinator:

Dr. M. Nabeel Abdel-Salam

Housing & Building National Research Center

87 El-Tahrir St., Dokki, Giza 11511

P.O.Box : 1770 Cairo, EGYPT

Phone: (+202) 7617062, 3351564, 7617057

Fax : (+202) 3351564, 3367179

E_mail : BMSHBRC@hbrc.edu.eg or BMSHBRC@netscape.net



Title : A Study Of Geological, Geotechnical & Hydrological Soil Characteristics And Some Foundation Applications At Sohag

Institute of Soil Mechanics & Geotechnical Engineering

ABSTRACT

The objective of the study is to form a geological, geotechnical and hydrological soil data base for Sohag Governorate. This study area of Sohag Governorate was chosen because abundant soil data were available from geotechnical reports carried out by soil mechanics and foundation engineering department.

Soil characteristics data from the available geotechnical reports were classified and stored in tables designed as data base forms. In order to be able to draw geotechnical sections reflecting the general soil formations in the studied area, representative boring log for each site was formed. These geotechnical sections included soil properties and ground water levels information.

The study comprised the determination of topographic and geological features of the governorate, geotechnical data base, maps and longitudinal cross-sections clarifying soil layers formation and their engineering characteristics. This study could be of great help to engineers and decision makers to optimize safely and economically the choice of projects location on scientific bases. Also as guidance in planning detailed site investigations for future projects, and provide bases of the evaluation of the possible natural or man-made hazards.

Furthermore, in the present work it was found that, the use of computer artificial intelligence program in suggesting the proper foundation types, according to soil nature and structures types, proved to be applicable compared to recommendations given by soil mechanics reports.

This research is considered to be a pilot study that can be applied on other governorates as well as new communities and expansions.



HBRC Journal

Board of Directors :

Prof. Ali S. Abdel Faiad (Chairman HBRC)
Prof. Omaina A. S. El-Din (Board Head)
Prof. Adel I. El-Mallawany (Deputy)
Prof. Hamdy A. El-Sayed
Prof. Fayrouz F. El-Dib
Prof. Shadia N. El-Ibiary
Prof. Heba H. Bahnasawy
Prof. Khadiga I. Abdel-Ghani
Prof. Mohamed M. Abdel-Razik

Board of Editors :

Prof. Adel I. El-Mallawany (Head)
Prof. Amira Abd El-Rahman (Deputy)
Dr. Nadia M. Nofal
Dr. Khalid M. El-Zahaby
Dr. Dina K. Shehayeb
Dr. Ashraf M. Kamal
Dr. Ashraf M. Fadel
Dr. Amr A. El-Hefinawy
Dr. Tarek M. El-Sokkary
Dr. Tarek M. Bahaa
Dr. Tarek M. Attia
Dr. Mohamed M. Abd El-Rahman
Mr. Mohamed El Sayed Metwally

Editorial Office :

Eng. Bastamy El-Touny
Eng. Ghada Diaa
Eng. Anwar M. Mohamed



Housing & Building National Research Center has the pleasure to announce the commencement of its new scientific refereed journal "HBRC Journal"

The journal is a semi-annual publication and covers the following areas:

1. Engineering Materials
2. Material Science
3. Architecture, Housing and Urban Development
4. Environmental Engineering and Building Physics
5. Structural Engineering
6. Geotechnical Engineering
7. Construction Engineering and Management

The first issue was published in Dec. 2004

Deadlines for Submission :

Receipt of full paper: May 1st (July issue); Oct. 1st (Jan. issue)

Interested authors are invited to submit their contribution (2 hard copies and a soft copy) to the following address according to the attached format

Email : journal@hbrc.edu.eg
Address : Housing & Building National Research Center
HBRC Journal
P.O.Box 1770 Cairo, Egypt

General Note:

Only Microsoft Word formatted articles will be accepted using the following guidelines:

General:

- Trade-names are not mentioned in the manuscript. Company or Organization names may, however, be included under "Acknowledgement" only
- Footnotes are not used in the text of the manuscript
- Only laser printer should be used

Paper Format:

- All text is in ARIAL.
- Page Standard Size A4
- Margins: 3.0 cm from all sides, for all pages including the first page.
- Maximum 12 pages (each extra page up to 18 Pages will be charged additional fees)

Title of Paper:

- Arial 14 pt bold, UPPER CASE
- Maximum 2 lines
- 3 blank lines are left above the title (single spaced at 10 pt)

Authors' Names:

- Arial 10 pt, Upper and Lower Case
- First name, middle (initial), followed by last name
- Titles are not included
- Authors from the same organization are grouped together

Authors' Affiliation:

- Arial 10 pt, italic, Upper and Lower Case
- Maximum 2 lines

Abstract:

- Arial 10 pt, single-line spacing
- Maximum 300 words
- Keywords maximum 7

Main Headings:

- Arial 12 pt bold, UPPER CASE
- Separated from preceding text by 20 pt (2 lines)
- Separated from subsequent text by 10 pt (1 line)

Secondary Headings:

- 10 pt bold, Upper and Lower case
- Separated from preceding text by 10 pt, and from subsequent text by 10 pt.

Text:

- Arial 10 pts, single-line spacing, full justified
- All Paragraphs have no indent

Figures/Illustrations:

- Caption heading in Arial 10 pt bold, centered below figure.
- Figures are in black and white (colour figures are not allowed).
- Figures are in high resolution, sharp enough for reproduction.
- No more Than 2 Blank Lines Should be Left Before or After Figures.
- Figures should be placed inside the text just after they cited.

Tables:

- Tables are centered; no text to wrap around the tables.
- Caption heading in Arial 10 pt bold, centered above table.
- Text and numbers are in Arial 10 pt.
- Tables are not split over two pages.
- Tables shall be surrounded with single normal lines.

Mathematical Text:

- All symbols are in italic
- All numbers are non-italic (e.g., 0.5 f_y)
- All equations are left justified and numbered in sequence
- All equation numbers are right justified

Units:

- The International system of units (SI) should be used, Equivalents in other units may be given in parentheses

References:

- All references are cited in the text between square brackets (e.g. [2] , [4-6] and listed in the end of the paper under word REFERENCES
- Reference follow the format in the following examples:

REFERENCES

1. Ghobarah, A., Aziz T.S. & Biddah, A. (1997), "Rehabilitation of Reinforced Concrete Frame Connections Using Corrugated Steel Jacketing", ACI Structural Journal, 94(33), pp. 283–294.
2. Nawy, E. G.(2000), "Prestressed Concrete: A fundamental Approach", 3rd Edition, Prentice Hall, NJ.
3. Tjandra, A.R. & Tan, K.H. (2003), "Strengthening of Reinforced Concrete Continuous Beams with External Tendons", 6th International Symposium on FRP Reinforcement for Concrete Structures (FRPRCS-6), Singapore, Vol.1, pp. 723–732.
4. "Product Review", http://in_site.bidcom.html/overview.html, (1999), accessed Feb. 3, 2000.
5. Use the paper sample template found in hbrc website.

Housing & Building National Research Center

87 El Tahrir St., Dokki, Giza EGYPT

P.O.Box (1770) Cairo

www.hbrc.edu.eg

Email : journal@hbrc.edu.eg

Tel : (20)(2)3356722, (20)(2)3356853, (20)(2)3351564, (20)(2)7617062 Fax: (20)(2)3351564, (20)(2)3367179, (20)(2)7617062